Imperial College London

Department of Physics

A novel approach to quantum transition rate theory using open quantum dynamics

Author:
Chiara Liverani

Supervisors:
Prof. Mike W. Finnis
Dr. Eva-Maria Graefe

Dissertation for the degree of Doctor of Philosophy

December 2017

The work contained in this thesis is my own, and otherwise I have inserted appropriate references.

The copyright of this thesis rests with the author and is made available under a Creative Commons Attribution Non-Commercial No Derivatives licence. Researchers are free to copy, distribute or transmit the thesis on the condition that they attribute it, that they do not use it for commercial purposes and that they do not alter, transform or build upon it. For any reuse or redistribution, researchers must make clear to others the licence terms of this work.

IMPERIAL COLLEGE LONDON

Abstract

Department of Physics

Doctor of Philosophy

A novel approach to quantum transition rate theory using open quantum dynamics

by Chiara LIVERANI

This work is about a quantum-mechanical generalisation of transition rate theory that accounts for temperature-dependent quantum-dynamical effects. The starting point of this investigation is a formulation of the classical transmission coefficient where the activated dynamics is needed to obtain the time evolution of the classical state function and the rate is expressed as an average flux in momentum space. Traditional approaches to quantum transition rate theory are briefly discussed, with emphasis on the fact that these do not generally require knowledge of the open quantum dynamics. The latter can be studied by means of the Lindblad equation for mixed states, which is shown to be analogous to an average over realisations of a certain type of stochastic Schrödinger dynamics. The stochastic evolution in Hilbert space is used in combination with an ansatz for the wave function as a Gaussian wave packet to show that under appropriate assumptions the stochastic Schrödinger equation converges to the classical Langevin equation. A novel formulation of the quantum transmission coefficient is presented which features a quantum-mechanical version of the state function obtained via the density operator, so that the activated quantum dynamics can be taken into account by solving the Lindblad equation. A numerical investigation of the quantum transmission coefficient thus obtained for different temperatures is carried out, along with a comparison to the classical results. The quantum-mechanical transmission coefficient is found to display some expected features, such as vanishing in the limit as $t \to 0^+$, displaying a "plateau" value for certain values of the temperature, and decaying to zero exponentially fast when the fundamental assumptions of TRT do not hold. Additionally the plateau value of the quantum transmission coefficient is found to be smaller than the classical counterpart in all regimes, and to approach the corresponding classical value in the limit of large temperatures.

Contents

Abstract ii

1 Introduction 1

2 Traditional approaches to classical and quantum transition rate theory 8
2.1 Classical transition rate theory . . . 9
2.2 Activated processes and open classical dynamics: Langevin equation . . . 21
2.3 Classical TRT in a 1-d double-well system . . . 24
2.4 Traditional approaches to quantum transition rate theory . . . 39
2.4.1 Discretised path-integrals and quantum TRT . . . 42

3 Open quantum dynamics 46
3.1 The Lindblad equation . . . 47
3.2 The quantum-state diffusion method . . . 51
3.3 Semiclassical limit of QSD pure state dynamics . . . 54
3.3.1 General case . . . 55
3.3.2 Example: particle moving in an external potential under the influence of a heat bath . . . 61

4 Quantum transition rate theory of a 1-d double-well system 72
4.1 Novel formulation of quantum transition rate theory . . . 73
4.2 Model and implementation . . . 77
4.3 Results – quantum and classical dynamics . . . 80
4.4 Results – quantum transition rate theory . . . 92

5 Conclusions and outlook 103

A Derivation of the classical Langevin equation 107

B A system of dimensionless units of measure 109

C Methods of numerical integration for open dynamics 111
C.1 Classical Langevin equation . . . 111
C.2 Semiclassical dynamics . . . 112

C.3 Lindblad and QSD equations 112

D Brownian motion and Itô calculus **114**

Bibliography **116**

Chapter 1

Introduction

Processes that can be described by means of *reaction* or *transition rates* are ubiquitous in nature. While originally conceived in chemistry to model reactions between chemical compounds, transition rates have implications in a variety of areas of research, including atomic physics, solid state and semi-conductor physics, diffusion dynamics, cosmology, celestial machanics and studies of the rearrangements of clusters [1].

An important aspect regarding transition rates is their relationship to Einstein's model of diffusion, where the diffusion coefficient D is related to the mean square displacement of a Brownian particle diffusing through a liquid [2]. If the Brownian particle is described as a random walker moving through a lattice of points x_i at distance d and the probability of hopping between any two points is k, then one has that the diffusion coefficient can be approximated as:

$$D = \Omega d^2 k, \tag{1.1}$$

where Ω is a constant depending on the dimensionality of the problem and the number of neighbouring sites the Brownian particle can jump to. For a detailed discussion on the equation above, see for example reference [3]. The transition probability k can be alternatively called *transition rate*.

Equation (1.1) makes transition rates useful tools to study diffusion as well as various meso- and macroscopic phenomena related to it. An example of such phenomena we find in engineering is *hydrogen embrittlement* (HE), which takes place when hydrogen atoms

enter the metal's structure and interact with its atoms in such a way that the metal loses its ductility and becomes brittle. One of the basic processes involved in HE is the diffusion of hydrogen through the metal lattice and this can be studied by means of a transition rate giving the probability that the hydrogen atom makes a transition from one local minimum of the potential energy surface to another [4], [5], [6].

Transition rate theory (TRT) was initially a purely phenomenological discipline, concerned with chemical reactions and the environmental factors influencing the value of the associated reaction rates. Amongst these we have temperature, pressure, concentration of the chemical compounds, and the nature of the reaction taking place. The first expression for the transition rate k was proposed by Arrhenius at the end of the XIX century and describes the dependence of k on the temperature [7]:

$$k_A = \nu e^{-\beta E_b}, \tag{1.2}$$

where β indicates the inverse temperature $\beta = (k_B T)^{-1}$, and k_B is the Boltzmann constant; E_b is the activation energy of the chemical reaction and the ν is a constant reaction-specific prefactor, with the dimensions of inverse time for unimolecular reactions. Arrhenius obtained equation (1.2) by observing and recording the data relative to a large number of chemical reactions. The resulting law is very powerful in that it captures a couple of key features of transition rates: they characterise thermally activated effects; they can be described in terms of two separate contributions of which one depends only on the temperature of the system and the energy barrier between initial and final states.

For a full characterisation of the multiplicative factor ν appearing in equation 1.2 we have to wait long after Arrhenius' work. In fact it was not until about a century later that efforts towards a mathematical formulation of transition rates in terms of time correlation functions started, mainly thanks to Kubo ([8], [9]) and Chandler [10]. This is when TRT went from being a phenomenological discipline based solely on the observation of macroscopic chemical systems to being a theory encompassing the microscopic *statistical* features of the system of interest. Not only did these developments enable the formulation of transition rates to be linked to the theory of non-equilibrium and noise-driven effects,

they also confirmed what Arrhenius had implicitly found with his formula: that the rate constant k can be expressed as the product of two distinct contributions, which we call κ and k^{TS}:

$$k = \kappa k^{TS}, \tag{1.3}$$

where κ is related to the dynamical, or non-equilibrium features of the system and k^{TS} is determined by the equilibrium-statistical features of the system. The label "TS" in the equation above refers to *transition-state theory* (TST), an approximation whereby the transition rate is expressed solely by its equilibrium-statistical contribution, while all dynamical contributions are neglected. We will discuss about this in greater detail in the following chapters.

Reaction rate theory began as a classical theory of chemical kinetics; the question of how to include quantum-mechanical effects into the theory and in particular in the description of reaction rates has been haunting scientists working in this field for a long time, and still does nowadays. The necessity of including quantum effects in TRT was acknowledged early on by Burgouin ([11]) and shortly after by Wigner ([12]), however it took about 30 years for attempts to systematically generalise classical TRT to quantum-mechanics to start [13], [14], [15].

Miller's *trace formula* for the transition rate ([15]) is a rigorously-derived quantum-mechanical expression encoding both dynamical and equilibrium contributions to the rate. A feature of this expression is that it implies the equilibrium contribution to the rate, k^{TS}, is zero in the quantum-mechanical case ([16]), and the dynamical contribution enters as a non-vanishing correction to the equilibrium part. However shortly after the publication of the work by Miller a number of other works were produced, by Miller himself and several others, that went in the direction to find a suitable approximation for k^{TS}. The rationale was that in most cases κ would be too expensive to compute, and hence focussing on ways to devise a non-zero estimate for k^{TS} would be more worthwhile. A large class of such efforts made use of the *discretised path-integral* (DPI) formalism derived from Feynman's path-integral formulation of quantum-mechanics [17], [18]. In the DPI approach to quantum transition rate theory, one estimates k^{TS} by expressing it as a ratio of quantum partition functions which are approximated in terms of classical

partition functions of a suitably defined ensemble of classical particles. According to Feynman's results, this mapping is exact in the limit as the number of classical particles in the ensemble tends to infinity.

Initial contributions in DPI-quantum-TRT were concerned with devising a convenient approximation for k^{TS} in the knowledge that the true quantum-mechanical version of this quantity is always zero [19], [20], [21]. Subsequent efforts in this area went as far as trying to demonstrate that the DPI version of the quantum-mechanical equilibrium rate k^{TS} is in fact its true version ([22], [23]), and even postulated that the DPI mapping between quantum and classical systems could be used to estimate the dynamical contribution to the rate, κ, in the quantum-mechanical case [24], [25], [26], [27], [28]. Despite the fact that the theoretical fundament for using DPI techniques to study quantum-dynamical effects is still being investigated, when applied to the case of hydrogen diffusion in metals they have produced meaningful results [29], [30].

We take a completely different approach to the study of quantum-mechanical effects in transition rate theory. Instead of applying *ad hoc* methods such as DPI, we formulate the open quantum dynamics giving rise to quantum TRT explicitly in terms of Gaussian wave packets evolving according to a quantum master equation that models the time evolution in the presence of a Markovian heat bath. We define the dynamical contribution to the quanutm rate, κ, by translating the classical *path-sampling* correlation function expression proposed by Chandler for the classical rate [31]. This allows us to calculate the quantum time correlation function κ for a symmetric double-well system at a range of temperatures as well as to study the associated quantum dynamics in each temperature regime. Our methodology to investigate quantum TRT is entirely novel to the best of our knowledge.

In our investigation of quantum TRT, Gaussian wavepackets are used to assign a minimum-uncertainty state to the initial configuration of the system, which is then allowed to evolve following a *Lindblad equation* modelling the combination of Hamiltonian and dissipative, temperature-dependent dynamics. This approach originates from the work done by Heller, who used Gaussian wave packets to devise a semiclassical scheme for the quantum evolution based upon expressing the external potential as a Taylor series up

to quadratic order ([32], [33]). We also use Heller's ideas to prove an important result, which is the correspondence between a certain type of stochastic Schrödinger equation and the classical Langevin equation. This result, while significant on its own, is very relevant within quantum TRT in that, as we stressed before, transition rates are defined within the realm of thermally activated processes, which can be modelled by means of stochastic or noise-driven systems. In fact, to the best of our knowledge, the relation between the classical stochastic dynamics given by the Langevin equation and the quantum stochastic dynamics given by this type of Schrödinger equation had never been shown before.

The outline of the thesis is as follows. In chapter 2 I review the formulation of classical transition rate theory, and show that the transition rate can be expressed in terms of a time correlation known as the reactive flux. I then introduce our main quantity of interest, the transmission coefficient, in the classical case. By manipulating the equation obtained for the transmission coefficient I show that this can be written in its transition path-sampling formulation as an average flux in momentum space. I discuss how this formulation relies on the knowledge of the classical "activated" dynamics, *i.e.*, on coupling the classical trajectories to a heat bath. In section 2.2 I present the classical open dynamics by introducing the Langevin equation and the Fokker-Planck equation. Next, in section 2.3 I apply the concepts of classical TRT to a 1-dimensional system given by a hydrogen atom moving in a symmetric double-well potential, where the open classical dynamics is obtained via the Langevin equation. I discuss how well TRT applies to this system depending on the values taken by the temperature and the coupling to the heat bath, and identify the regions in parameter space where the TST approximation to the transition rate is more accurate among the values tested. The numerical results presented here are all original, although the general topic of classical TRT is well-known in the literature. In the last part of chapter 2 I review some of the traditional approaches to the generalisation of classical TRT to quantum mechanics. I present Miller's trace formula for the quantum rate and other approaches based on the discretised version of Feynman's path intergral formulation of quantum-statistics.

Chapter 3 dives into the topic of open quantum dynamics. Here I firstly present the

Lindblad equation, which governs the time evolution of the density operator in the non-unitary case. Similarly to the classical case with Langevin and Fokker-Planck dynamics, in quantum mechanics the Lindblad equation for mixed states is analogous to an average of Schrödinger equations for pure states. The latter constitutes the so-called *quantum-state diffusion* (QSD) approach to open quantum dynamics, discussed in section 3.2. In section 3.3 I show that the QSD equation converges to the Langevin equation in the classical limit. This is achieved by means of a coherent states representation of quantum states, and in particular by writing the wave function as a Gaussian wave packet in phase space. By assuming that the external potential is quadratic near the centre of the wave packet I derive the stochastic dynamics of the parameters appearing in the Gaussian ansatz, and find that the classical position and momentum obey the Langevin equation in the limit as $\hbar \to 0$. Mention of this result can be found in the literature, however to my knowledge an explicit derivation based on coherent states is new. In section 3.3.2 I proceed to compare the semiclassical, quantum-mechanical and classical dynamics by numerically solving the corresponding equations of motion at a range of temperatures and values of the coupling coefficient. I find that the semiclassical scheme correctly predicts delocalisation effects at low temperatures, however it does not appear to capture interference effects which brings about unphysical results in cases where the coupling to the heat bath is very low.

In chapter 4 I introduce a novel formulation of the quantum-mechanical transition rate. This is based on the classical path-sampling expression for the transmission coefficient, which is interpreted in quantum-mechanical terms via the expectation values of the position and momentum operators and a quantum-mechanical state function that depends on time through the density operator. Here the crucial ingredient is the open quantum dynamics, which enters with the time-dependent density operator, and to my knowledge is not featured in any of the previous formulations of the quantum rate. In sections 4.3 and 4.4, I investigate quantum TRT using our formulation of the quantum rate and compare the results obtained for different values of the temperature and the coupling coefficient to the corresponding classical results. I also study the open quantum and classical trajectories giving rise to various transmission coefficients, and examine how

different types of dynamics generate different types of correlation functions in both classics and quantum-mechanics. I find that the quantum transmission coefficient shares some qualitative features with the classical counterpart, including a "plateau" value corresponding to the rate constant in certain regions of parameter space and an exponential decay in high-temperature regimes where the assumptions of TRT do not hold. I find that the quantum correlation function is zero at $t = 0$, confirming that the classical definition of the TST rate cannot be applied *ipso facto* in quantum mechanics. However my results show that there is a small-time non-zero value of the quantum correlation function which is of the same order of magnitude as the classical TST value and approaches the classical counterpart as temperature gets large. I find that the plateau displayed by the quantum transmission coefficient, corresponding to the "true" quantum transition rate, is generally smaller than the classical counterpart. Lastly, in chapter 5 I summarise my results and discuss potential further developments of my work.

Chapter 2

Traditional approaches to classical and quantum transition rate theory

In this chapter we present classical and quantum-mechanical transition rate theory by discussing their traditional formulations. In classical mechanics we show how to derive the transition rate using the time correlation function approach developed in reference [34]. Here one exploits Onsager's *regression hypothesis* to relate the macroscopic rate equations to the autocorrelation of microscopic equilibrium fluctuations taking place in the system. The rate is obtained via the so-called *reactive flux* correlation function by assuming that there is a separation of time scales between macroscopic transitions and microscopic fluctuations. We show that the classical transmission coefficient, encoding the dynamical information entering the transition rate, can be expressed as an average flux in momentum space by writing it in a transition path-sampling form. The latter was derived by Chandler in reference [31]. We discuss the transition-state theory (TST) approximation to the classical rate and show how it can be obtained as the limit as $t \to 0^+$ of the reactive flux.

The computation of the "full" transition rate, or, alternatively, of the transmission coefficient, requires that the corresponsing classical dynamics is temperature-dependent – *i.e.*, "open": in a closed system there are no transitions in the sense of activated processes [31]. We discuss how the classical temperature-dependent dynamics can be described by

means of the Langevin equation for single trajectories, or via the Fokker-Planck equation for the density in phase space. In Langevin dynamics, the coupling of the trajectory to a heat bath at thermal equilibrium is described via two parameters, the temperature T and the coupling coefficient γ.

We apply classical TRT to a 1-dimensional model of hydrogen in iron where the potential surface is a symmetric double-well potential. By numerically evaluating the Langevin equation we obtain the classical transmission coefficient at a range of temperatures and values of the coupling coefficient. We recover the results predicted by classical TRT and discuss how well the theory fits our system in different regions of (T, γ)-space.

Lastly we present the traditional formulations of quantum TRT. The main example here is Miller's *trace formula* which introduces quantum-dynamical corrections to the transition-state value of the rate obtained via the closed-system dynamics. We briefly discuss approaches to quantum transition-state theory based on *discretised path-integrals*, as they constitute a popular and successful method for including approximate quantum-mechanical effects in TRT.

2.1 Classical transition rate theory

At its very beginning transition rate theory (TRT) was conceived in chemistry as a way to determine the probability of molecular reactions to take place as a function of the activation energy E_b separating reactant and product and the temperature T.

However it was not until the work by Chandler that the so-called *reactive flux* method for computing the classical rate, which is the one of interest here, was formulated [10], [34], [35].

We are now going to derive the central quantity in classical transition rate theory, the classical transition rate k^c, by closely following the presentation in reference [34]. For clarity we are going to restrict the discussion to a 1-dimensional system. Imagine a classical particle of mass m travelling along a potential energy surface in figure 2.1 which we call $V(q)$; for simplicity, in what follows we assume that $V(q)$ is symmetric. We call

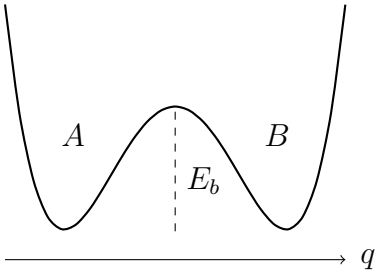


FIGURE 2.1: A 1-dimensional two-state system.

A the "state" associated to the region of space $q < 0$, and B the one associated to $q > 0$. Let $q^* = 0$ be such that $V(q^*)$ is the saddle point of $V(q)$. In TRT, the time evolution of the macroscopic probabilities $n_A(t)$ and $n_B(t)$ is assumed to follow the phenomenological rate equations:

$$\dot{n}_A(t) = k_{AB} n_B(t) - k_{BA} n_A(t) \tag{2.1}$$

$$\dot{n}_B(t) = k_{BA} n_A(t) - k_{AB} n_B(t), \tag{2.2}$$

where the transition rates k_{AB} and k_{BA} give the average frequency of the transitions from state A to state B and from state B to state A respectively. In what follows we deal with one value of the classical transition rate for the two-state system in figure 2.1, which is defined as:

$$k^c = \frac{1}{2}(k_{BA} + k_{AB}). \tag{2.3}$$

We define a microscopic state function $\theta_B(t) = H_B[q(t)]$, which is given by a heaviside step function of the position of the particle $q(t)$, that is it returns 1 when the particle is in state B, identified by the positive q-semiaxis, and returns 0 otherwise.

$$\theta_B(t) = H[q(t)] = 1 \text{ for } q(t) > q^* \tag{2.4}$$

$$= 0 \text{ for } q(t) < q^*; \tag{2.5}$$

the state function relative to state A, on the other hand, is defined as $\theta_A(t) = 1 - \theta_B(t)$. Note that although in what follows we denote the classical state functions as explicit functions of time, they are actually functions of a time-dependent variable, such as $q(t)$.

The state functions can be related to the macroscopic probabilities n_A and n_B of finding

the particle in state A and B respectively; by sampling a large number of initial positions and velocities from a non-equilibrium distribution $f(p_0, q_0)$, where we denote $p(0) = p_0$ and $q(0) = q_0$ for clarity, the probability of finding the particle in state X at time t, with $X = A, B$, is obtained as:

$$n_X(t) = \int_{-\infty}^{\infty} \int_{-\infty}^{\infty} \mathrm{d}p_0 \mathrm{d}q_0 f(p_0, q_0) \theta_X(t), \tag{2.6}$$

where $\theta_X(t)$ depends on time through the trajectory $q(t)$, with $q(t) = q(t; p_0, q_0)$.

The validity of equations (2.1) and (2.2) relies on the existence of two distinct energy scales, one corresponding to the activation energy E_b and one corresponding to the thermal energy $k_B T$. The fundamental assumption of TRT is that these two energy scales are separated, and in particular that:

$$\frac{k_B T}{E_b} \ll 1. \tag{2.7}$$

The numerator in the equation above identifies the thermal energy arising from keeping the system at temperature T, where k_B is the Boltzmann constant [36]. In other words, equation (2.7) states that a trajectory crossing the energy barrier should constitute a *rare event* in comparison to the frequency of its thermal fluctuations. This is a central assumption in transition rate theory; in fact TRT and all the theories derived from it cannot be expected to yield meaningful results whenever $T \geq \frac{E_b}{k_B}$.

The objective of TRT is to predict the value of k^c using the microscopic dynamics of the system, rather than equations (2.1) and (2.2). This can be achieved by employing a central result in non-equilibrium statistical mechanics: Onsager's *regression hypothesis*, which states that the relaxation of a macroscopic variable towards equilibrium and the regression of the corresponding microscopic thermal equilibrium fluctuations follow the same law ([37], [38]). In the present case, the hypothesis can be expressed as [34]:

$$\frac{n_X(t) - \langle n_X \rangle}{n_X(0) - \langle n_X \rangle} = \frac{\langle \delta\theta_X(0) \delta\theta_X(t) \rangle}{\langle [\delta\theta_X(0)]^2 \rangle}, \tag{2.8}$$

where $\langle\rangle$ denotes the canonical ensemble average:

$$\langle g \rangle = \frac{1}{Z} \int_{-\infty}^{\infty} \int_{-\infty}^{\infty} \mathrm{d}p_0 \mathrm{d}q_0 e^{-\beta H(p_0,q_0)} g(p_0, q_0); \tag{2.9}$$

here $H(p_0, q_0)$ is the Hamiltonian of the system, $\beta = (k_b T)^{-1}$ is the inverse temperature and $\delta\theta_X(t) = \theta_X(t) - \langle\theta_X\rangle$ are the microscopic equilibrium fluctuations of the system. We call Z the classical canonical partition function:

$$Z = \int_{-\infty}^{\infty} \int_{-\infty}^{\infty} \mathrm{d}p_0 \mathrm{d}q_0 e^{-\beta H(p_0,q_0)}. \tag{2.10}$$

In equation (2.8), the left-hand-side represents the relaxation of the macroscopic probability to find the particle in state X towards its equilibrium value, while the right-hand-side identifies the autocorrelation of microscopic equilibrium fluctuations taking place in the system. The ensemble average of the product of any two microscopic equilibrium fluctuations at times t_1 and t_2 defines the classical correlation function:

$$\langle \delta\theta_X(t_1)\delta\theta_X(t_2)\rangle = \langle \theta_X(t_1)\theta_X(t_2)\rangle - \langle\theta_X\rangle^2 = C_{\theta_X}(|t_1 - t_2|), \tag{2.11}$$

where the second equality is obtained using the stationarity of the equilibrium ensemble, which implies that $\langle\theta_X(t)\rangle = \langle\theta_X\rangle$.

We are now going to manipulate equation (2.8) in order to obtain a correlation function expression for the transition rate k^c. First we insert the expression for $n_A(t)$ obtained by solving the rate equations:

$$n_A(t) = [n_A(0) - \langle n_A\rangle]e^{-\frac{t}{\tau_r}} + \langle n_A\rangle, \tag{2.12}$$

where we have defined the inverse rate:

$$\tau_r = \frac{1}{k_{BA} + k_{AB}} = \frac{1}{2k^c}. \tag{2.13}$$

This yields:

$$e^{-\frac{t}{\tau_r}} = \frac{\langle\theta_A(0)\theta_A(t)\rangle - \langle\theta_A\rangle^2}{\langle\theta_A^2\rangle - \langle\theta_A\rangle^2}. \tag{2.14}$$

In the denominator of the expression above, we note that because of how the state functions are defined we have that $\langle \theta_X^2 \rangle = \langle \theta_X \rangle$ for $X = A, B$; hence we can re-write equation (2.14) as:

$$e^{-\frac{t}{\tau_r}} = \frac{\langle \theta_A(0)\theta_A(t) \rangle - \langle \theta_A \rangle^2}{\langle \theta_A \rangle \langle \theta_B \rangle}, \tag{2.15}$$

where we have used the fact that $\langle \theta_B \rangle = 1 - \langle \theta_A \rangle$. While the classical transition rate k^c could in principle be computed from equation (2.15), by taking the time derivative of both sides of equation (2.15) we are able to obtain an expression for k^c that is significantly easier to evaluate. We have:

$$-\frac{1}{\tau_r} e^{-\frac{t}{\tau_r}} = \frac{\langle \theta_A(0)\dot{\theta}_A(t) \rangle}{\langle \theta_A \rangle \langle \theta_B \rangle}; \tag{2.16}$$

using the fact that $\langle \dot{\theta}_X(0)\theta_X(t) \rangle = -\langle \theta_X(0)\dot{\theta}_X(t) \rangle$, we rewrite the expression above as:

$$\frac{1}{\tau_r} e^{-\frac{t}{\tau_r}} = \frac{\langle \dot{\theta}_A(0)\theta_A(t) \rangle}{\langle \theta_A \rangle \langle \theta_B \rangle} = -\frac{\langle \dot{q}_0 \delta(q_0 - q^*)\theta_A(t) \rangle}{\langle \theta_A \rangle \langle \theta_B \rangle}, \tag{2.17}$$

where in the last equality we have inserted the time derivative $\dot{\theta}_A(0) = -\dot{q}_0 \delta(q_0 - q^*)$. If we now substitute the definition $\theta_A(t) = 1 - \theta_B(t)$ in equation (2.17), we find:

$$\frac{1}{\tau_r} e^{-\frac{t}{\tau_r}} = \frac{\langle \dot{q}_0 \delta(q_0 - q^*)\theta_B(t) \rangle}{\langle \theta_A \rangle \langle \theta_B \rangle}, \tag{2.18}$$

since the integral in $\langle \dot{q}_0 \delta(q_0 - q^*) \rangle$ vanishes as it involves the product of an even by an odd function of $p_0 = m\dot{q}_0$. Equation (2.18) can be equivalently written as:

$$\frac{1}{\tau_r} e^{-\frac{t}{\tau_r}} = \frac{\langle \dot{\theta}_B(0)\theta_B(t) \rangle}{\langle \theta_A \rangle \langle \theta_B \rangle}, \tag{2.19}$$

or

$$\frac{1}{\tau_r} e^{-\frac{t}{\tau_r}} = \frac{\varrho(t)}{\langle \theta_A \rangle \langle \theta_B \rangle}, \tag{2.20}$$

with the so-called *reactive-flux* correlation function $\varrho(t)$ defined as:

$$\varrho(t) = \langle \dot{\theta}_B(0)\theta_B(t) \rangle = \langle \dot{q}_0 \delta(q_0 - q^*)\theta_B(t) \rangle. \tag{2.21}$$

Hence the classical rate is given by an average flux of trajectories across q^* provided that

the they are found in state B at time t [10]. This can also be seen by considering a more conventional formula for the rate involving an average flux across q^* provided that $q(t) > q^*$, *and* that at an earlier time $-t$, $q(-t) < q^*$. This results in writing the reactive flux as

$$\tilde{\varrho}(t) = \langle \dot{q}_0 \delta(q_0 - q^*) \theta_B(t) \theta_A(-t) \rangle, \tag{2.22}$$

but the difference between the equation above and equation (2.21) is given by:

$$\langle \dot{q}_0 \delta(q_0 - q^*) \theta_B(t) \theta_B(-t) \rangle, \tag{2.23}$$

which is an average flux across the surface $q_0 = q^*$ and vanishes by Liouville's theorem [10]. Hence $\varrho(t)$ and $\tilde{\varrho}(t)$ are identical.

Equation (2.19), following from Onsager's regression hypothesis, tells us that the correlation of $\dot{\theta}_A(0)$ with $\theta_A(t)$ on the right-hand-side, describing the regression of microscopic equilibrium thermal fluctuations, evolves in time following the same decay to zero as the exponential on the left-hand-side, which arises the evolution of the macroscopic probability $n_A(t)$. However, the equalities in (2.19) and (2.20) will not hold on all time scales. If we assume the separartion of time scales encoded in expression (2.7), we can distinguish between two distinct time regimes: a macroscopic time scale τ_r corresponding to the relaxation of the non-equilibrium probabilities $n_X(t)$ to their equilibrium values, and a microscopic time scale τ_{sr}, which relates to the short-time relaxation of the equilibrium thermal fluctuations taking place in the system, described by the quantities $\delta\theta_X$. This reflects the assumption we made with equation (2.7) that two different energy scales co-exists in the system: a much smaller one, given by the thermal energy $k_B T$, and a much larger one, related to the barrier height E_b. Hence for τ_{sr} and τ_r we have:

$$\tau_r \gg \tau_{sr}. \tag{2.24}$$

This idea is not in contradiction with Onsager's hypothesis: it only tells us that the microscopic variables describing our system display two distinct dynamical behaviours that can be appreciated depending on whether we choose to study the system's correlations over a short or a longer time range. On the longer time scale, τ_r, the short-time

behaviour cannot be resolved and the fluctuations of $\delta\theta_X$ decay on average like $n_X(t)$. On the shorter time scale, τ_{sr}, the regression of the microscopic system fluctuations may not be characterised by the exponential law prescribed by Onsager's hypothesis. In other words we can say that Onsager's law is observed upon "coarse-graining" the dynamics of the system in time.

While equations (2.19) or (2.20) could in principle be used to obtain the rate constant, we saw that this quantity is meaningful only when the fundamental assumption of TRT is valid, that is when we do have the separation of time scales expressed in equation (2.24). For times t such that:

$$\tau_{sr} < t \ll \tau_r, \tag{2.25}$$

the exponential in equation (2.19) is approximately equal to 1. That is, on these intermediate time scales the function $\varrho(t)$ in equation (2.21) is approximately a constant, *i.e.* it exhibits a "plateau" value, which we associate with the rate constant k^c via:

$$k^c = \frac{k_{AB} + k_{BA}}{2} = \frac{\langle \dot{\theta}_B(0)\theta_B(t_{pl})\rangle}{2\langle\theta_A\rangle\langle\theta_B\rangle}. \tag{2.26}$$

The detailed balance condition associated to the rate equations (2.1) and (2.2) states that

$$k_{BA} = \frac{\langle n_B\rangle}{\langle n_A\rangle} k_{AB}. \tag{2.27}$$

By substituting this expression into equation (2.20), and using the fact that

$$\langle\theta_X\rangle = \frac{\langle n_X\rangle}{\langle n_A\rangle + \langle n_B\rangle}, \tag{2.28}$$

we obtain the following expressions for the rates:

$$k_{BA} = \frac{1}{\langle\theta_A\rangle}\langle\dot{\theta}_B(0)\theta_B(t_{pl})\rangle = \frac{\varrho(t_{pl})}{\langle\theta_A\rangle}, \tag{2.29}$$

and

$$k_{AB} = \frac{1}{\langle\theta_B\rangle}\langle\dot{\theta}_B(0)\theta_B(t_{pl})\rangle = \frac{\varrho(t_{pl})}{\langle\theta_B\rangle}. \tag{2.30}$$

Here t_{pl} denotes a time at which the value of $\varrho(t)$ is in the plateau region. Overall, using the fact that in a symmetric system $\langle\theta_A\rangle = \langle\theta_B\rangle$, we have:

$$k^c = \frac{1}{\langle\theta^c\rangle}\langle\dot{\theta}^c(0)\theta^c(t_{pl})\rangle = \frac{\varrho(t_{pl})}{\langle\theta^c\rangle}, \tag{2.31}$$

where we have introduced the notation $\theta^c = \theta_B = 1 - \theta_A$.

We can further consider the time dependent quantity on the right-hand-side of equation (2.31) for times both inside and outside the plateau region. We will refer to this as the time-dependent transition rate $k^c(t)$ in what follows:

$$k^c(t) = \frac{\varrho(t)}{\langle\theta^c\rangle} = \frac{1}{\langle\theta^c\rangle}\langle\dot{\theta}^c(0)\theta^c(t)\rangle. \tag{2.32}$$

Often in the literature the classical rate is colloquially defined in terms of the limit of $\varrho(t)$ for $t \to \infty$, and in such cases $\varrho(t)$ is called classical *flux-side* correlation function, $c^c_{fs}(t)$ [39]. While identifying the long-time beahviour of $\varrho(t)$ with the rate is a widely used convention in certain areas of the literature, it is important to note that even if one assumes the separartion of time scales that allows to derive k^c from $\varrho(t)$ *a priori*, strictly speaking $\lim_{t\to\infty}\varrho(t) = 0$ and the expression has to be interpreted as the limit for long but finite times.

Equation (2.32) allows us to introduce a widely used approximation for the classical transition rate, known as the *transition-state theory* (TST) value, k^c_{TS}. This is obtained as the short-time limit of the $k^c(t)$:

$$k^c_{TS} = \lim_{t\to 0^+} k^c(t). \tag{2.33}$$

The TST value approximates the rate constant given by TRT under the assumption that the trajectory does not recross the dividing surface, and, as we will see later, it follows that $k^c_{TS} \geq k^c(t)$. A schematic representation of the behaviour expected from $k^c(t)$ according to the theory presented above is given in figure 2.2. Here we see that as $t \to 0^+$ the rate k^c equals its TST approximation k^c_{TS}. For small times $t \approx \tau_{sr}$ we are able to observe the relaxation of microscopic equilibrium fluctuations taking place in the

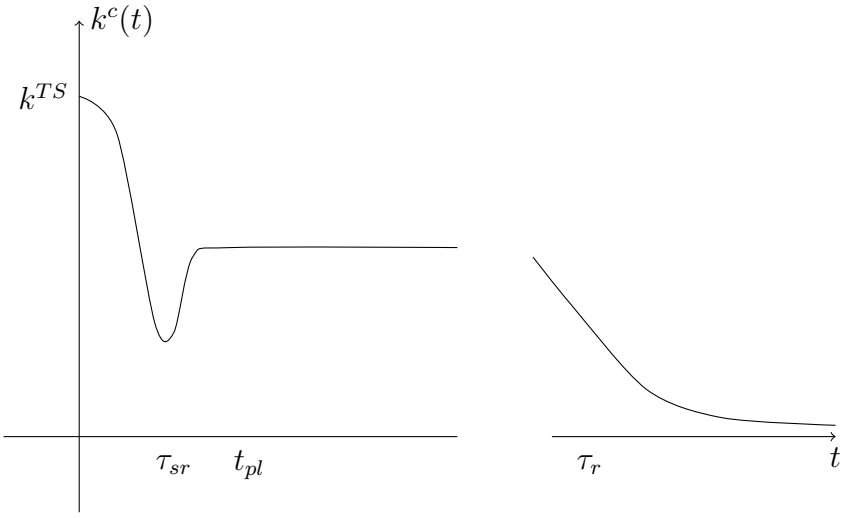


FIGURE 2.2: Expected time dependence of the classical transition rate $k^c(t)$ in equation (2.32).

system, which do not follow an exponential decay. As $t \approx t_{pl}$, $k^c(t)$ reaches a plateau value, which is associated to the true transition rate k^c. On longer time scales τ_r, we have the exponential decay prescribed by Onsager's regression hypothesis.

We are now going to obtain a more explicit expression for k^c_{TS} for the case of the 1-dimensional Hamiltonian $H(p_0, q_0) = \frac{p_0^2}{2m} + V(q_0) = K(p_0) + V(q_0)$. The time correlation function in equation (2.32) can be written as:

$$k^c(t) = \frac{1}{Z\langle\theta^c\rangle}\int_{-\infty}^{\infty} \mathrm{d}p_0 \int_{-\infty}^{\infty} \mathrm{d}q_0 \frac{p_0}{m}\delta(q_0 - q^*)\theta^c(t)e^{-\beta H(p_0,q_0)}; \tag{2.34}$$

for the short-time limit of equation (2.32) we have:

$$\begin{aligned}\lim_{t\to 0^+} \varrho(t) &= \int_{-\infty}^{\infty} \mathrm{d}p_0 p_0 H[\dot{q}(0)]e^{-\beta K(p_0)} \int_{-\infty}^{\infty} \mathrm{d}q_0 \delta(q_0 - q^*)e^{-\beta V(q_0)} \\ &= \frac{1}{m}\int_0^{\infty} \mathrm{d}p_0 p_0 e^{-\beta K(p_0)}e^{-\beta V(q^*)},\end{aligned} \tag{2.35}$$

where we have used the fact that $\lim_{t\to 0}\theta_B(t) = \lim_{t\to 0} H[q(t)] = H[\dot{q}(t)]$ [10]. The denominator of equation (2.32) can be simplified as follows:

$$\langle\theta^c\rangle Z = \frac{1}{Z}\int_{-\infty}^{\infty}\int_{-\infty}^{\infty} \mathrm{d}p_0\mathrm{d}q_0\theta^c(0)e^{-\beta H(p_0,q_0)}Z = \int_{-\infty}^{\infty}\mathrm{d}p_0\int_0^{\infty}\mathrm{d}q_0 e^{-\beta H(p_0,q_0)} = Z_+. \tag{2.36}$$

Overall we thus find:

$$k_{TS}^{c} = \frac{1}{m} \frac{\int_0^\infty \mathrm{d}p_0 p_0 e^{-\beta K(p_0)}}{\int_{-\infty}^\infty \mathrm{d}p_0 e^{-\beta K(p_0)}} \frac{e^{-\beta V(q^*)}}{\int_0^\infty \mathrm{d}q_0 e^{-\beta V(q_0)}}. \tag{2.37}$$

The second factor in the expression above is the average over positive momenta of the momentum p_0, which can be easily computed as

$$\langle p_0 \rangle_{p_0^+} = \frac{\int_0^\infty \mathrm{d}p_0 p_0 e^{-\beta \frac{p_0^2}{2m}}}{\int_{-\infty}^\infty \mathrm{d}p_0 e^{-\beta \frac{p_0^2}{2m}}} = \sqrt{\frac{m}{2\pi\beta}}. \tag{2.38}$$

Therefore for the transition-state approximation of the classical rate we find:

$$k_{TS}^{c} = \frac{1}{\sqrt{2\pi m\beta}} \frac{e^{-\beta V(q^*)}}{\int_0^\infty \mathrm{d}q_0 e^{-\beta V(q_0)}}, \tag{2.39}$$

which can be expressed as a ratio of partition functions:

$$k_{TS}^{c} = \langle v \rangle \frac{Z^\ddagger}{Z_+}, \tag{2.40}$$

where we have introduced:

$$Z^\ddagger = \int_{-\infty}^\infty \int_{-\infty}^\infty \mathrm{d}p_0 \mathrm{d}q_0 \delta(q_0 - q^*) e^{-\beta H(p,q_0)}, \tag{2.41}$$

and the velocity factor $\langle v \rangle$ is defined as:

$$\langle v \rangle = \frac{1}{m} \langle p_0 \rangle_{p_0^+}. \tag{2.42}$$

Thus, while the calculation of k^c relies on the knowledge of the microscopic dynamics of the system, its TST approximation solely relies on equilibrium-statistical information about the system, making it a useful tool for obtaining an upper bound for the transition rate at a fraction of the difficulty and the computational cost.

In order to distinguish between time-independent and time-dependent contributions to

the transition rate it is common practice in this field to introduce the so-called *transmission coefficient* $\kappa^c(t)$ and write the "full", time-dependent transition rate as

$$k^c(t) = \kappa^c(t) k^c_{TS}, \tag{2.43}$$

where the TST factor k^c_{TS} is defined as above. In terms of trajectories crossing the energy barrier E_b, the transmission coefficient is related to the fraction of trajectories that successfully cross from the dividing point into the final state, while the TST approximation is a rate expression that assumes *all* trajectories successfully cross from the dividing point into the final state, or in other words, that no recrossings of the dividing point are taking place.

While a large amount of literature in the field of classical and quantum-mechanical TRT is concerned with defining and computing the TST approximation to the transition rate, the focus of this thesis is on the transmission coefficient $\kappa^c(t)$. Clearly k^c_{TS} is a quantity that offers a computational advantage over $\kappa^c(t)$, as stressed above, however three points should be apparent: *i*) the TST rate is only an approximation to the true rate k^c; *ii*) if it exists, k^c can only be calculated by including the dynamical information encoded in $\kappa^c(t)$; *iii*) only by looking at the evolution of the transmission coefficient are we able to determine whether the system we study allows for transition rate theory to be applied at all.

The formulation we adopt is the so-called *path-sampling* expression for $\kappa^c(t)$, which was first derived by Chandler ([31]) and we shall briefly outline in what follows. Firstly use the fact that $\kappa^c(t) k^c_{TS} = \frac{\varrho(t)}{\langle \theta^c \rangle}$, that is:

$$\kappa^c(t) = \frac{1}{k^c_{TS}} \frac{\varrho(t)}{\langle \theta^c \rangle}. \tag{2.44}$$

Let us write out the reactive flux $\varrho(t)$ explicitly for our 1-dimensional system:

$$\begin{aligned}
\varrho(t) &= \langle \dot{q_0}\delta(q_0 - q^*)\theta^c[q_t]\rangle && (2.45)\\
&= \frac{1}{Z}\int_{-\infty}^{\infty} \mathrm{d}p_0 e^{-\beta\frac{p_0^2}{2m}}\frac{p_0}{m}\int_{-\infty}^{\infty}\mathrm{d}q_0 e^{-\beta V(q_0)}\delta(q_0 - q^*)\theta^c(t) && (2.46)\\
&= \frac{1}{Z}e^{-\beta V(q^*)}\int_{-\infty}^{\infty}\mathrm{d}p_0 e^{-\beta\frac{p_0^2}{2m}}\frac{p_0}{m}\theta^c(t)|_{q_0=q^*}. && (2.47)
\end{aligned}$$

By inserting equations (2.39) and (2.47) into equation (2.44) we find:

$$\kappa^c(t) = \sqrt{\frac{2\pi\beta}{m}}\frac{\int_{-\infty}^{\infty}\mathrm{d}p_0 e^{-\beta\frac{p_0^2}{2m}}p_0\theta^c(t)|_{q_0=q^*}}{\int_{-\infty}^{\infty}\mathrm{d}p_0 e^{-\beta\frac{p_0^2}{2m}}} = \frac{1}{\langle p_0\rangle_{p_0^+}}\langle p_0\theta^c(t)|_{q_0=q^*}\rangle_{p_0}. \qquad (2.48)$$

This is the ratio of the expectation value of the initial momentum of those trajectories that are in state B at time t, and that of those that crossed the energy barrier at time zero.

From equation (2.48) we see that $\kappa^c(t)$ is strictly bounded by -1 and 1: when all trajectories starting at $q^* = 0$ with a positive momentum are in $q > 0$ at time t the numerator reaches its maximum value, and it equals the denominator. On the other hand, when all trajectories found in the positive q-semiaxis at time t had a negative momentum at time zero, the numerator equals the demoninator, multiplied by -1. It follows that for the TST rate in equation (2.43) we must have:

$$k^c \leq k^c_{TS}. \qquad (2.49)$$

Moreover we see that the long-time limit of $\kappa^c(t)$ is zero, because in this case the configuration of the system at time t is uncorrelated to that at time zero, and the numerator reduces to an average over initial momenta, which is an integral from $-\infty$ to ∞ of an even by an odd function.

There is also a computational advantage in evaluating the transition rate via equation (2.48) as opposed to computing the canonical average in equation (2.45): in practice, one would invoke the ergodic assumption and write the phase space average as an intergal over time, which yields the same result as the average over p_0 and q_0 provided that

one considers times long enough to observe a large number of transitions. Because of the rare-event assumption underlying the calculation of transition rates this approach proves very costly. With the path-sampling method, on the other hand, we focus only on the region of time for which there are transitions. Because knowledge of microsopic temperature-dependent dynamics is central to the calculation of $\kappa^c(t)$ we are going to discuss open classical dynamics in the next section.

2.2 Activated processes and open classical dynamics: Langevin equation

We have seen in the previous section that a central aspect to transition rate theory is that the system under investigation undergoes *activated processes*. By this we mean that the rare events mentioned above which bring the system from one metastable state to another through an energy barrier, or activated state, require energy to be provided to the particle by its surrounding, and removed from the particle by its surrounding. From now on we call "system" the ensemble given by the particle and its surrounding, or environment. We think of this environment as a bath of (classical) degrees of freedom to which the particle is coupled, thus generating the energy fluctuations necessary for the reaction coordinate to be activated and de-activated. It is therefore clear that if we are interested in studying the dynamics of the particle alone, as required to compute the classical transmission coefficient in the reactive-flux approach outlined above, such classical dynamics will be open or non-Hamiltonian.

Here we consider the following: a particle of mass m in a 1-dimensional potential $V(q)$ coupled to a heat bath of harmonic oscillators. Under certain approximations this is described by the Langevin equation [40]:

$$\dot{q} = \frac{1}{m}p \tag{2.50}$$

$$\dot{p} = -V_q(q) - \frac{1}{m}\gamma p + \xi(t), \tag{2.51}$$

where $\xi(t)$ is a stochastic force acting on the particle at each time t, and $V_q(q) = \mathrm{d}V(q)/\mathrm{d}q$. The well-known case of Brownian motion for which the Langevin equation was originally introduced ([41]), is given by the equations above with $V_q = 0$. A detailed derivation of the classical Langevin equation is presented in appendix A.

The random force in the Langevin equation arises from a fully deterministic equation involving the intial conditions for the bath's degress of freedom by means of a coarse-graining procedure – see appendix A for details. In the Langevin picture we choose not to include the details of the dynamics of the bath but only the average effect such dynamics has on the coordinates of interest, resulting in the definition of a random process $\xi(t)$ whose average properties are designed to capture the overall behaviour of the heat bath [42]. In the case of interest to us ξ is assumed to be memory-less, *i.e.* Markovian, and characterised by a Gaussian distribution, which implies that its moments obey

$$\langle \xi(t) \rangle = 0 \qquad \text{and} \tag{2.52}$$

$$\langle \xi(t)\xi(t') \rangle = \lambda \delta(t - t'). \tag{2.53}$$

The Langevin equation (2.50)-(2.51) with average properties for $\xi(t)$ given by equations (2.52)-(2.53) generates the dynamics of a system in thermal contact with a heat bath at temperature T, which makes it an effective way to study thermally activated processes such as TRT. If k_B is the Boltzmann constant and T is the bath's temperature, by the fluctuation-dissipation theorem the above implies that $\lambda = \sqrt{2\gamma k_B T}$, hence in Langevin dynamics it is not possible to uniquely interpret γ as a damping coefficient in that the strength of the random "kicks" the particle receives at each time steps is proportional to both T and γ [40].

While the Langevin equation describes the stochastic dynamics of single temperature-dependent trajectories, one can alternatively introduce a classical phase space density whose dynamics describes the evolution of an ensemble of temperature-dependent trajectories in terms of a deterministic equation of motion, known as the Fokker-Planck equation. We now derive the Fokker-Planck equation associated to the Langevin equation (2.50)-(2.51). Let us firstly consider a simplified expression for equations (2.50) and

(2.51):

$$\dot{y} = u(y) + \xi(t), \tag{2.54}$$

where $y = (p, q)$ is the phase space vector and u is a function of the phase space coordinates. We consider a phase space density $f(y, t)$ which is normalised at all times:

$$\int_{-\infty}^{\infty} \mathrm{d}y f(y, t) = 1. \tag{2.55}$$

In analogy with other cases where a density such as $f(y, t)$ obeys the conservation law above, we expect the time derivative of the density to be equal to the divergence of a flux – examples where this is the case are the continuity equations in electromagnetism and fluid dynamics, and the law of conservation of energy. Hence we write:

$$\dot{f} + \frac{\partial}{\partial y}(\dot{y}f) = 0, \tag{2.56}$$

where we sue the notation $\dot{f} = \frac{\partial f}{\partial t}$. By inserting equation (2.54) into this we find

$$\dot{f} = -\frac{\partial}{\partial y}\left[u(y)f(y, t) + \xi(t)f(y, t)\right], \tag{2.57}$$

which, if we define $\mathcal{L}\Phi = \partial_y[u(y)\Phi]$, can also be expressed as:

$$\dot{f} = -\mathcal{L}f - \frac{\partial}{\partial y}\left[\xi(t)f\right]. \tag{2.58}$$

By integrating equation (2.58) over time we obtain [40]:

$$f(y, t) = e^{-t\mathcal{L}}f(y, 0) - \int_0^t \mathrm{d}s e^{-(t-s)\mathcal{L}} \frac{\partial}{\partial y}\left[\xi(s)f(y, s)\right]. \tag{2.59}$$

We insert equation (2.59) into (2.58) to find:

$$\dot{f}(y, t) = -\mathcal{L}f(y, t) - \frac{\partial}{\partial y}\left[\xi(t)f(y, 0)\right] + \frac{\partial}{\partial y}\xi(t) \int_0^t \mathrm{d}s e^{-(t-s)\mathcal{L}} \frac{\partial}{\partial y}\left[\xi(s)f(y, s)\right]. \tag{2.60}$$

If the noise $\xi(t)$ satisfies the properties given by equations (2.52) and (2.53) upon taking the average over ξ (indicated by the symbol $\langle\ \rangle_\xi$) we obtain [40]:

$$\frac{\partial}{\partial t}\langle f(y,t)\rangle_\xi = -\frac{\partial}{\partial y}\left[u(y)\langle f(y,t)\rangle_\xi\right] + \lambda\frac{\partial^2}{\partial y^2}\langle f(y,t)\rangle_\xi; \tag{2.61}$$

for the Langevin equation (2.50)-(2.51) this implies:

$$\dot{f} = -\frac{\partial}{\partial q}\left(\frac{p}{m}f\right) - \frac{\partial}{\partial p}\left[-V_q(q) - \gamma\frac{p}{m}\right]f + \lambda\frac{\partial^2 f}{\partial p^2}. \tag{2.62}$$

In summary, open classical dynamics can be described either by means of a stochastic equation which determines the evolution of a single trajectory (here the Langevin equation), or alternatively by means of a linear deterministic equation which describes the dynamics of a phase space distribution (here the Fokker-Planck equation). Note that while one could in principle use the Fokker-Planck equation to compute the classical transition rate instead of the Langevin equation, this would not offer any computational advantage. In chapter 3 we will see that such dual description is mirrored in open quantum dynamics, with a type of stochastic Schrödinger equation and its corresponding Lindblad equation for the density operator. In the next section we apply Langevin dynamics to the study classical transition rate theory.

2.3 Classical TRT in a 1-d double-well system

Here we study classical transition rate theory applied to a 1-dimensional symmetric double-well system, using open classical dynamics based on the Langevin equation. A plot of the potential used is given in figure 2.3. We define a system of dimensionless units in which the mass of the particle equals 1, the distance between potential minima is 2, the height of the energy barrier is $\frac{3}{4}$, and the Boltzmann constant equals 1. For more details on the units of measure used, see appendix B. All our numerical investigations are meant to model a system given by a hydrogen atom moving in a 1-d potential compatible with an iron lattice. This leads to the natural units of time being 8.016×10^{-2} ps. The dividing point is located at $q^* = 0$, and the particle coupled to a heat bath at temperature T

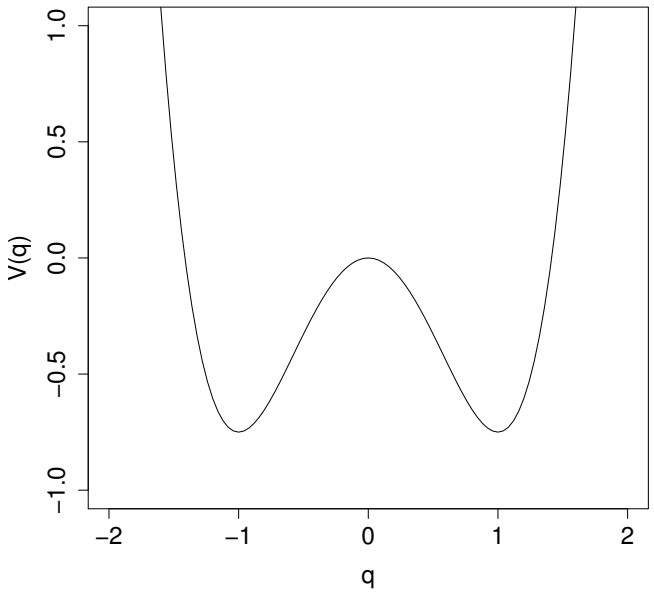


FIGURE 2.3: Schematic representation of the potential used in the classical simulations. Both q and $V(q)$ are represented in dimensionless units.

evolves according to the Langevin dynamics, which we write here by expressing equations (2.50) and (2.51) in differential form:

$$\mathrm{d}q_t = \frac{1}{m} p_t \mathrm{d}t \tag{2.63}$$

$$\mathrm{d}p_t = -V_q(q_t)\mathrm{d}t - \gamma p_t \mathrm{d}t + \lambda \mathrm{d}w_t, \tag{2.64}$$

where the notation x_t indicates the value taken by the variable x at time t, V_q as before indicates the derivative of V with respect to q and $\mathrm{d}w$ indicates a Wiener process such that:

$$w_t = \int_0^t \mathrm{d}s \xi_s, \tag{2.65}$$

and ξ has the average properties given in equations (2.52) and (2.53). We also have that $\lambda = \sqrt{2\gamma k_b T}$. The stochastic differential equations above can be evaluated numerically by means of a modified version of the Verlet algorithm ([43]), which we present in appendix C.

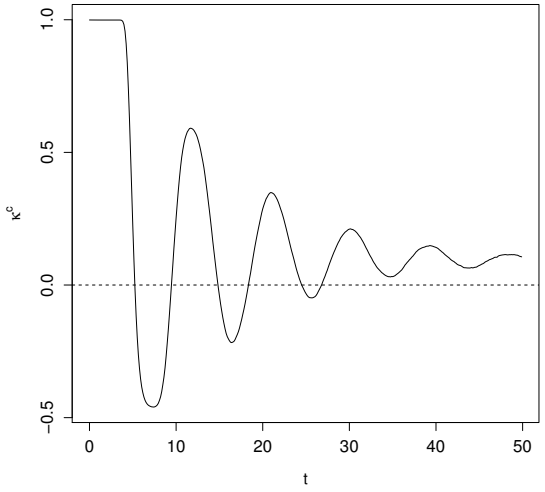
We are then able to compute the transmission coefficient κ^c given in equation (2.48). Numerically, this is obtained by computing the finite sum:

$$\kappa^c_K(t) = \frac{1}{K}\sqrt{\frac{2\pi\beta}{m}}\sum_{j=0}^{K} p_0^j \theta^c(q_t^j)|_{q_0^j=q^*}, \tag{2.66}$$

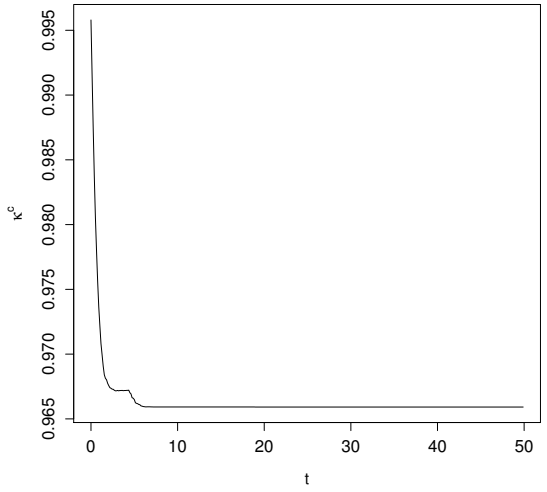
where $\{p_0^1, ...p_0^K\}$ are sampled from a Boltzmann distribution, and K is chosen sufficiently large for the sum to converge. In practice, because this is actually a double average, in the sense that we need both a large number of initial momenta to sample from and a large number of stochastic realisations of the dynamics, the values of K we use tend to be quite large, of the order of 10^4.

We are now going to present some numerical simulations of the classical transmission coefficient and the associated open classical trajectories using the methodology outlined above. Recall that a separation of time scales $k_BT \ll E_b$ is required for transition rate theory to be applicable. With $E_b = \frac{3}{4} = 0.75$ in our system of units, we have three broad temperature regions: low temperatures around $T = 0.01$; medium temperatures around $T = 0.1$; and we consider two high-temperature examples, $T = 0.25$ and $T = 0.5$. When $k_BT \gtrsim E_b$ we know that the separation of time scales required by TRT does not hold and therefore we cannot define a transition rate. For each temperature considered we use a few different values of γ. The advantage of using a system of dimensionless units is that our results would still apply to a different system, simply with rescaled time scales and rescaled values of T and γ.

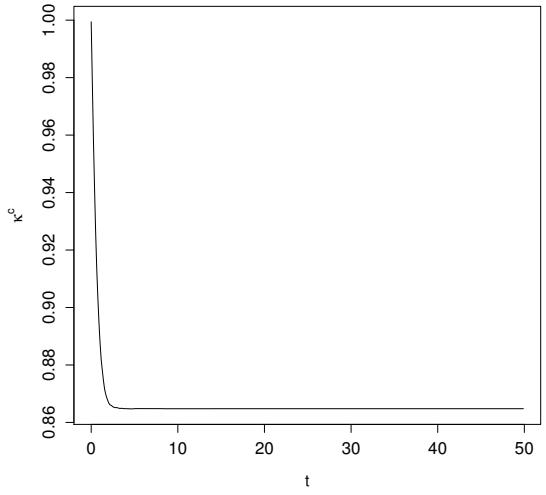
In figure 2.4 we show $\kappa^c(t)$ computed for a low value of the temperature, $T = 0.01$, and three different values of the coupling coefficient γ: 0.001, 0.1 and 0.5. In all following examples we observe that $\kappa^c(t)$ indeed has value 1 at $t = 0$, as it follows from equation (2.43) and the definition of k^{TS} given in equation (2.33). When $T = 0.01$ and $\gamma = 0.001$, shown in figure 2.4a, no plateau is reached within the duration of the simulation of 50 units of time. However the figure suggests that over a longer period of time the short-time fluctuations will relax giving rise to a plateau, which is indeed the case as can be verified by running the same simulation for over 200 units of time, the result of which is shown in figure 2.5. This can be interpreted by considering that when the temperature is very low and so is the coupling to the heat bath, regular oscillations about the potential



(A) $T = 0.01$, γ=0.001



(B) $T = 0.01$, γ=0.1



(C) $T = 0.01$, γ=0.5

FIGURE 2.4: Classical transmission coefficient κ^c computed via equation (2.48) and the numerical scheme in equations (C.1) and (C.2), for $T = 0.01$ and different values of γ.

minima contribute significantly to the overall dynamics, giving rise to the oscillatory behaviour shown by the correlation function in the figure. The trajectories in figure 2.6 show precisely this behaviour, with frequent transitions over the barrier, followed by prolonged trapping in either metastable state characterised by wide oscillations near the minimum. The rare events where a trajectory is kicked strongly enough to cross over the energy barrier from a metastable state give rise to the plateau at longer times. Because of the frequent intial recrossing of the dividing point the value of the plateau in $\kappa^c(t)$ is

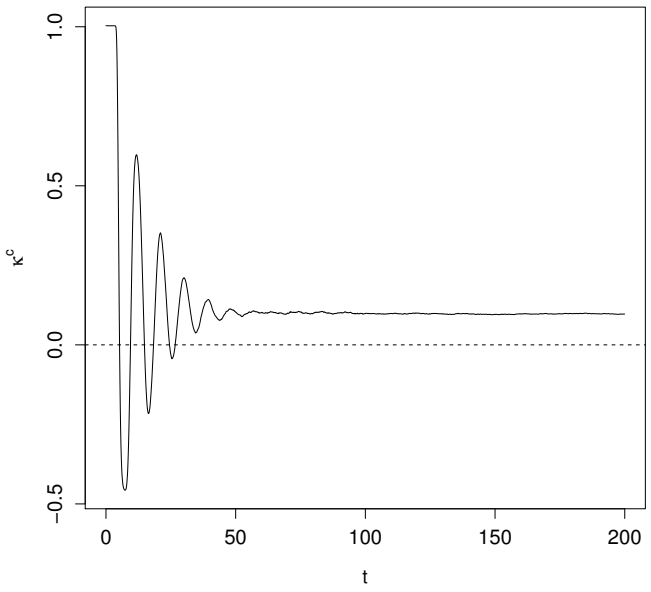
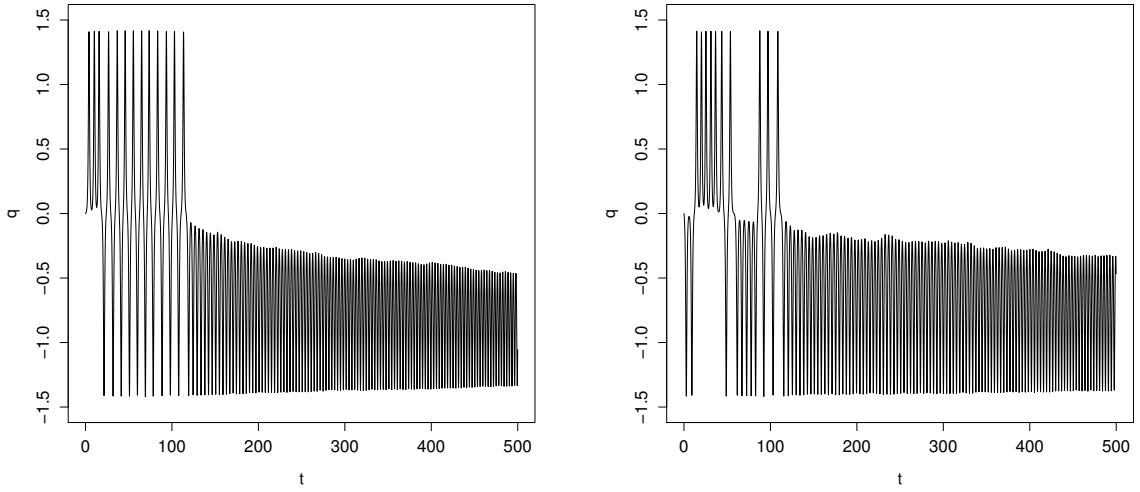


FIGURE 2.5: $T = 0.01$ and $\gamma = 0.001$. Longer simulation (200 units of time) of the classical transmission coefficient shown in figure 2.4a.

rather small, below 0.25.

By raising the value of the coupling coefficient to $\gamma = 0.1$ we find a radically different behaviour, with a well-defined "plateau" at $\kappa^c(t_{pl}) \approx 0.965$. A value of the plateau so close to 1 suggests that this regime would be optimal for approximating the classical rate k^c with its TST version, k^{TS}; from the point of view of the dynamics, we are in a region of (T, γ)-space where very few recrossings of the energy barrier take place. In figure 2.7 we show the associated trajectories. We see that with the temperature very low and the coupling coefficient not so low, the trajectories get trapped very quickly into the potential minima and remain there for long times; additionally the oscillations taking place at the metastable states have a very small amplitude: this explains why figure 2.4b featured almost no short-time fluctuations and a high plateau.

When $T = 0.01$ and $\gamma = 0.5$ dimensionless units (2.4c) we have a similar scenario: the plateau associated to k^c is reached very quickly, with $t_{pl} \approx 5$, and $\kappa^c(t)$ shows no short-time fluctuations. As before, the type of dynamics we expect to be associated with this behaviour for $\kappa^c(t)$ is one where the trajectory gets trapped for very long periods of time in the metastable states due to the low temperature, thus making transitions over

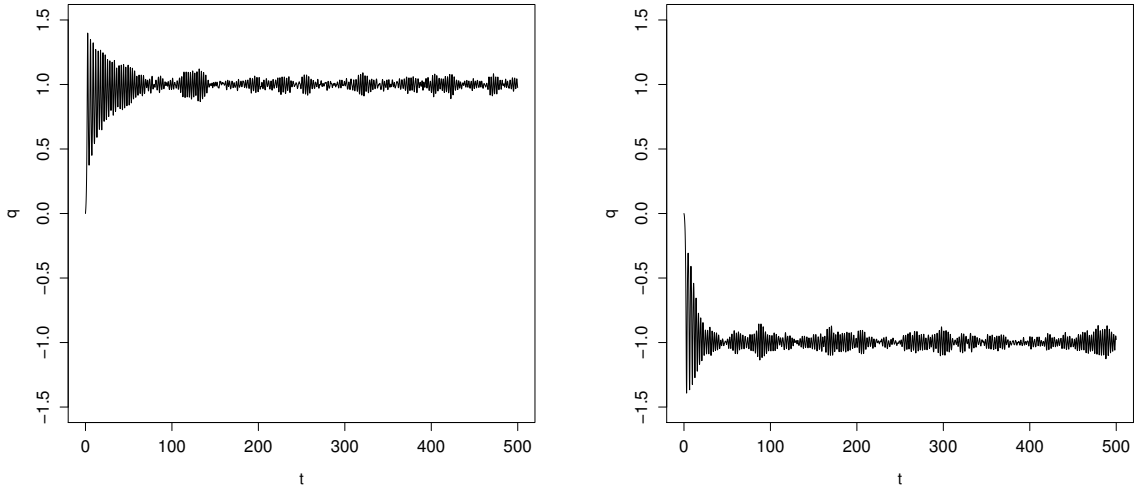


(A) (B)

FIGURE 2.6: $T = 0.01$ and $\gamma = 0.001$. Two stochastic realisations of the dynamics corresponding to the classical transmission coefficient in figure 2.4a. Obtained by integrating the classical equations of motion (2.63) and (2.64) using the numerical scheme in equations (C.1) and (C.2).

the barrier truly rare events, but also, due to the high coupling to the heat bath, the harmonic oscillations about the minima are strongly damped and do not generate visible short-time relaxations in the time correlation function. This is precisely what we find in figure 2.8, showing the trajactories associated with the rate in figure 2.4c. However we note that with $\gamma = 0.5$ the transmission coefficient reaches a plateau whose value is smaller than that we had with $\gamma = 0.1$, which can be explained by recalling that γ regulates both the damping and the strength of the random "kicks" the particle is subject to as it evolves.

In figure 2.9 we show the classical transmission coefficient $\kappa^c(t)$ computed for a medium value of the temperature, $T = 0.1$, and three different values of the coupling coefficient γ: 0.01, 0.1 and 0.5. In figure 2.9a, where $T = 0.1$ and $\gamma = 0.01$, we have an example where the system's short-time relaxations are visible and bring about oscillations in $\kappa^c(t)$ up until about $\tau_{sr} \approx 30$ dimensionless units, after which a highly oscillatory plateau-like region is observed. As in the case of figure 2.4a, we expect the corresponding classical dynamics to feature ample oscillations about the minima and to display trapping only after fairly long periods of time. This is the type of behaviour we can associate with low

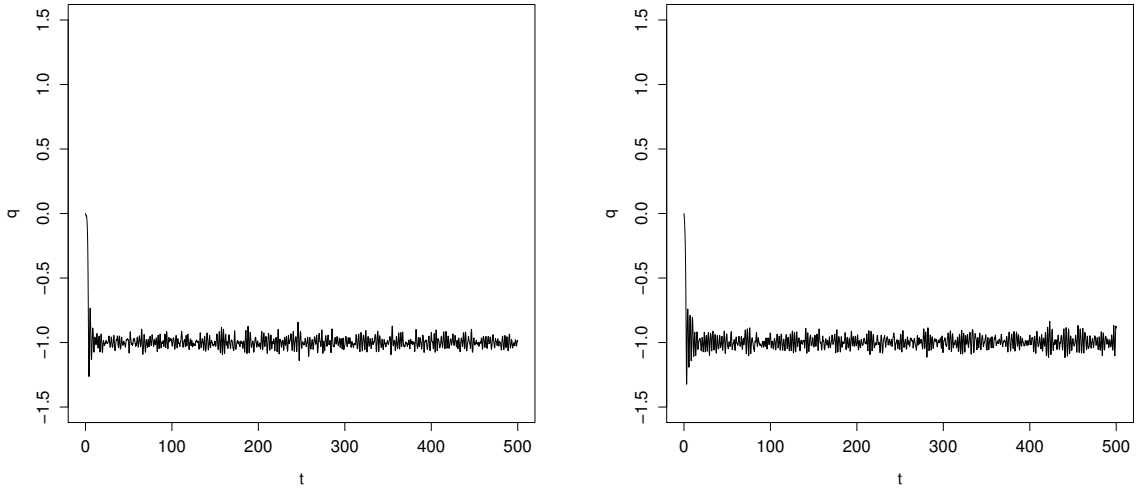


(A) (B)

FIGURE 2.7: $T = 0.01$ and $\gamma = 0.1$. Two stochastic realisations of the dynamics corresponding to the classical transmission coefficient in figure 2.4b. Obtained by integrating the classical equations of motion (2.63) and (2.64) using the numerical scheme in equations (C.1) and (C.2).

and very low γ-regimes. Figure 2.10 show that the combination $(T, \gamma) = (0.1, 0.01)$ can give rise to slightly different types of classical dynamics: in our first stochastic realisation, figure 2.10a, the trajectory oscillates across the barrier up until $t \approx 200$ units, when it is trapped; on the other hand in figure 2.10b we see that the trajectory is trapped almost immediately. In both cases the oscillations about the metastable states are quite wide, suggesting that the corresponding time correlation function features a visible short-time relaxation, which is what we find in figure 2.9a. The fact that in these trajectories trapping takes place but possibly after long periods of time matches with the beahviour of $\kappa^c(t)$, which only displays a plateau at $t_{pl} \approx 35$ units of time.

An example with $T = \gamma = 0.1$ is shown in figure 2.9b. In comparison to figures 2.4b and 2.4c, by raising the temperature we obtain an analogous behaviour of the time correlation function, which shows a plateau as before, but we also find an initial short-time relaxation, with $\tau_{sr} \approx 10$ units of time. With $T = \gamma = 0.1$ the relatively high temperature tends to activate trajectories over the energy barrier, while the relatively high coupling does not allow transitions to take place too often. However we notice that the plateau in this case decays more rapidly than we saw with $T = 0.01$ and $\gamma = 0.1$

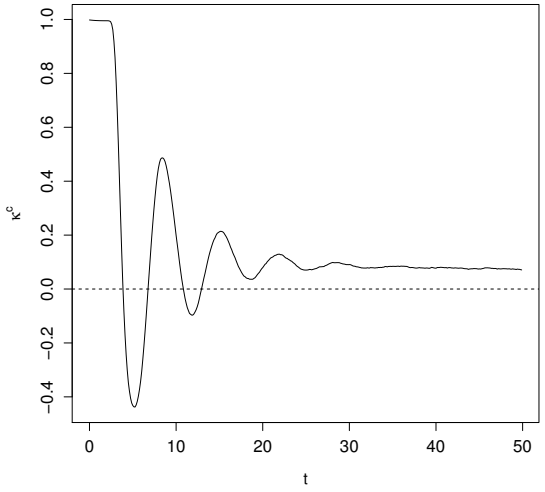


(A) (B)

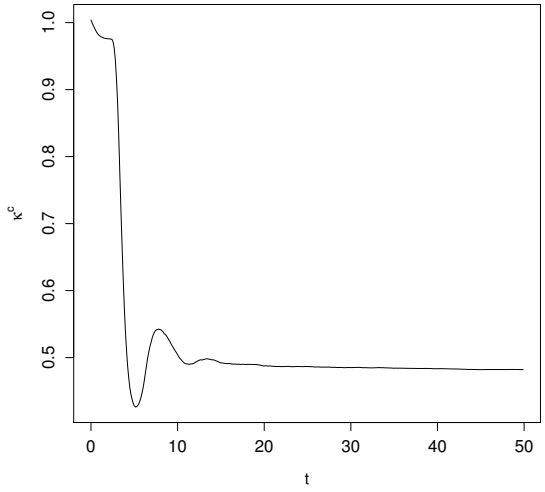
FIGURE 2.8: $T = 0.01$ and $\gamma = 0.5$. Two stochastic realisations of the dynamics corresponding to the classical transmission coefficient in figure 2.4c. Obtained by integrating the classical equations of motion (2.63) and (2.64) using the numerical scheme in equations (C.1) and (C.2).

or $\gamma = 0.5$, suggesting that transitions take place more often in this case than they do when $T = 0.01$. It is also interesting to notice that because the plateaus we found in figures 2.4b and 2.4c correspond to a higher value of $\kappa^c(t)$ than in the case of figure 2.9b, we can conclude that in the present case the TST approximation to the true rate is less accurate and we expect the corresponding dynamics to feature more recrossings over the energy barrier. If we look at the dynamics at $T = \gamma = 0.1$, shown in figures 2.11, we observe trajectories that are trapped in one of the metastable states and stay trapped for over 500 units of time, while performing oscillations about the minimum, which fits with the behaviour we find for $\kappa^c(t)$.

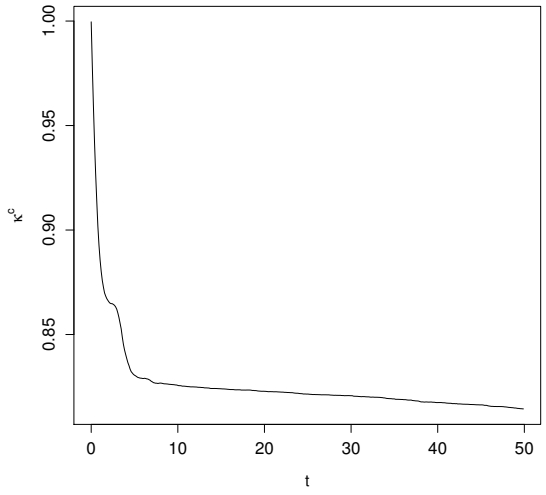
When $T = 0.1$ and $\gamma = 0.5$ as in figure 2.9c, we no longer have a flat "plateau": here, similarly to the case of figure 2.9b, we expect the trajectories to get trapped due to the high coupling coefficient, but also to get activated over the barrier fairly often due to the relatively high temperature. However the comparison with the plot in figure 2.9b also allows us to appreciate a feature of our model based on the Langevin dynamics: it is not possible to uniquely interpret γ as a damping in that the strength of the random "kicks" the particle receives at each time steps is proportional to both T and γ, as we saw in



(A) $T = 0.1$, γ=0.01



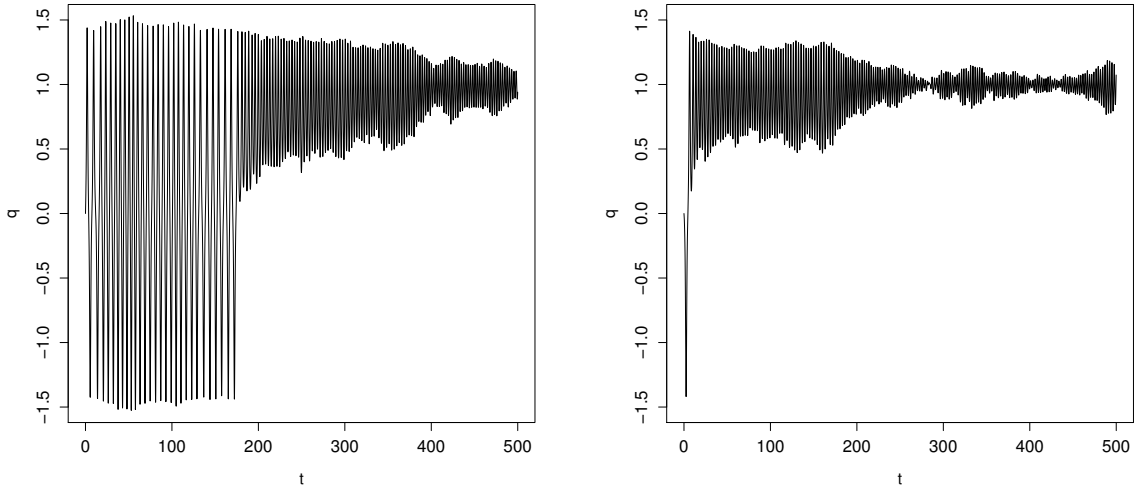
(B) $T = \gamma = 0.1$



(C) $T = 0.1$, γ=0.5

FIGURE 2.9: Classical transmission coefficient κ^c computed via equation (2.48) and the numerical scheme in equations (C.1) and (C.2), for $T = 0.1$ and different values of γ.

equations (2.63) and (2.64). In fact one could expect that the transmission coefficient obtained with $T = 0.1$ and $\gamma = 0.5$ displays a better-defined plateau than the one found for $T = \gamma = 0.1$ since in the former case the value of γ is higher, and therefore the corresponding trajectories feature fewer recrossings. However we see that in fact the opposite is true, and the lower value of γ leads to a "flatter" plateau. On the other hand the fact that the plateau we find with $T = 0.1$ and $\gamma = 0.5$ is higher than that we have for $T = \gamma = 0.1$ reflects the fact that with higher damping recrossings are less

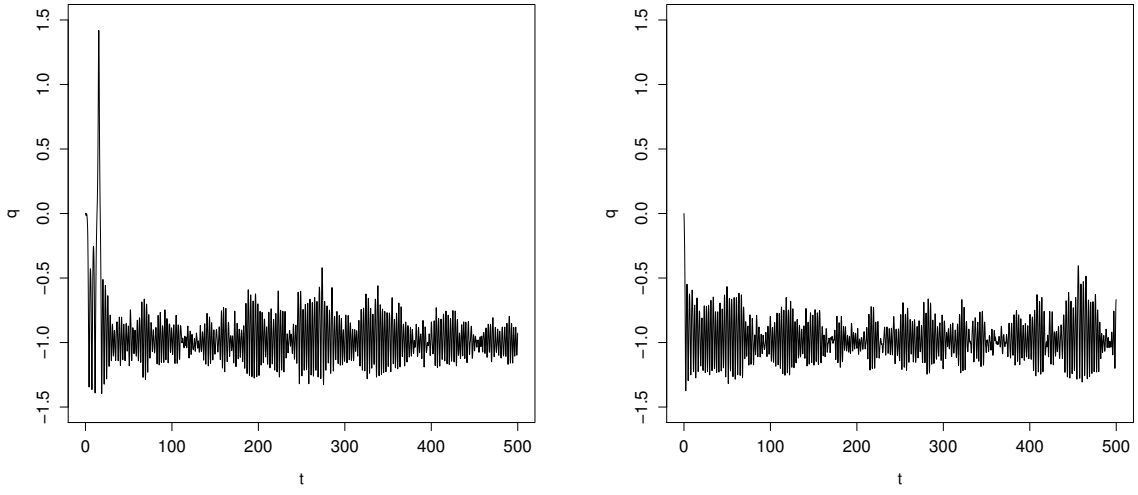


(A) (B)

FIGURE 2.10: $T = 0.1$ and $\gamma = 0.01$. Two stochastic realisations of the dynamics corresponding to the classical transmission coefficient in figure 2.9a. Obtained by integrating the classical equations of motion (2.63) and (2.64) using the numerical scheme in equations (C.1) and (C.2).

frequent. In figure 2.12 the trajectories display fluctuations of relatively large amplitude, as expected, suggesting that activation over the energy barrier is more likely in this case compared to the one with lower γ. However because the value of the coupling coefficient is high the trajectories also do get trapped. This result is the linearly decaying "plateau" we observe in figure 2.9c. The fact that the value of the coupling coefficient is quite large also means that there are few recrossings, resulting in a higher value of the "plateau" here compared to the case with $T = \gamma = 0.1$, in figure 2.9b. As noted earlier in this section, the apparent contradiction between the effects brought about by the coupling γ is due to the fact that γ acts both as damping and as coefficient of the "random force" dw in the Langevin equation (2.63)-(2.64).

Lastly we test two high values of the temperature, $T = 0.25$ and $T = 0.5$, with $\gamma = 0.001$ and $\gamma = 0.5$ respectively. This is shown in figure 2.13. While many qualitative features of the short-time behaviour resemble those of lower temperatures, in neither case it is possible to identify a plateau from the plot of $\kappa^c(t)$, meaning that compared to previous examples now the time scales separation required for the transition rate to be defined does not apply. As stressed at the beginning of the discussion, this makes sense as $E_b = 0.75$

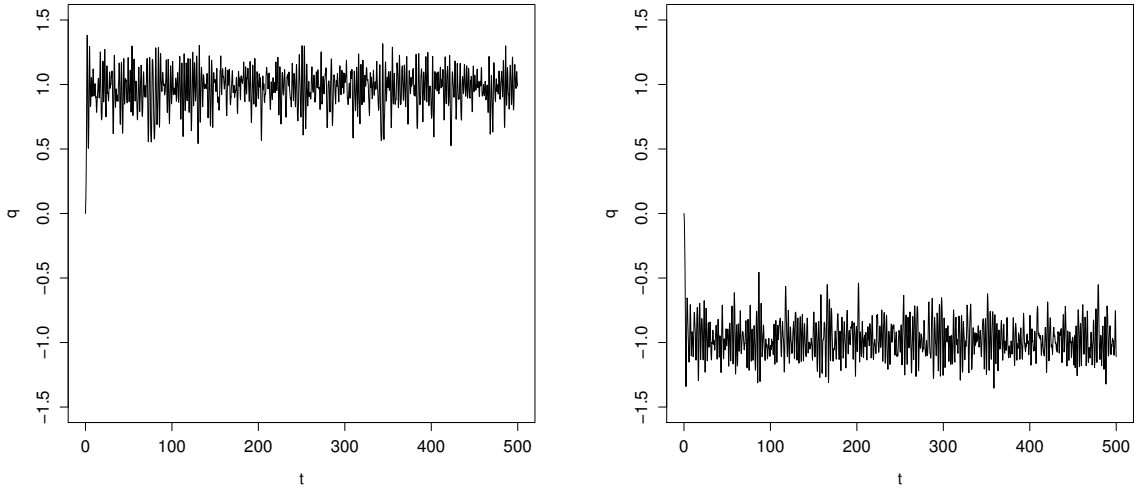


(A) (B)

FIGURE 2.11: $T = \gamma = 0.1$. Two stochastic realisations of the dynamics corresponding to the classical transmission coefficient in figure 2.9b. Obtained by integrating the classical equations of motion (2.63) and (2.64) using the numerical scheme in equations (C.1) and (C.2).

which means that we expect TRT to be applicable when $T \ll 0.75$. Nevertheless the behaviour of $\kappa^c(t)$ provides some insights. In the case where $T = 0.25$ and $\gamma = 0.001$, shown in figure 2.13a, the exponential decay we expect from $\kappa^c(t)$ in a high-temperature regime is almost not visible as it is strongly modulated by short-time relaxations that bring the transmission coefficient to rapidly oscillate to zero. This is because the value of γ is so low that despite the high temperature the trajectories are able to perform ample regular oscillations about the potential minima, as shown in the trajectories at $T = 0.25$ and $\gamma = 0.001$ in the upper panel of figure 2.14. This is analogous to the other examples with small γ we saw before, namely $T = 0.01$ and $\gamma = 0.001$, and $T = 0.1$ and $\gamma = 0.01$, shown in figures 2.6 and 2.10 respectively. Similarly here we have numerous recrossings when the particle is near the saddle point, however in the present case transitions from the minima over the energy barrier are no longer rare due to the high value of T.

On the other hand when $T = \gamma = 0.5$ we find a pronounced exponential decay with $\tau_r = \tau_{sr} \approx 5$, and no plateau is observed. As expected the trajectories corresponding to this regime, shown in the lower panel of figure 2.14, displayed very frequent transitions across $q^* = 0$ and are also heavily damped during the short periods of time they stay

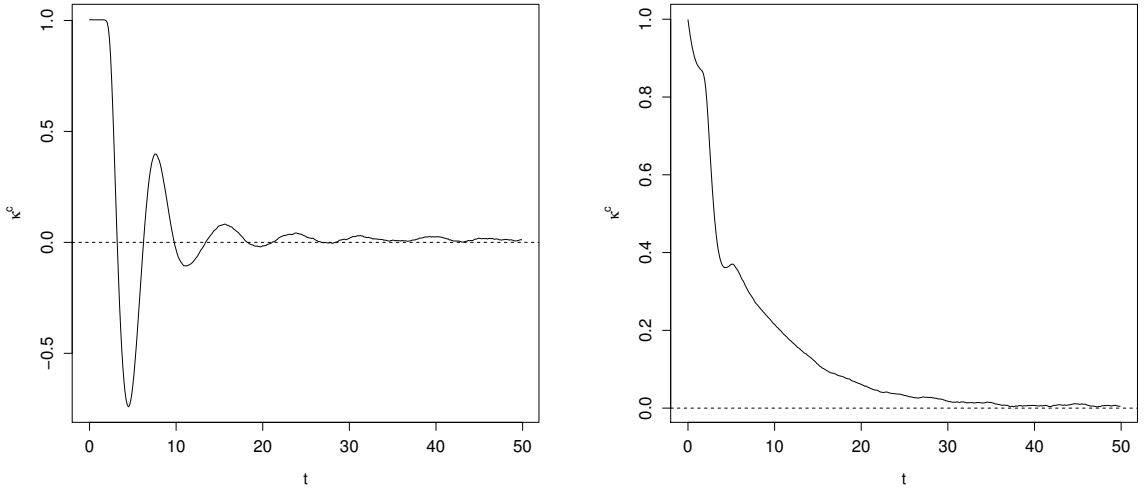


(A) (B)

FIGURE 2.12: $T = 0.1$ and $\gamma = 0.5$. Two stochastic realisations of the dynamics corresponding to the classical transmission coefficient in figure 2.9c. Obtained by integrating the classical equations of motion (2.63) and (2.64) using the numerical scheme in equations (C.1) and (C.2).

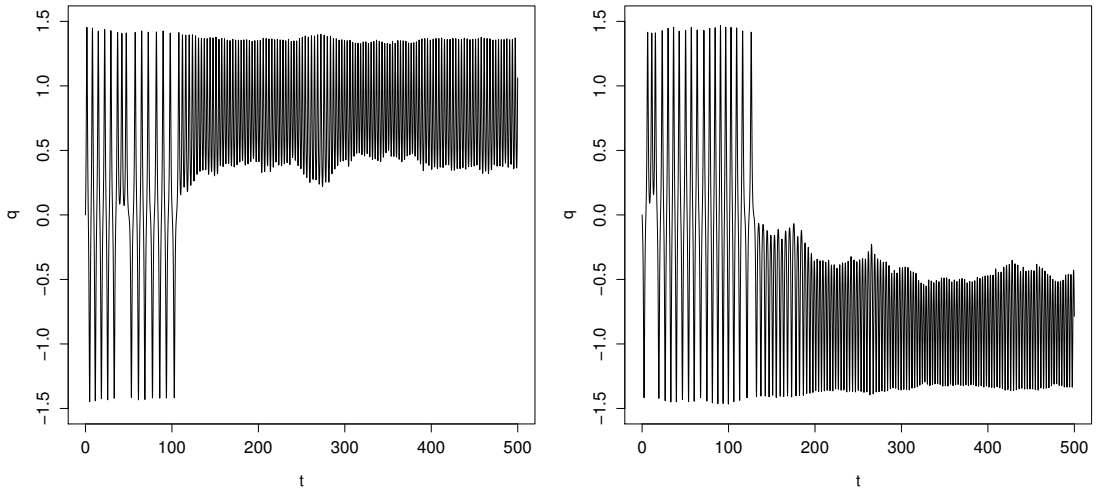
within a metastable state.

In summary we can distinguish between three regions in parameter space schematically displayed in figure 2.15. The regions are defined according to how well the concepts of TRT and TST discussed earlier in this chapter can be applied. Region (1) is where $\kappa^c(t)$ displays a plateau and the value taken by the plateau is such that k^c is 50% or more of k^{TS}. This is where the required separation of time scales between microscopic dynamics and macroscopic transitions across the barrier can certainly be made, and recrossings are very rare such that TST is a fair approximation. In region (2) the classical transmission coefficient shows a plateau but this is lower than 0.5. That is, the TST approximation to the true rate constant is not very accurate. In this regime trajectories are characterised by prolonged trapping but recrossings can take place as well. Region (3) is where TRT cannot be applied and equally the TST approximation to the rate is not a meaningful concept to use: $\kappa^c(t)$ here never reaches a plateau due to the fact that crossings over the barrier are very frequent as $T \sim \frac{E_b}{k_B}$. Having studied classical TRT in detail, we are now going to review some of the traditional approaches to generalising this theory to quantum mechanics.

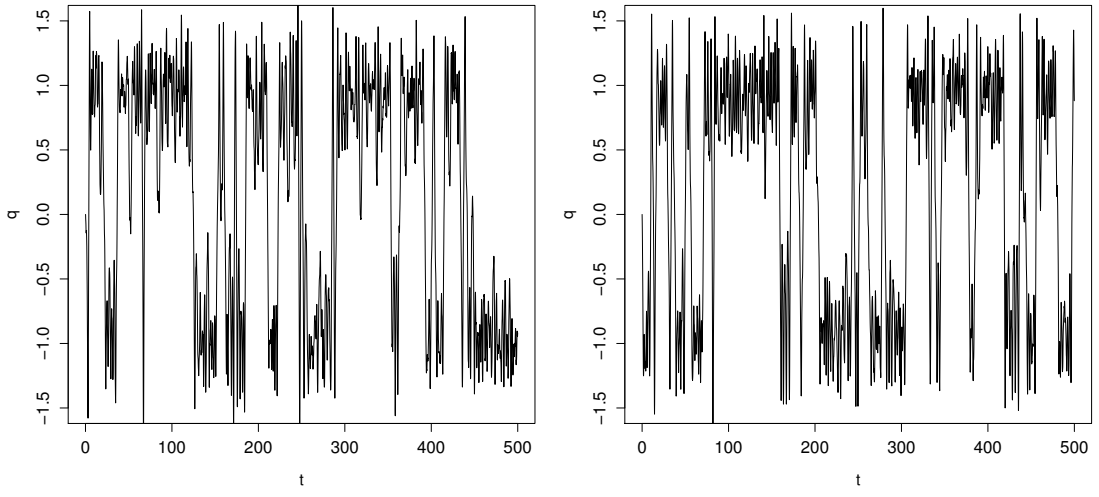


(A) $T = 0.25$, γ=0.001 (B) $T = \gamma$=0.5

FIGURE 2.13: Classical transmission coefficient κ^c computed via equation (2.48) and the numerical scheme in equations (C.1) and (C.2).



(A) (B)



(C) (D)

FIGURE 2.14: Stochastic realisations of the dynamics corresponding to the classical transmission coefficient in figures 2.13a and 2.13b. Upper panel: two stochastic realisations with $T = 0.25$ and $\gamma = 0.001$. Lower panel: two stochastic realisations with $T = \gamma = 0.5$. Obtained by integrating the classical equations of motion (2.63).

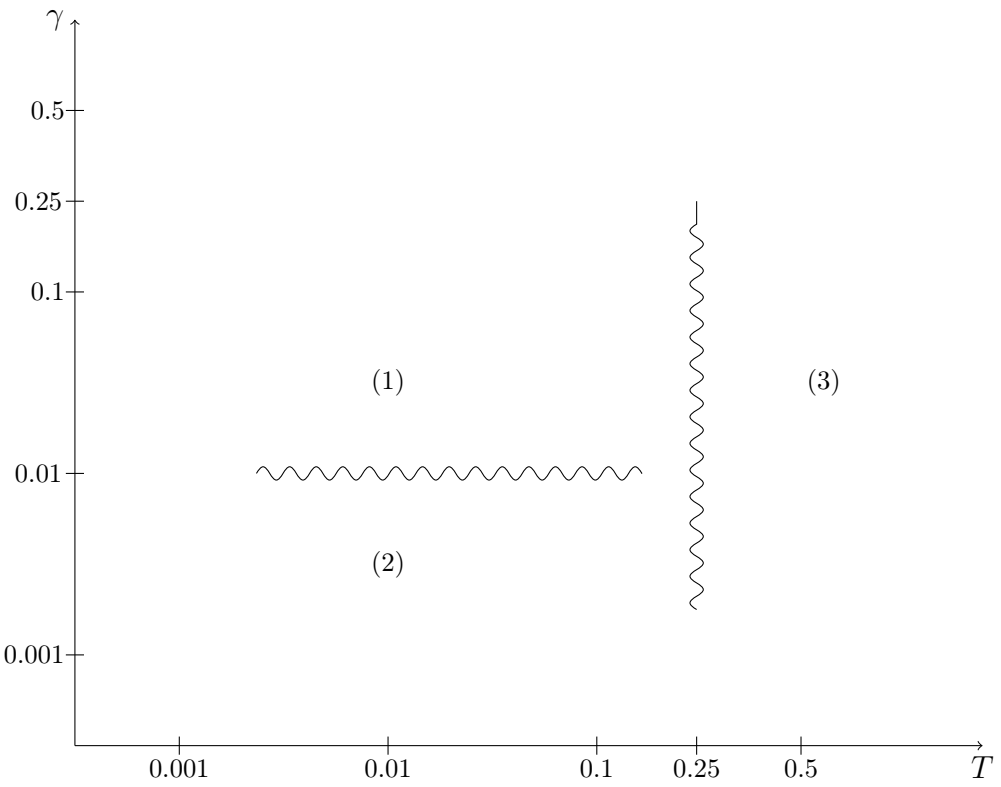


FIGURE 2.15: Summary of the results obtained for $\kappa^c(t_{pl})$ in different (T, γ) regimes. In region (1), $\kappa^c(t_{pl}) \geq 0.5$; in region (2), $\kappa^c(t_{pl}) \leq 0.5$; in region (3) we have no plateau. All values are shown in dimensionless units.

2.4 Traditional approaches to quantum transition rate theory

Attempts to generalise the classical theory of transition rates to quantum mechanics started roughly at the same time as the inception of TRT itself, with the work of Bourgin ([11]) and, shortly after, with that of Wigner [12]. Initial formulations of quantum-mechanical rate theory focussed on determining appropriate corrections to the classical TST rate to take into account tunneling and other quantum dynamical effects; a crucial contribution to this field was made by Miller in 1974 [15]. Miller's formulation is analogous to an earlier formulation due to Yamamoto ([13]), who used results in linear response theory obtained by Kubo ([8]) to derive a quantum-mechanical expression for the rate; however the formula by Miller presents a computational advantage compared to that by Yamamoto [44]. Note that in Miller's theory the dynamical contributions to the quantum rate appear as corrections to a quantum TST expression. We will now briefly review how Miller's expression for the quantum rate is derived by following a didactical presentation by Manolopoulos [39].

In analogy to the framework we used to derive the classical transition rate, in the quantum-mechanical case let us imagine that two states identified by the two coordinate semiaxes $q < 0$ and $q > 0$ are separated by an energy barrier. Unlike in the derivation we presented of the classical rate however, here the quantum rate k is obtained in the context of a 1-dimensional barrier transmission problem, and not in a double-well system. The dividing point is, as before, $q^* = 0$. Miller's formulation starts from a general expression for the quantum mechanical transition rate [39]:

$$Z_k = \frac{1}{2\pi\hbar}\int_0^\infty \mathrm{d}E e^{-\beta E} N(E), \tag{2.67}$$

where Z_- indicates the partition function relative to the negative q semiaxis and $N(E)$ gives the probability of crossing the energy barrier. Note that the average is taken over a distribution of *free* particle energies $E = \frac{p^2}{2m}$. Through scattering theory Miller derives

a quantum-mechanical expression for $N(E)$ as follows [39]:

$$N(E) = 2\pi\hbar\frac{m}{p}\langle\psi|\hat{F}|\psi\rangle, \tag{2.68}$$

where $|\psi\rangle$ are the outgoing eigenstates of the scattering Schrödinger equation $\hat{H}|\psi\rangle = E|\psi\rangle$ and $\hat{F}$ is the Heisenberg time derivative of the projection operator $h(\hat{x} - q^*)$ onto the positive semiaxis, giving the flux of particles passing through the dividing point q^*:

$$\hat{F} = \frac{\mathrm{i}}{\hbar}[\hat{H}, h(\hat{x} - q^*)], \tag{2.69}$$

with:

$$h(q - q^*) = \begin{cases} 1, & \text{if } q > q^* \\ 0, & \text{if } q < q^*. \end{cases} \tag{2.70}$$

In position representation $\hat{F}$ can be written as

$$\hat{F}(q^*) = -\frac{\mathrm{i}\hbar}{2m}\left[\delta(q - q^*)\frac{\mathrm{d}}{\mathrm{d}q} + \frac{\mathrm{d}}{\mathrm{d}q}\delta(q - q^*)\right]. \tag{2.71}$$

By inserting equation (2.68) into equation (2.67) one finds:

$$Z_k = \int_0^\infty \mathrm{d}E\frac{m}{p}e^{-\beta E}\langle\psi|\hat{F}|\psi\rangle; \tag{2.72}$$

this equation can be alternatively written as:

$$Z_k = \int_0^\infty \mathrm{d}p\langle\psi|e^{-\frac{\beta}{2}\hat{H}}\hat{F}e^{-\frac{\beta}{2}\hat{H}}|\psi\rangle, \tag{2.73}$$

where we have used the substitution $p = \sqrt{2mE}$ and the fact that $\hat{H}|\psi\rangle = E|\psi\rangle$. Further, the expression above can be modified to obtain Miller's *trace formula* for the quantum rate [39]:

$$Z_k = \mathrm{tr}\left(e^{-\frac{\beta}{2}\hat{H}}\hat{F}e^{-\frac{\beta}{2}\hat{H}}\lim_{t\to\infty}e^{-\frac{\mathrm{i}}{\hbar}\hat{H}t}h(\hat{p})e^{\frac{\mathrm{i}}{\hbar}\hat{H}t}\right). \tag{2.74}$$

Physically, the equation above features a thermal flux through the dividing point at $t = 0$, $e^{-\frac{\beta}{2}\hat{H}}\hat{F}e^{-\frac{\beta}{2}\hat{H}}$, and the factor $\lim_{t\to\infty}e^{-\frac{\mathrm{i}}{\hbar}\hat{H}t}h(\hat{p})e^{\frac{\mathrm{i}}{\hbar}\hat{H}t}$ indicates the projection onto states with positive momentum. With several additional manipulations equation (2.74)

can be expressed as:

$$Z_k = -\lim_{t\to\infty} \text{tr } e^{-\frac{\beta}{2}\hat{H}}\hat{F}e^{-\frac{\beta}{2}\hat{H}}e^{-\frac{\mathrm{i}}{\hbar}\hat{H}t}\hat{h}e^{\frac{\mathrm{i}}{\hbar}\hat{H}t}, \tag{2.75}$$

with $\hat{F}$ defined as in equation (2.69). In an important work by Miller *et al.* it is shown that the quantum-mechanical transition rate in equation (2.75) can be equivalently written in terms of a *side-side*, *flux-side* and *flux-flux* correlation function, which we indicate as $c_{ss}(t)$, $c_{fs}(t)$ and $c_{ff}(t)$ respectively [44]:

$$Z_k = \lim_{t\to\infty} \frac{\mathrm{d}}{\mathrm{d}t} c_{ss}(t) = \lim_{t\to\infty} c_{fs}(t) = \int_0^\infty \mathrm{d}t c_{ff}(t), \tag{2.76}$$

where we have:

$$c_{fs}(t) = \text{tr } e^{-\frac{\beta}{2}\hat{H}}\hat{F}e^{-\frac{\beta}{2}\hat{H}}e^{\frac{\mathrm{i}}{\hbar}\hat{H}t}\hat{h}e^{-\frac{\mathrm{i}}{\hbar}\hat{H}t}, \tag{2.77}$$

$$c_{ss}(t) = \text{tr } e^{-\frac{\beta}{2}\hat{H}}\hat{h}e^{-\frac{\beta}{2}\hat{H}}e^{\frac{\mathrm{i}}{\hbar}\hat{H}t}(1-\hat{h})e^{-\frac{\mathrm{i}}{\hbar}\hat{H}t}, \quad \text{and} \tag{2.78}$$

$$c_{ff}(t) = \text{tr } e^{-\frac{\beta}{2}\hat{H}}\hat{F}e^{-\frac{\beta}{2}\hat{H}}e^{\frac{\mathrm{i}}{\hbar}\hat{H}t}\hat{F}e^{-\frac{\mathrm{i}}{\hbar}\hat{H}t}. \tag{2.79}$$

It can be shown that equation (2.79) is analogous to the quantum rate expression proposed by Yamamoto:

$$Z_k = \int_0^\infty \mathrm{d}t c_{ff}(t) = \frac{1}{\beta}\int_0^\beta \mathrm{d}\lambda \lim_{t\to\infty} \text{tr } \left(\hat{F}e^{\frac{\mathrm{i}}{\hbar}\hat{H}t}e^{-\lambda\hat{H}}\hat{h}e^{-(\beta-\lambda)\hat{H}}e^{-\frac{\mathrm{i}}{\hbar}\hat{H}t}\right). \tag{2.80}$$

A key feature of the flux-side correlation function $c_{fs}(t)$ defined in equation (2.77) is that it smoothly goes to zero as $t \to 0^+$ [16]. This differentiates it from its classical analogue, $\varrho(t)$, which we introduced in equation (2.21). This is summarised in the qualitative sketch in figure 2.16. This is a central result in that it demonstrates that any quantum-mechanical formulation of the transition rate compatible with Miller's formula does not allow for a transition-state theory approximation in the sense of a $t \to 0$ limit. In the next section we review another important approach to approximate quantum TRT based on discretised path-integrals.

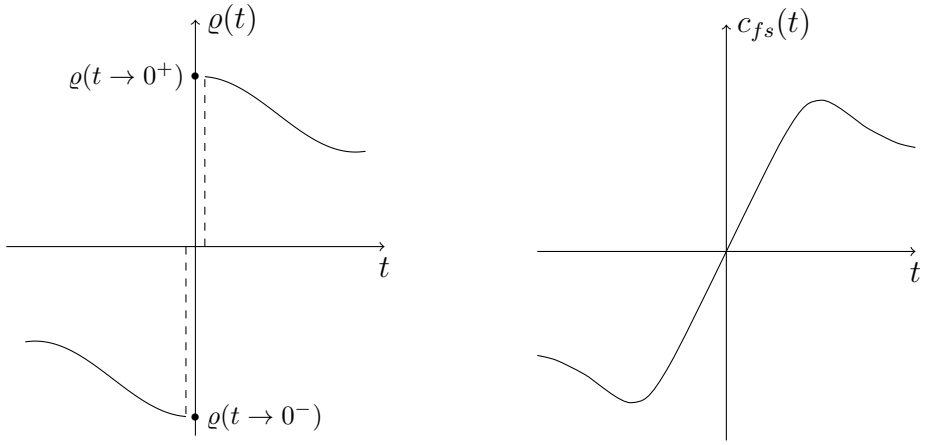


FIGURE 2.16: Qualitative sketch portraying the behaviour of classical (left-hand-side) and quantum-mechanical (right-hand-side) time correlation functions, $\varrho(t)$ and $c_{fs}(t)$, defined in equations (2.21) and (2.77) respectively. The classical and quantum-mechanical rates are defined in terms of these correlation functions in equations (2.32) and (2.80) respectively.

2.4.1 Discretised path-integrals and quantum TRT

One of the most commonly used approaches in quantum transition rate theory involves using the a *discretised path-integral* (DPI) formalism to express quantum rates. While we are not going to use a DPI-based approach in the present work, for completeness we briefly review this alternative method to study quantum TRT as it could offer future exciting opportunities for comparison to our formulation, which will be introduced in chapter 4. Originally due to Feynman and Hibbs ([17], [18]), the path-integral technique for quantum statistical mechanics exploits the analogy between the canonical density operator $\hat{\rho}(\beta) = e^{-\beta\hat{H}}$ and the time propagator $\hat{U}$ evaluated in imaginary time [42]:

$$\hat{\rho}(\beta) = \hat{U}(-\mathrm{i}\beta\hbar), \quad \hat{U}(t) = \hat{\rho}\left(\frac{\mathrm{i}t}{\hbar}\right). \tag{2.81}$$

It can be shown that the expression for $\hat{\rho}$ as an imaginary time propagator can be used to derive a discretised path-integral formulation for the quantum-mechanical partition function Z, which in one dimension reads:

$$Z_P = \left(\frac{mP}{2\pi\beta\hbar^2}\right)^{\frac{P}{2}} \int_D \mathrm{d}x_1 ... \mathrm{d}x_P e^{-\beta\chi(x_1,...,x_P)}, \tag{2.82}$$

with:

$$\chi(x_1, ..., x_P) = \sum_{i=1}^{P} \frac{1}{2} m\omega_P^2 (x_i - x_{i+1})^2 + \frac{1}{P} V(x_i), \tag{2.83}$$

where $\omega_P = \frac{\sqrt{P}}{\beta\hbar}$, D indicates the domain over which we wish to compute the partition function, and the coordinates x_i form a closed loop: $x_{P+1} = x_1$. In the limit as $P \to \infty$ the discretised expression for Z tends to the true value:

$$\lim_{P\to\infty} Z_P = Z. \tag{2.84}$$

While a detailed derivation of the equation above is beyond the scope of the present discussion, we note that one can obtain equation (2.82) by writing the matrix elements of $\hat{\rho}(\beta)$ in coordinate representation [42]:

$$\rho(x, x'; \beta) = \langle x' | e^{-\beta \hat{H}} | x \rangle, \tag{2.85}$$

and observing that this can be factorised as follows:

$$\rho(x', x; \beta) = \lim_{P\to\infty} \int_{-\infty}^{\infty} \mathrm{d}x_2 ... \mathrm{d}x_P \langle x' | \hat{\Omega} | x_P \rangle \langle x_P | \hat{\Omega} | x_{P-1} \rangle ... \langle x_2 | \hat{\Omega} | x \rangle, \tag{2.86}$$

where:

$$\hat{\Omega} = e^{-\frac{\beta}{2P} V(\hat{x})} e^{-\frac{\beta}{P} \frac{\hat{p}^2}{2m}} e^{-\frac{\beta}{2P} V(\hat{x})}. \tag{2.87}$$

Equation (2.82) is an interesting result. Firstly we notice that the expression essentially allows us to map the problem of determining the partition function of a quantum-mechanical particle of mass m moving in a potential $V(\hat{x})$ onto that of finding the partition function of an ensemble of P classical particles that are harmonically coupled via temperature-dependent spring constants and are subject to the potential $\frac{1}{P} V(x)$. Also, in the expression (2.82) high-temperature and classical limit coincide: as $\beta \to 0$, $\omega_P \to \infty$ and the classical "particles" collapse to one single point.

The main use of the DPI method in quantum transition rate theory is to provide an estimate for the TST approximation for the quantum rate. We saw in the previous section that the rigorous formulation of the quantum rate obtained by Miller involves a time correlation function whose limit as $t \to 0$ is zero, thus making it impossible in

principle to obtain a quantum-mechanical analogue of k_{TS}^{c}. Because it is computationally much cheaper to compute the TST approximation of the transition rate versus its full expression in the classical case, significant efforts have been made in order to by-pass this issue by postulating various DPI forms for a quantum-mechanical TST rate. One of the first works where the discretised path-integral approach is related to quantum TST rate theory is due to Gillan [19]. In his work Gillan states that the probability of finding the "centre of mass" of the DPI chain at the saddle point of the energy barrier separating two metastable states can be used to find the rate of transitions between such states. A detailed argument for why this approximation should be suitable was developed shortly after by Voth and co-workers [21], [45]. Here the DPI formulation is employed to translate expressions for k_{TS}^{c} as a ratio of partition functions, like the type given in equation (2.40), into quantum-mechanics, where the approximation in equation (2.82) can be used to compute the quantum partition functions.

A great deal of work has been put into providing rigurous arguments why such estimates should identify the "true" quantum rate. One example of work carried out in this direction is that by Althorpe and co-workers [27], [22], [22]. The key assumption within this class of contributions is that the quantum-mechanical TST rate is assumed *a priori* to be in DPI form, from which it is shown that such expressions validate several features expected from a legitimate quantum TST rate.

On the other hand, DPI-based approaches have recently been proposed for the computation of dynamical effects arising in quantum transition rate theory. An example is the so-called ring-polymer molecular dynamics (RPMD) technique, which was introduced by Manolopulos *et al.* [24], [25]. Here one estimates the dynamics of the quantum-mechanical system, which contributes to the rate via what we call the transmission coefficient, by computing the classical dynamics of the "polymer" of P harmonically interacting classical particles instead of that of a single quantum particle. It is shown that for large enough values of P this provides a reasonable estimate for $\kappa(t)$.

The key ingredient needed to compute the classical transmission coefficient is the "activated" classical dynamics, which, as we showed, can be described via the Langevin

equation for single trajectories. We aim to generalise this perspective to the quantum-mechanical case by writing an expression for the quantum transmission coefficient where the open quantum dynamics appears explicitly. Before we proceed to this formulaiton, in the next chapter we discuss how one can model temperature-dependance in quantum mechanics.

Chapter 3

Open quantum dynamics

In this chapter we discuss open quantum dynamics in terms of two analogous formulations: the *Lindblad equation* for the density operator, and the *quantum-state diffusion* (QSD) equation for pure states. The Lindblad equation is a deterministic linear differential equation, while the QSD equation is a nonlinear stochastic differential equation. By averaging over stochastic realisations we show that the two descriptions of the dynamics coincide.

We are interested in formulating an expression for the quantum rate that we can compare directly to the classical transmission coefficient obtained via the Langevin dynamics. To this end we define the *Lindblad operator* $\hat{L}$ appearing in both the Lindblad and QSD equations in such a way that it models an analogous type of coupling to the heat bath as we had in the classical case. The form for $\hat{L}$ we use is taken from reference [46] and it features a temperature-dependent non-Hermitian combination of the position and momentum operators.

By using coherent states in the same fashion as was proposed by Heller ([33]), we show that the classical limit of the QSD dynamics is the Langevin equation. This is obtained as a special case of a general semiclassical scheme we derive for a quadratic Hamiltonian and linear Lindblad operators. We carry out a detailed numerical investigation where we compare the open semiclassical, quantum-mechanical and classical dynamics for our toy model of hydrogen in iron.

3.1 The Lindblad equation

In classical mechanics we saw that the Fokker-Planck equation describes the evolution of the probability distribution of a set of variables which obey the Langevin dynamics in the case of Gaussian and Markovian noise. A similar duality can be established in quantum-mechanics where the open-system dynamics is described in terms of a deterministic Lindblad equation governing the density operator of the system, and the dissipative single-trajectory dynamics is given by a stochastic process in the Hilbert space of state vectors.

Let us briefly introduce the *density operator* $\hat{\rho}$ by following reference [47]. Note that with all quantum-mechanical quantities we denote expectation values with $\langle\ \rangle$ and ensemble averages with $\mathcal{M}$. Call u the coordinates of the system of interest and v those of the environment the system is in contact with and let $\psi_i(u)$ be a complete set of wave functions. A general wave function Ψ can be written:

$$\Psi(u,v) = \sum_i C_i(v)\psi_i(u). \tag{3.1}$$

In bra-ket notation, the above can be expressed as

$$\Psi(u,v) = \sum_{ij} C_{ij}\langle u|\psi_i\rangle\langle v|\eta_j\rangle, \tag{3.2}$$

where $\eta_i(v) = \langle v|\eta_i\rangle$ and we have taken $C_i(v) = \sum_j C_{ij}\langle v|\eta_j\rangle$. If $\hat{O}$ is an operator acting on the system, its expectation value with respect to product states of the system and the environment is given by:

$$\langle\hat{O}\rangle = \langle\Psi|\hat{O}|\Psi\rangle = \sum_{ijk} C^*_{ij}C_{kj}\langle\psi_i|\hat{O}|\psi_k\rangle = \sum_{ik}\langle\psi_i|\hat{O}|\psi_k\rangle\rho_{ki}, \tag{3.3}$$

where the *density matrix* is defined as

$$\rho_{ki} = \sum_j C^*_{ij}C_{kj}. \tag{3.4}$$

The density operator $\hat{\rho}$ is defined such that:

$$\rho_{ki} = \langle \psi_k | \hat{\rho} | \psi_i \rangle. \tag{3.5}$$

Hence for the expectation value of $\hat{O}$ we have:

$$\langle \Psi | \hat{O} | \Psi \rangle = \sum_i \langle \psi_i | \hat{O} \hat{\rho} | \psi_i \rangle = \text{tr } \hat{\rho} \hat{O}. \tag{3.6}$$

It follows from equation (3.4) that $\hat{\rho}$ is Hermitian and it can therefore be diagonalised using a complete set of orthonormal eigenvectors $|\phi_i\rangle$ with real eigenvalues w_i:

$$\hat{\rho} = \sum_i w_i |\phi_i\rangle\langle\phi_i|. \tag{3.7}$$

It can be shown that the following properties apply [47]:

$$w_i \geq 0 \quad \forall i, \quad \text{and} \tag{3.8}$$

$$\sum_i w_i = 1. \tag{3.9}$$

Now the expectation value of a physical observable $\hat{O}$ can be expressed as

$$\langle \hat{O} \rangle = \text{tr } \hat{\rho} \hat{O} = \sum_{i,j} w_i \langle \psi_j | \phi_i \rangle \langle \phi_i | \hat{O} | \psi_j \rangle = \sum_i w_i \langle \phi_i | \hat{O} | \phi_i \rangle; \tag{3.10}$$

so we can interpret the quantities w_i as the probability that the system is in state ϕ_i. It follows that the density operator is normalised to unity: tr $\hat{\rho} = 1$. A system is said to be in a *pure state* when all but one of the w_i are zero, and we say it is in a *mixed state* otherwise. When the operator we consider is a projector onto one of the eigenstates $|o_i\rangle$ of $\hat{O}$, that is $\hat{P} = |o_j\rangle\langle o_j|$, the expectation value of this operator can be written using $\hat{\rho}$ as

$$\langle \hat{P} \rangle = \text{tr } \hat{\rho} \hat{P} = \sum_k w_k \langle \phi_k | o_j \rangle \langle o_j | \phi_k \rangle = \sum_k w_k |\langle o_j | \phi_k \rangle|^2. \tag{3.11}$$

The above can be seen as a weighted average of the possible outcomes of a measurement of $\hat{O}$. We can interpret $|\phi_i\rangle$ as a complete set of microscopic states with probabilities w_i given by the density operator. In this sense $\hat{\rho}$ is analogous to the phase space density

$f(y,t)$ we encountered in chapter 2.

In position representation, the density matrix is defined as follows:

$$\rho(x',x) = \langle x'|\hat{\rho}|x\rangle = \sum_i w_i \langle x'|\phi_i\rangle\langle\phi_i|x\rangle = \sum_i w_i \phi_i(x')\phi_i^*(x); \tag{3.12}$$

and the expectation value of $\hat{O}$ becomes:

$$\langle O\rangle = \text{tr } \hat{\rho}\hat{O} = \int_{-\infty}^{\infty} \mathrm{d}x \int_{-\infty}^{\infty} \mathrm{d}x' \rho(x,x')O(x',x). \tag{3.13}$$

We now proceed to discuss the dynamics of the density operator $\hat{\rho}$.

When the quantum system under study is closed the evolution of the density operator is thought of as a *unitary map*; for open systems the requirement is loosened to *completely positive* maps, that is: $\hat{\rho} \to \sum_j \hat{O}_j \hat{\rho} \hat{O}_j$ where the linear operators $\hat{O}_j$ are such that $\sum_j \hat{O}_j^\dagger \hat{O}_j = 1$, which guarantees that the trace of $\hat{\rho}$ stays conserved over time [48]. In his seminal paper, Lindblad showed that this implies that the linear differential equation describing the evolution of $\hat{\rho}(t)$ can be written as follows [49]:

$$\frac{\mathrm{d}}{\mathrm{d}t}\hat{\rho} = -\frac{\mathrm{i}}{\hbar}[\hat{H},\hat{\rho}] + \sum_j (2\hat{L}_j\hat{\rho}\hat{L}_j^\dagger - \hat{\rho}\hat{L}_j^\dagger\hat{L}_j - \hat{L}_j^\dagger\hat{L}_j\hat{\rho}), \tag{3.14}$$

where $[\ ,\ ]$ indicates the commutator and $\hat{L}_j$ are called *Lindblad operators*, which may or may not be Hermitian. On the right-hand side of equation (3.14) the first term represents the unitary dynamics associated to the Hamiltonian $\hat{H}$, while the second term describes the interaction of the system with the environment, which constitutes the irreversible and non-unitary contribution to the overall time-evolution of the density operator. The definition of the Lindblad operators will depend on the type of interaction between the system and the environment one desires to achieve; to model measurements, one can introduce an Hermitian Lindblad operator, while dissipation is usually described via non-Hermitian Lindblad operator [50].

It is possible to introduce a Lindblad operator $\hat{L}$ such that the Lindblad equation (3.14) models a quantum system in contact with a heat bath. In particular quantum Brownian motion can be studied by means of a particular system-reservoir model known as

the Caldeira-Leggett model [51]. This is derived in a completely analogous way to the Langevin equation. We have a quantum particle of unitary mass which in the absence of heat bath has Hamiltonian $\hat{H}_p$:

$$\hat{H}_p = \frac{\hat{p}^2}{2} + V(\hat{x}), \tag{3.15}$$

and bath of quantum oscillators with masses m_i frequencies ω_j, with Hamiltonian $\hat{H}_b$:

$$\hat{H}_b = \sum_j \left(\frac{1}{2m_j}\hat{p}_j^2 + \frac{1}{2}m_j\omega_j\hat{x}_j^2 \right) = \sum_j \hbar\omega_j \left(\hat{b}_j^\dagger \hat{b}_j + \frac{1}{2} \right), \tag{3.16}$$

where $\hat{b}$ and $\hat{b}^\dagger$ indicate the annihilation and creation operators of the bath respectively. Similarly to the classical case, here the quantum particle is coupled linearly to the bath's coordinates $\hat{x}_j$, leading to the interaction Hamiltonian $\hat{H}_i$:

$$\hat{H}_i = -\hat{x}\sum_j \zeta_j \hat{x}_j, \tag{3.17}$$

where ζ_j are coupling constants. The resulting total Hamiltonian is:

$$\hat{H} = \frac{1}{2}\hat{p}^2 + \tilde{V}(\hat{x}) + \sum_j \left(\frac{1}{2m_j}\hat{p}_j^2 + \frac{1}{2}m_j\omega_j\hat{x}_j^2 \right) - \hat{x}\sum_j \zeta_j\hat{x}_j, \tag{3.18}$$

where the potential $\tilde{V}$ is introduced in order to compensate for a renormalisation of $V(\hat{x})$ [46]:

$$\tilde{V}(\hat{x}) = V(\hat{x}) + \hat{x}^2 \sum_j \frac{\zeta_j^2}{2m_j\omega_j^2}. \tag{3.19}$$

The Caldeira-Leggett quantum master equation is obtained in the Markov approximation; it reads [46]:

$$\frac{\mathrm{d}}{\mathrm{d}t}\hat{\rho} = \frac{\mathrm{i}}{\hbar}[\hat{H}_p, \hat{\rho}] - \frac{\mathrm{i}\gamma}{\hbar}[\hat{x}, [\hat{p}, \hat{\rho}]_+] - \frac{2\gamma}{\beta\hbar^2}[\hat{x}, [\hat{x}, \hat{\rho}]], \tag{3.20}$$

where the symbol $[\ ,\ ]_+$ indicates the anticommutator and γ is the constant coupling coefficient. This equation, however, is not in Lindblad form, a fact that is often mentioned in the literature (see for example the review in reference [48]). In particular equation (3.20) is not positivity preserving, thus violating some of the probability interpretation

of quantum mechanics. However it is beyond the scope of our work to go into details, and we use a pragmatic solution proposed in reference [46]. Here, in order to bring equation (3.20) in Lindblad form, it is proposed to add the following *minimally invasive* modification to the master equation:

$$-\frac{\gamma\beta}{8}[\hat{p},[\hat{p},\hat{\rho}]]; \tag{3.21}$$

by doing this and defining the non-Hermitian Lindblad operator:

$$\hat{L}=\sqrt{\frac{2}{\beta\hbar^2}}\hat{x}+\frac{\mathrm{i}}{2}\sqrt{\frac{\beta}{2}}\hat{p}, \tag{3.22}$$

the Caldeira-Leggett equation (3.20) reduces to the Lindblad equation (3.14) with a modified Hamiltonian that includes the anticommutator term $\hat{H}_\gamma=\frac{\gamma}{2}[\hat{p},\hat{q}]_+$. This represents the unitary contribution to the dynamics brought about by the introduction of dissipative terms in the quantum master equation. Other similar modifications to the Caldeira-Leggett quantum master equation have been proposed among others by Diósi [52].

3.2 The quantum-state diffusion method

In classical dynamics, we saw that an open system can be described via a stochastic differential equation, the Langevin equation. We also saw that given an ensemble of classical trajectories evolving according to the Langevin dynamics, the evolution of their density is described by the Fokker-Planck equation. In quantum-mechanics, if a mixed state evolves according to a quantum master equation, the evolution can be *unravelled* in terms of the so-called *quantum-state diffusion* (QSD) trajectories [53],[54],[50]. Similarly to how the Langevin equation models the diffusion of a particle in the classical coordinate space, a QSD trajectory describes the diffusion of pure state vectors in Hilbert space.

The quantum-state diffusion approach to open quantum dynamics states that if the dynamics of pure states $|\psi\rangle$ follows the stochastic Schrödinger equation [54]:

$$|\mathrm{d}\psi\rangle = -\frac{\mathrm{i}}{\hbar}\hat{H}|\psi\rangle\mathrm{d}t + \gamma(2\langle\hat{L}^\dagger\rangle\hat{L} - \hat{L}^\dagger\hat{L} - \langle\hat{L}^\dagger\rangle\langle\hat{L}\rangle)|\psi\rangle\mathrm{d}t + \sqrt{\gamma}(\hat{L} - \langle\hat{L}\rangle)|\psi\rangle\mathrm{d}\xi, \tag{3.23}$$

the mean over stochastic realisations gives the Lindblad dynamics:

$$\frac{\mathrm{d}\hat{\rho}}{\mathrm{d}t} = -\frac{\mathrm{i}}{\hbar}[\hat{H}, \hat{\rho}] + \gamma(2\hat{L}\hat{\rho}\hat{L}^\dagger - \hat{\rho}\hat{L}^\dagger\hat{L} - \hat{L}^\dagger\hat{L}\hat{\rho}); \tag{3.24}$$

that is ([53],[54]):

$$\hat{\rho} = \mathcal{M}_\psi|\psi\rangle\langle\psi|, \tag{3.25}$$

where $\mathcal{M}_\psi$ indicates the mean over stochastic wave vectors $|\psi\rangle$. The term $\langle\hat{L}\rangle$ stands for the expectation value of $\hat{L}$ with respect to $|\psi\rangle$, that is $\langle\hat{L}\rangle = \langle\psi|\hat{L}|\psi\rangle$, and similarly for $\hat{L}^\dagger$; this dependence brings about a nonlinearity that guarantees the QSD equation conserves the norm of the state vector. In appendix D we introduce the properties of a complex Brownian motion $\mathrm{d}\xi$. These can be expressed as:

$$\mathcal{M}_{\mathrm{d}\xi}\mathrm{d}\xi = 0, \quad \mathcal{M}_{\mathrm{d}\xi}(\mathrm{d}\xi)^2 = 0 \quad \text{and} \quad \mathcal{M}_{\mathrm{d}\xi}|\mathrm{d}\xi|^2 = 2\mathrm{d}t, \tag{3.26}$$

where $\mathcal{M}_{\mathrm{d}\xi}$ indicates the mean over stochastic processes $\mathrm{d}\xi$. In other words the QSD approach interprets the state vector dynamics in terms of a stochastic Markovian process where the covariance matrix of the state vector is given by the density operator [48]. Following reference [54], we show that by taking the average over pure states that evolve according to equation (3.23) one indeed obtains the Lindblad equation (3.24). To this end we wish to evaluate equation (3.25) by explicitly averaging over the stochastic dynamics (3.23).

To simplify the notation we introduce the vectors $|v\rangle$ and $|u\rangle$ such that equation (3.23) can be rewritten as:

$$|\mathrm{d}\psi\rangle = |v\rangle\mathrm{d}t + |u\rangle\mathrm{d}\xi, \tag{3.27}$$

According to Itô's lemma the differential of $\hat{\rho}$ is given by

$$\mathrm{d}\hat{\rho} = \mathcal{M}_{\mathrm{d}\psi}(|\psi\rangle\langle \mathrm{d}\psi| + |\mathrm{d}\psi\rangle\langle\psi| + |\mathrm{d}\psi\rangle\langle \mathrm{d}\psi|), \tag{3.28}$$

where $\mathcal{M}_{\mathrm{d}\psi}$ refers to the mean over stochastic differentials $|\mathrm{d}\psi\rangle$. Using the notation in (3.27) we have:

$$\mathrm{d}\hat{\rho} = \mathcal{M}_{\mathrm{d}\psi}(|\psi\rangle\langle v|\mathrm{d}t + |v\rangle\langle\psi|\mathrm{d}t + |u\rangle\langle u|\mathrm{d}\xi\mathrm{d}\xi^*), \tag{3.29}$$

where we used the properties (3.26). By applying the properties of the mean of independent Wiener processes, equation (3.26), for $\frac{\mathrm{d}\hat{\rho}}{\mathrm{d}t}$ we find:

$$\frac{\mathrm{d}\hat{\rho}}{\mathrm{d}t} = |\psi\rangle\langle v| + |v\rangle\langle\psi| + 2|u\rangle\langle u| \tag{3.30}$$

With reference to equation (3.23), the three terms on the right-hand side of the equation above are:

$$|\psi\rangle\langle v| = \frac{\mathrm{i}}{\hbar}|\psi\rangle\langle\psi|\hat{H} + \gamma|\psi\rangle\langle\psi|(2\langle\hat{L}\rangle\hat{L}^\dagger - \hat{L}^\dagger\hat{L} - \langle\hat{L}\rangle\langle\hat{L}^\dagger\rangle), \tag{3.31}$$

$$|v\rangle\langle\psi| = -\frac{\mathrm{i}}{\hbar}\hat{H}|\psi\rangle\langle\psi| + \gamma(2\langle\hat{L}^\dagger\rangle\hat{L} - \hat{L}^\dagger\hat{L} - \langle\hat{L}^\dagger\rangle\langle\hat{L}\rangle)|\psi\rangle\langle\psi|, \tag{3.32}$$

and

$$|u\rangle\langle u| = \gamma(\hat{L}|\psi\rangle\langle\psi|\hat{L}^\dagger - \hat{L}|\psi\rangle\langle\psi|\langle\hat{L}^\dagger\rangle - \langle\hat{L}\rangle|\psi\rangle\langle\psi|\hat{L}^\dagger + \langle\hat{L}\rangle\langle\hat{L}^\dagger\rangle|\psi\rangle\langle\psi|). \tag{3.33}$$

Overall we have:

$$\frac{\mathrm{d}\hat{\rho}}{\mathrm{d}t} = -\frac{\mathrm{i}}{\hbar}[\hat{H},\hat{\rho}] + \gamma(2\hat{L}\hat{\rho}\hat{L}^\dagger - \hat{\rho}\hat{L}^\dagger\hat{L} - \hat{L}^\dagger\hat{L}\hat{\rho}). \tag{3.34}$$

Equation (3.23) displays a structure analogous to that of the classical Langevin equation we found in chapter 2 (equations (2.63)-(2.64)): we have a Hamiltonian, or unitary term, a drift term proportional to the coupling coefficient γ, and a stochastic term proportional to $\sqrt{\gamma}$.

In the following section we show in detail how upon choosing the Lindblad operator $\hat{L}$ appropriately one recovers the Langevin equation in the classical limit. This will enable us to use the Lindblad-QSD framework for open quantum dynamics to compute the quantum mechanical transmission coefficient in chapter 4 and compare it to the classical

results obtained using the Langevin equation.

3.3 Semiclassical limit of QSD pure state dynamics

Following the approach by Heller ([33]), in the present section we use a position representation of coherent states, that is we write quantum states as Gaussian wave packets of the form:

$$\psi(x) = N \exp\left\{\frac{\mathrm{i}}{\hbar}\left[\alpha(x-q)^2 + p(x-q) + \phi\right]\right\}, \tag{3.35}$$

where $p, q \in \mathbb{R}$ are the expectation values of $\hat{p}$ and $\hat{x}$ respectively, and $\alpha, \phi \in \mathbb{C}$ with $\Re(\alpha) > 0$. Let us briefly consider the properties of the Gaussian wave packet in equation (3.35). By applying the normalisation condition $|N|^2 = 1$ we find:

$$N = \left[\frac{2\Im(\alpha)}{\hbar\pi}\right]^{\frac{1}{4}} e^{-\frac{1}{\hbar}\Im(\phi)}. \tag{3.36}$$

The paratemeter α is related to the uncertainty in q and p. In particular we have:

$$\Delta q = \frac{1}{2}\sqrt{\frac{\hbar}{b}}, \quad \Delta p = |\alpha|\sqrt{\frac{\hbar}{b}}, \tag{3.37}$$

where a and b are defined as the real and imaginary part of α respectively. Note that in comparison to the notation often found in the literature we are using scaled coordinates such that:

$$X = \frac{x}{\sqrt{m\omega_0}}, \quad Q = \frac{q}{\sqrt{m\omega_0}} \quad \text{and} \quad P = \sqrt{m\omega_0}p \tag{3.38}$$

are the standard harmonic oscillator coordinates, where m and ω_0 indicate the mass and the frequency of the particle respectively. Also to avoid confusion we do not set $\hbar = 1$, as explained in appendix B.

In the next section we use the Gaussian states presented above to derive a set of semiclassical equations of motion given a stochastic Schrödinger dynamics such as the one appearing in the QSD method, discussed in section 3.2. We also demonstrate that with a particular choice of Lindblad operators the semiclassical dynamics reduces to the Langevin equation in the limit $\hbar \to 0$.

3.3.1 General case

Building upon the work done by Heller, let us now investigate the semiclassical behaviour of stochastic quantum dynamics by means of Gaussian wavepackets. We employ the Gaussian ansatz in equation (3.35) for the wave vector appearing in the stochastic Schrödinger equation (3.23) and derive the equations of motion of the parameters α, p, q and ϕ. This reflects the procedure adopted by Heller, however to our knowledge his semiclassical approach had not been applied to stochastic dynamics before.

In his seminal work ([33]), Heller used the dynamics of localised wave packets to compute a semiclasiscal approximation to quantum dynamics. Taking inspiration from comments made by Dirac about the "classical approximation" of quantum systems described in terms of wave packets ([55]), Heller formulates an ansatz for the wave function as a time-dependent Gaussian wave packet centred at the expected values of the position and momentum operators. For quadratic Hamiltonians Gaussian wave packets stay Gaussian for all times and the centre of the wave packet moves according to classical dynamics. However this method can be generalised to *locally* quadratic potentials as well. If the Hamiltonian is not quadratic, because the wave packet is localised on the order of $\hbar$ (see equations (3.37)) we can replace the Hamiltonian with its Taylor expansion up to second order around the centre of the wave packet. Under this local quadratic approximation the wave packet stays Gaussian and the centre moves according to the classical equations of motion. In what follows we mirror Heller's analysis and apply it to the case of a quadratic Hamiltonian first, and to the case of a locally quadratic Hamitonian next; in addition here we consider the open quantum dynamics based on the QSD Schrödinger equation.

Firstly we study the dynamics associated to a quadratic Hamiltonian operator, which we express as a Taylor series in $(x - q)$, where q represents the instantaneus location of the expected value of the position operator and x is the position coordinate in phase space; the Lindblad operators are linear operators, so overall the nonlinear equation (3.23) is quadratic and the dynamics of Gaussian wave packets is exact. In the next section we will concentrate on the example of relevance in this thesis, where the Hamiltonian and the Lindblad operator $\hat{L}$ are chosen to model a quantum particle moving under the

influence of a heat bath. There we will show that under certain conditions it is possible to recover the Langevin equation from the stochastic Schrödinger equation (3.23) using Heller's approach.

From this point on we will be using a simpler notation: $\Re(\alpha) = a$, $\Im(\alpha) = b$ and for all other complex quantities $\{u\}$ we let $\Re(u) = u^R$ and $\Im(u) = u^I$. Let us re-write equation (3.23) here:

$$|\mathrm{d}\psi\rangle = -\frac{\mathrm{i}}{\hbar}\hat{H}|\psi\rangle\mathrm{d}t + \gamma[2\langle\hat{L}^\dagger\rangle\hat{L} - \hat{L}^\dagger\hat{L} - \langle\hat{L}^\dagger\rangle\langle\hat{L}\rangle]|\psi\rangle\mathrm{d}t + \sqrt{\gamma}[\hat{L} - \langle\hat{L}\rangle]|\psi\rangle\mathrm{d}\xi, \tag{3.39}$$

where $\mathrm{d}\xi$ is a complex Wiener process defined in terms of two real independent Wiener processes $\mathrm{d}\xi^R$ and $\mathrm{d}\xi^I$: $\mathrm{d}\xi = \mathrm{d}\xi^R + \mathrm{i}\mathrm{d}\xi^I$; these obey the properties summarised in equation (3.26). Now assume the Hamiltonian can be written:

$$\hat{H} = H_0 + H_x(\hat{x}-q) + H_p(\hat{p}-p) + \frac{1}{2}H_{xx}(\hat{x}-q)^2 + \frac{1}{2}H_{pp}(\hat{p}-p)^2 + \frac{1}{2}H_{xp}[(\hat{x}-q)(\hat{p}-p) + (\hat{p}-p)(\hat{x}-q)], \tag{3.40}$$

where H_0 indicates the zeroth order in $(\hat{x} - q)$ and $H_x = \frac{\partial\hat{H}}{\partial\hat{x}}|_{\hat{x}=q}$, $H_{xx} = \frac{\partial^2\hat{H}}{\partial\hat{x}^2}|_{\hat{x}=q}$, and similarly for H_p and H_{pp}. the Lindblad operator, which in general is non-Hermitian, is written:

$$\hat{L} = L_0 + L_x(\hat{x} - q) + L_p(\hat{p} - p) \quad \text{and} \quad \hat{L}^\dagger = L_0^* + L_x^*(\hat{x} - q) + L_p^*(\hat{p} - p). \tag{3.41}$$

Going back to the wave packet in equation (3.35), in what follows we will set $\Im(\phi) = 0$; let us re-write our Gaussian ansatz for the wavefunction here:

$$\psi = \left(\frac{2b}{\pi\hbar}\right)^{\frac{1}{4}} \exp\left\{\frac{\mathrm{i}}{\hbar}[\alpha(x - q)^2 + p(x - q) + \phi]\right\}. \tag{3.42}$$

Firstly we will compute the total differential of ψ by taking its derivative with respect to all variables $\{y\}$. Being the dynamics of all such variables governed by stochastic processes we need to take into account Itô's lemma (see appendix D, equation (D.5)) and include second order derivatives in the computation of $\mathrm{d}\psi$:

$$\mathrm{d}\psi = \sum_j \frac{\partial\psi}{\partial y_j}\mathrm{d}y_j + \frac{1}{2}\sum_{j,k}\frac{\partial^2\psi}{\partial y_j y_k}\mathrm{d}y_j\mathrm{d}y_k. \tag{3.43}$$

We gather terms obtained from the total differential $\mathrm{d}\psi$ according to powers of $(x-q)$; we find:

$$(x-q)^2\left[\frac{\mathrm{i}}{\hbar}\psi\mathrm{d}a-\frac{1}{\hbar}\psi\mathrm{d}b-\frac{2}{\hbar^2}\alpha^2\psi\mathrm{d}q^2-\frac{1}{2\hbar^2}\psi\mathrm{d}p^2+\frac{2}{\hbar^2}\alpha\psi\mathrm{d}q\mathrm{d}p\right], \tag{3.44}$$

$$(x-q)\left[-\frac{2\mathrm{i}}{\hbar}\alpha\psi\mathrm{d}q+\frac{\mathrm{i}}{\hbar}\psi\mathrm{d}p-\frac{2}{\hbar^2}\alpha p\psi\mathrm{d}q^2-\frac{1}{\hbar^2}\psi\mathrm{d}p\mathrm{d}\phi+\frac{2}{\hbar^2}\alpha\psi\mathrm{d}q\mathrm{d}\phi+\frac{1}{\hbar^2}p\psi\mathrm{d}q\mathrm{d}p\right], \tag{3.45}$$

$$(x-q)^0\left[\frac{1}{4\alpha^I}\psi\mathrm{d}\alpha^I-\frac{\mathrm{i}}{\hbar}p\psi\mathrm{d}q+\frac{\mathrm{i}}{\hbar}\psi\mathrm{d}\phi+\left(\frac{\mathrm{i}}{\hbar}\alpha-\frac{1}{2\hbar^2}p^2\right)\psi\mathrm{d}q^2-\frac{1}{2\hbar^2}\psi\mathrm{d}\phi^2-\frac{\mathrm{i}}{\hbar}\psi\mathrm{d}q\mathrm{d}p+\frac{1}{\hbar^2}p\psi\mathrm{d}q\mathrm{d}\phi\right]. \tag{3.46}$$

So far we have computed the left-hand-side of equation (3.39). To compute the right-hand side we act the operators appropriately expanded in series (equations (3.40) and (3.41)) onto ψ in equation (3.42). As before we gather terms according to powers of $(x-q)$, to obtain:

$$(x-q)^2\left\{-\frac{\mathrm{i}}{2\hbar}H_{xx}-\frac{\mathrm{i}}{\hbar}2\alpha^2H_{pp}-\frac{\mathrm{i}}{\hbar}2\alpha H_{xp}-\gamma[|L_x|^2+4\alpha^2|L_p|^2+2\alpha(L_x^*L_p+L_p^*L_x)]\right\}\psi\mathrm{d}t, \tag{3.47}$$

$$(x-q)\left(\left\{-\frac{\mathrm{i}}{\hbar}H_x-\frac{\mathrm{i}}{\hbar}2\alpha H_p+\gamma[L_0^*L_x-L_0L_x^*+2\alpha(L_0^*L_p-L_0L_p^*)]\right\}\psi\mathrm{d}t+\sqrt{\gamma}(L_x+2\alpha L_p)\psi\mathrm{d}\xi\right), \tag{3.48}$$

$$(x-q)^0\left[-\frac{\mathrm{i}}{\hbar}H_0-\alpha H_{pp}-\frac{1}{2}H_{xp}+\mathrm{i}\hbar\gamma(2\alpha|L_p|^2+L_p^*L_x)\right]\psi\mathrm{d}t. \tag{3.49}$$

Before coupling up the factors of $(x-q)^0$, $(x-q)$ and $(x-q)^2$ in equations (3.44)-(3.49), we need to separate the equations into real and imaginary parts. Then, we insert expressions for the stochastic differentials $\mathrm{d}y$, where $y=\{a,b,q,p,\phi\}$; these will be of the form:

$$\mathrm{d}y=\mu_y\mathrm{d}t+\sigma_y^R\mathrm{d}\xi^R+\sigma_y^I\mathrm{d}\xi^I. \tag{3.50}$$

From the quadratic order $(x-q)^2$, we obtain:

$$\mu_a=-\frac{1}{2}H_{xx}-2(a^2-b^2)H_{pp}-2aH_{xp}-\hbar\gamma\left[8ab|L_p|^2+4b(L_x^RL_p^R+L_x^IL_p^I)\right], \tag{3.51}$$

$$\mu_b=-4abH_{pp}-2bH_{xp}+\hbar\gamma\left[|L_x|^2+4\left(a^2-b^2\right)|L_p|^2+4a(L_x^RL_p^R+L_x^IL_p^I)\right], \tag{3.52}$$

$$\sigma_{a,b}^{R,I}=0. \tag{3.53}$$

From the linear order $(x-q)$ we find, for q:

$$\mu_q = H_p - 2\hbar\gamma(L_0^R L_p^I - L_0^I L_p^R) \tag{3.54}$$

$$\sigma_q^R = \frac{\hbar\sqrt{\gamma}}{2}\left[\frac{L_x^R}{b} + 2\left(\frac{a}{b}L_p^R - L_p^I\right)\right] \tag{3.55}$$

$$\sigma_q^I = -\frac{\hbar\sqrt{\gamma}}{2}\left[\frac{L_x^I}{b} + 2\left(\frac{a}{b}L_p^I + L_p^R\right)\right], \tag{3.56}$$

and for p:

$$\mu_p = -H_x + 2\hbar\gamma(L_0^R L_x^I - L_0^I L_x^R) \tag{3.57}$$

$$\sigma_p^R = \hbar\sqrt{\gamma}\left[L_x^I + \frac{a}{b}L_x^R + \frac{2}{b}\left(a^2+b^2\right)L_p^R\right] \tag{3.58}$$

$$\sigma_p^I = -\hbar\sqrt{\gamma}\left[-L_x^R + \frac{a}{b}L_x^I + \frac{2}{b}\left(a^2+b^2\right)L_p^I\right]. \tag{3.59}$$

From the zeroth order in $(x-q)$ we find:

$$\begin{aligned}\mu_\phi^R &= pH_p - 2\hbar\gamma p(L_0^R L_p^I - L_0^I L_p^R) + \hbar^2\gamma\left[\frac{1}{4}\frac{a}{b^2}|L_x|^2 + \frac{a}{b^2}(a^2+3b^2)|L_p|^2\right.\\ &\left. + \frac{a}{b}(L_p^R L_x^I - L_x^R L_p^I) + \left(\frac{a^2+b^2}{b^2}\right)(L_x^R L_p^R + L_x^I L_p^I)\right],\end{aligned} \tag{3.60}$$

$$\sigma_\phi^{R,I} = p\sigma_q^{R,I}. \tag{3.61}$$

If we put terms back together using equation (3.50) we have:

$$\mathrm{d}a = \left\{-\frac{1}{2}H_{xx} - 2(a^2-b^2)H_{pp} - 2aH_{xp} - \hbar\gamma\left[8ab|L_p|^2 + 4b(L_x^R L_p^R + L_x^I L_p^I)\right]\right\}\mathrm{d}t, \tag{3.62}$$

$$\mathrm{d}b = \left\{-4abH_{pp} - 2bH_{xp} + \hbar\gamma\left[|L_x|^2 + 4\left(a^2-b^2\right)|L_p|^2 + 4a(L_x^R L_p^R + L_x^I L_p^I)\right]\right\}\mathrm{d}t, \tag{3.63}$$

$$\begin{aligned}\mathrm{d}q &= [H_p - 2\hbar\gamma(L_0^R L_p^I - L_0^I L_p^R)]\mathrm{d}t + \frac{\hbar\sqrt{\gamma}}{2}\left[\frac{L_x^R}{b} + 2\left(\frac{a}{b}L_p^R - L_p^I\right)\right]\mathrm{d}\xi^R\\ &\quad - \frac{\hbar\sqrt{\gamma}}{2}\left[\frac{L_x^I}{b} + 2\left(\frac{a}{b}L_p^I + L_p^R\right)\right]\mathrm{d}\xi^I,\end{aligned} \tag{3.64}$$

$$\begin{aligned} \mathrm{d}p &= [-H_x + 2\hbar\gamma(L_0^R L_x^I - L_0^I L_x^R)]\mathrm{d}t + \hbar\sqrt{\gamma}\left[L_x^I + \frac{a}{b}L_x^R + \frac{2}{b}\left(a^2+b^2\right)L_p^R\right]\mathrm{d}\xi^R \\ &\quad -\hbar\sqrt{\gamma}\left[-L_x^R + \frac{a}{b}L_x^I + \frac{2}{b}\left(a^2+b^2\right)L_p^I\right]\mathrm{d}\xi^I, \end{aligned} \tag{3.65}$$

$$\begin{aligned} \mathrm{d}\phi &= [pH_p - 2\hbar\gamma p(L_0^R L_p^I - L_0^I L_p^R)]\mathrm{d}t + \hbar^2\gamma\left[\frac{1}{4}\frac{a}{b^2}|L_x|^2 + \frac{a}{b^2}(a^2+3b^2)|L_p|^2\right. \\ &\quad \left. + \frac{a}{b}(L_p^R L_x^I - L_x^R L_p^I) + \left(\frac{a^2+b^2}{b^2}\right)(L_x^R L_p^R + L_x^I L_p^I)\right]\mathrm{d}t \\ &\quad + \frac{\hbar\sqrt{\gamma}}{2}p\left[\frac{L_x^R}{b} + 2\left(\frac{a}{b}L_p^R - L_p^I\right)\right]\mathrm{d}\xi^R - \frac{\hbar\sqrt{\gamma}}{2}p\left[\frac{L_x^I}{b} + 2\left(\frac{a}{b}L_p^I + L_p^R\right)\right]\mathrm{d}\xi^I. \end{aligned} \tag{3.66}$$

By comparing the equations above with those obtained by Heller in reference [33] we observe that whenever $\gamma = 0$ our equations match with his. We note that, as expected, when $\hbar = \gamma = 0$ the equations for p and q reduce to Hamilton's equations. Another feature of the equations above is that α does not display a stochastic motion, while the classical parameters p and q as well as the phase ϕ all do.

While the complexity of the equations above make it fairly difficult to interpret them, we can try to investigate the geometrical structure associated to them, analogously to what is done in references [56] and [57], where a similar procedure is applied in the case of a non-Hermitian Hamiltonian and in the absence of Lindblad operators. To this end let us introduce the covariance matrix G, defined in terms of the real and imaginary parts of α:

$$G = \begin{pmatrix} G_{pp} & G_{pq} \\ G_{qp} & G_{qq} \end{pmatrix} = \begin{pmatrix} \frac{1}{2b} & -\frac{a}{b} \\ -\frac{a}{b} & 2\frac{(a^2+b^2)}{b} \end{pmatrix}, \tag{3.67}$$

where we note that $\det G = 1$. We can then rewrite the equations for p and q in terms of the elements of G as follows:

$$\begin{aligned} \mathrm{d}q &= [H_p - 2\hbar\gamma(L_0^R L_p^I - L_0^I L_p^R)]\mathrm{d}t + \hbar\sqrt{\gamma}\left(G_{pp}L_x^R - G_{pq}L_p^R - L_p^I\right)\mathrm{d}\xi^R \\ &\quad -\hbar\sqrt{\gamma}\left(G_{pp}L_x^I - G_{pq}L_p^I + L_p^R\right)\mathrm{d}\xi^I \end{aligned} \tag{3.68}$$

$$\begin{aligned} \mathrm{d}p &= [-H_x + 2\hbar\gamma(L_0^R L_x^I - L_0^I L_x^R)]\mathrm{d}t + \hbar\sqrt{\gamma}\left(L_x^I - G_{pq}L_x^R + G_{qq}L_p^R\right)\mathrm{d}\xi^R \\ &\quad -\hbar\sqrt{\gamma}\left(-L_x^R - G_{pq}L_x^I + G_{qq}L_p^I\right)\mathrm{d}\xi^I \end{aligned} \tag{3.69}$$

or in vector form:

$$\begin{aligned} \mathrm{d}z &= \Omega\left[\nabla H - \hbar\gamma\left(L_0^R\nabla L^I - L_0^I\nabla L^R\right)\right]\mathrm{d}t - \hbar\sqrt{\gamma}\left(\Omega\nabla L^I - G^{-1}\nabla L^R\right)\mathrm{d}\xi^R \\ &\quad -\hbar\sqrt{\gamma}\left(\Omega\nabla L^R + G^{-1}\nabla L^I\right)\mathrm{d}\xi^I, \end{aligned} \tag{3.70}$$

where we have let $z^T = (p \quad q)$ and

$$\Omega = \begin{pmatrix} 0 & -1 \\ 1 & 0 \end{pmatrix}. \tag{3.71}$$

Similarly we can derive a vector equation for G by working out equations of motion for its elements. We have:

$$\dot{G}_{pp} = -2G_{pq}H_{pp} + 2G_{pp}H_{xp} + \hbar\gamma\left[-2G_{pp}^2|L_x|^2 - 2\left(G_{pq}^2 - 1\right)|L_p|^2 + 4G_{pq}G_{pp}(L_x^R L_p^R + L_x^I L_p^I)\right] \tag{3.72}$$

$$\dot{G}_{pq} = -G_{qq}H_{pp} + G_{pp}H_{xx} + \hbar\gamma\left\{-2G_{pq}G_{pp}|L_x|^2 - 2G_{pq}G_{qq}|L_p|^2 + 4G_{qq}G_{pp}(L_x^R L_p^R + L_x^I L_p^I)\right\} \tag{3.73}$$

$$\dot{G}_{qq} = 2G_{pq}H_{xx} - 2G_{qq}H_{xp} + \hbar\gamma\left[-2(G_{qq}G_{pp} - 2)|L_x|^2 - 2G_{qq}^2|L_p|^2 + 4G_{pq}G_{qq}(L_x^R L_p^R + L_x^I L_p^I)\right] \tag{3.74}$$

which can be expressed as

$$\dot{G} = H''\Omega G - G\Omega H'' - G\Omega^T D\Omega G + D, \tag{3.75}$$

with

$$D = 2\hbar\gamma\begin{pmatrix} |L_p|^2 & L_x^R L_p^R + L_x^I L_p^I \\ L_x^R L_p^R + L_x^I L_p^I & |L_x|^2 \end{pmatrix}. \tag{3.76}$$

Up to this point we focused on the case of a quadratic Hamiltonian, so that the dynamical scheme above provides an exact description of the open quantum dynamics. In the next section we apply this scheme to the case of a general external potential $V(\hat{x})$, which

yields a semiclassical approximation to the dynamics in terms of stochastic equations of motion for the parameters characterising the Gaussian wave packet.

3.3.2 Example: particle moving in an external potential under the influence of a heat bath

Having obtained the semiclassical dynamics for the stochastic Schrödinger equation (3.23) in the general quadratic case, we can now proceed to study a specific example by assigning a desired form to the Hamiltonian and to the Lindblad operator. As our focus is on the dynamics of a quantum particle moving in a potential $V(q)$ under the influence of a heat bath, we define $\hat{H}$ and $\hat{L}$ as follows [46], [58]:

$$\hat{H} = \frac{1}{2m}\hat{p}^2 + V(\hat{x}) + \frac{\gamma}{2}(\hat{x}\hat{p} + \hat{p}\hat{x}) \tag{3.77}$$

and

$$\hat{L} = \frac{r}{\hbar}\hat{x} + \frac{\mathrm{i}}{2r}\hat{p} \tag{3.78}$$

where $r = \sqrt{2mk_BT}$. Given equations (3.77) and (3.78), we can work out the terms appearing in the equations of motion (3.62)-(3.65) we found in the general quadratic case. Here we will not include the equation of motion for ϕ, being of little physical relevance. For the other variables we find:

$$\mathrm{d}a = \left[-\frac{1}{2}V_{xx} - \frac{2}{m}(a^2 - b^2) - 2\gamma a - \frac{2\hbar\gamma}{r^2}ab\right]\mathrm{d}t, \tag{3.79}$$

$$\mathrm{d}b = \left[-\frac{4}{m}ab - 2\gamma b + \frac{\gamma r^2}{\hbar} + \frac{\hbar\gamma}{r^2}(a^2 - b^2)\right]\mathrm{d}t, \tag{3.80}$$

$$\mathrm{d}q = \frac{p}{m}\mathrm{d}t + \frac{\sqrt{\gamma}}{2}\frac{r}{b}\mathrm{d}\xi^R - \frac{\hbar\sqrt{\gamma}}{2r}\mathrm{d}\xi^R - \frac{\hbar\sqrt{\gamma}}{2r}\frac{a}{b}\mathrm{d}\xi^I, \tag{3.81}$$

$$\mathrm{d}p = -(V_x + 2\gamma p)\mathrm{d}t + r\sqrt{\gamma}\frac{a}{b}\mathrm{d}\xi^R + r\sqrt{\gamma}\mathrm{d}\xi^I - \frac{\hbar\sqrt{\gamma}}{r}\left(\frac{a^2 + b^2}{b}\right)\mathrm{d}\xi^I. \tag{3.82}$$

We now wish to consider the classical limit of the equations above to determine whether we recover the Langevin equation. The latter, previously introduced in chapter 2, reads:

$$\mathrm{d}q = \frac{1}{m}p\mathrm{d}t \tag{3.83}$$

$$\mathrm{d}p = -(V_x + \gamma^c p)\mathrm{d}t + r\sqrt{\gamma^c}\mathrm{d}w, \tag{3.84}$$

where $\mathrm{d}w$ indicates a real Wiener process. Upon taking $\hbar \to 0$ in equations (3.79) and (3.80), one finds that both $\mathrm{d}a$ and $\mathrm{d}b$ go to infinity. However it is easy to verify numerically that:

$$\lim_{\hbar\to 0}\frac{a}{b} = 1. \tag{3.85}$$

In relation to equations (3.37), in the classical limit the wave packet is completely localised in q, while Δp goes to infinity. This is reflected by the covariant matrix G which becomes analogous to a δ-function, with $G_{pp} \to 0$, $G_{qq} \to \infty$ and the off-diagonal terms $G_{pq} = G_{qp} \to -1$ as $\hbar \to 0$. Overall, in the quantum-mechanical case we have:

$$\lim_{\hbar\to 0}\mathrm{d}q = \frac{1}{m}p\mathrm{d}t \tag{3.86}$$

$$\lim_{\hbar\to 0}\mathrm{d}p = -(V_x + 2\gamma p)\mathrm{d}t + r\sqrt{2\gamma}\mathrm{d}w. \tag{3.87}$$

where we have let $\mathrm{d}w = (\mathrm{d}\xi^R + \mathrm{d}\xi^I)/\sqrt{2}$. We have therefore shown that the stochastic Schrödinger equation postulated in the QSD approach to open quantum dynamics yields the Langevin equation in the classical limit provided the Lindblad operator is defined as in equation (3.78) and an appropriate modification is afforded to the Hamiltonian operator such that the resulting generator is of Lindblad form. Similar results to the ones presented above were obtained by Pokharel *et al.* in the case of a double-well potential with dissipation and sinusoidal driving [59], and for a general Hamiltonian by Percival and co-workers [60].

Let us now present some numerical examples that show how the semiclassical dynamics encoded in equations (3.79)-(3.82) compares to the classical and quantum-mechanical counterparts, which are obtained via equations (2.63), (2.64) and (3.39) respectively.

All trajectories are obtained via the numerical schemes outlined in appendix C. We use the same symmetric double-well potential as we did in chapter 2 (figure 2.3) to investigate

classical transition rate theory, as well as the system of dimensionless units of measure outlined, as before, in appendix B. Note that in our system of units the distance between metastable states is 2, the height of the energy barrier is $\frac{3}{4}$, $\hbar$ takes the value 0.123 and the tunnelling time is $t_T \sim 160 \times 10^3$. In the present chapter we compare trajectories starting at $q = 1$; this allows us to better appreciate the dynamical effects arising in the different regimes we analyse. In both the semiclassical and quantum-mechanical case we show the trajectory of the particle in black and its uncertainty in the position coordinate in red; the latter is defined as:

$$\Delta x = \sqrt{\langle \hat{x}^2 \rangle - \langle \hat{x} \rangle^2}. \tag{3.88}$$

In figures 3.1, 3.2, 3.3 and 3.4 we compare semiclassical, quantum and classical dynamics. For each we present two realisations of the stochastic time evolution. The four regimes we consider are: $T = 0.01$ and $\gamma = 0.1$, shown in figure 3.1; $T = 0.01$ and $\gamma = 0.5$, shown in figure 3.2; $T = \gamma = 0.1$, shown in figure 3.3; and $T = \gamma = 0.5$, shown in figure 3.4.

In the top panel of figure 3.1 we have the semiclassical dynamics at $T = 0.01$ and $\gamma = 0.1$. We notice how both trajectories in figures 3.1a and 3.1b perform frequent transitions across $q = 0$. By looking at the evolution of the position uncertainty Δq, we find that this oscillates between its initial value, 0.25, and values as high as 0.65. In the potential under study the distance between the saddle point at $q = 0$ and the intercepts of $V(q)$ with the q-axes is equal to $\sqrt{2} = 1.41$, hence with a spread Δq that reaches approximately 46% of the total width of the wells we can say that in these trajectories delocalisation effects play an important role.

By looking at figures 3.1c, 3.1d we see that although semiclassical and quantum-mechanical dynamics share some qualitative similarities, namely the fact they both display frequent transitions across the barrier and a large uncertainty in the position coordinate, from a quantitative standpoint the two dynamics are rather different. In particular the oscillations found in semiclassics are much wider than those we find in quantum-mechanics, and significantly more frequent. At the same time, interestingly, the position uncertainly in the quantum-mechanical trajectories, Δx, appears to be on average larger than the correposding quantity in semiclassics, Δq. An hypothesis as to why this happens

is that at low temperature we do not have strong decoherence effects taking place in the quantum-mechanical trajectories and while the wave packet is very spread it always stays roughly within the neighbourhood of the two energy minima. The semiclassical dynamics does capture a large position uncertainty but it does not take into account interference effects, and the semiclassical wave packet is allowed to sample a much larger region of the potential surface.

In figures 3.1e and 3.1f we observe that the classical trajectories at $T = 0.01$ and $\gamma = 0.1$ stay trapped near the minimum throughout the duration of the simulation, unlike the semiclassical and quantum-mechanical counterparts. Overall, for $T = 0.01$ and $T = 0.1$ we are in a regime where transitions are dominated by quantum delocalisation effects, which drive both semiclassical and quantum-mechanical trajectories frequently across the barrier. On the other hand the classical trajectories remain trapped an the fixed point located at $q = 1$ withour ever acquiring enough energy to move over the barrier.

In figure 3.2 we study all three types of dynamics with $T = 0.01$ and $\gamma = 0.5$. As in the previous case, we find that semiclassical and quantum-mechanical trajectories are qualitatively rather similar, while the classical ones behave in a totally different way: this makes sense as we are still in a low-temperature regime. In figures 3.2a and 3.2b, portraying the semiclassical trajectories, we find frequent transitions across the energy barrier and uncertainty Δq that stays roughly between 0.25 and 0.5; the trajectories in figures 3.2c and 3.2d, showing the corresponding quantum-mechanical case, display a similar behaviour. However, we observe that the uncertainty displayed by the quantum dynamics is on average much larger than the one we find in classics, similarly to the previous low-temperature example with $\gamma = 0.1$, in figure 3.1. Further, we notice that now the semiclassical dynamics undergoes fewer transitions than the quantum-mechanical counterpart, arguably as a result of the smaller width in q. By comparing the semiclassical and quantum-mechanical trajectories in figures 3.1 and 3.2 we observe another interesting feature: that raising the value of the coupling coefficient from 0.1 to 0.5 has opposite effects in the semiclassical and quantum-mechanical dynamics. In going from $T = 0.01$ and $\gamma = 0.1$ to $T = 0.01$ and $\gamma = 0.5$ the semiclassical trajectory is characterised by a smaller uncertainty and fewer transitions; the quantum-mechanical dynamics, on the other hand, features a larger uncertainty when $\gamma = 0.5$ and more

transitions. Determining the causes of this feature would be an interesting expansion to the investigation carried out here.

In figure 3.3 we show the dynamics for $T = \gamma = 0.1$. We find that in this case semiclassical, quantum-mechanical and classical dynamics all look very similar: they all feature trajectories that remain trapped in the metastable state throughout the duration of the simulation. This is explained by considering that with the temperature and the coupling coefficient at this medium level there is not enough thermal energy available to activate the trajectories across the barrier, and at the same time the temperature is not low enough for delocalisation effects to play a role in semiclassics and quantum-mechanics. Note that while here we are generally assuming that delocalisation effects are stronger at lower temperatures, the relationship between temperature and delocalisation is non-trivial, as discussed in reference [50]. It is interesting to notice that in this regime the classical dynamics is the one displaying wider oscillations about the minimum compared to semiclassical and quantum-mechanical counterparts, which remain highly localised in the neighbourhood of $q = 1$.

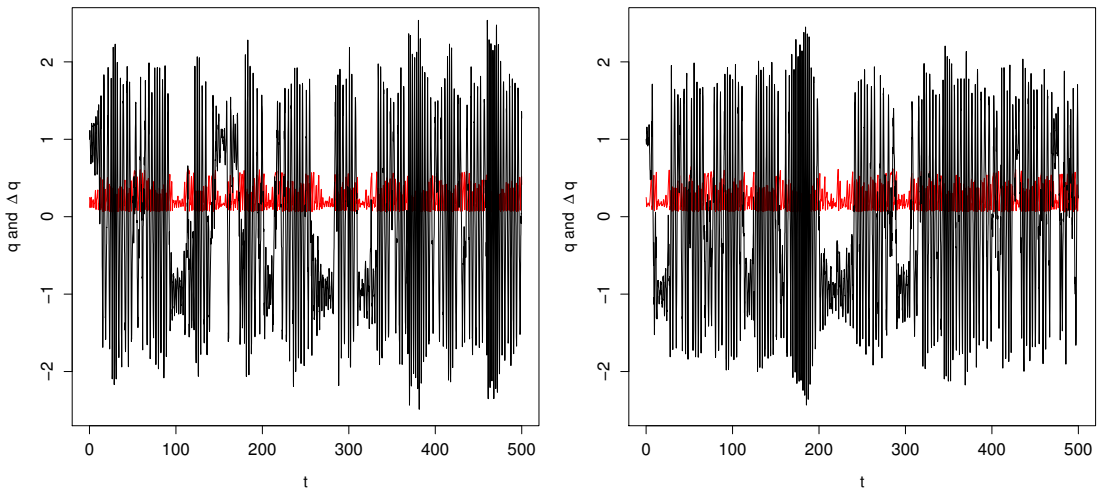
In the case where $T = \gamma = 0.5$, shown in figure 3.4, all three types of dynamics display frequent oscillations about $q = 0$. Curiously, in this high-temperature regime semiclassical and classical trajectories are very similar to each other, while the quantum-mechanical ones seem quantitatively rather different; in particular the number of crossings over the barrier observed in classics and semiclassics is significantly smaller than the one we have in quantum-mechanics. This fact should not come as a surprise in that, as we showed above, the semiclassical equations of motion reduce to the classical ones in the classical limit; while the quantum dynamics is expected to become increasingly similar to the classical one as T increases the equation governing it is fundamentally different. By comparing these results with the ones we found in figure 3.2 we see that in regimes with large γ the QSD trajectories appear to be more sensitive to the stochastic contribution to the dynamics, while the semiclassical ones display the dissipative effects more noticeably. This is another aspect which could be worthwhile investigating further in future work.

Overall we can say for $T \geq 0.1$ and $\gamma \geq 0.1$ we are in a region of parameter space where quantum effects are less significant and the semiclassical and quantum dynamics

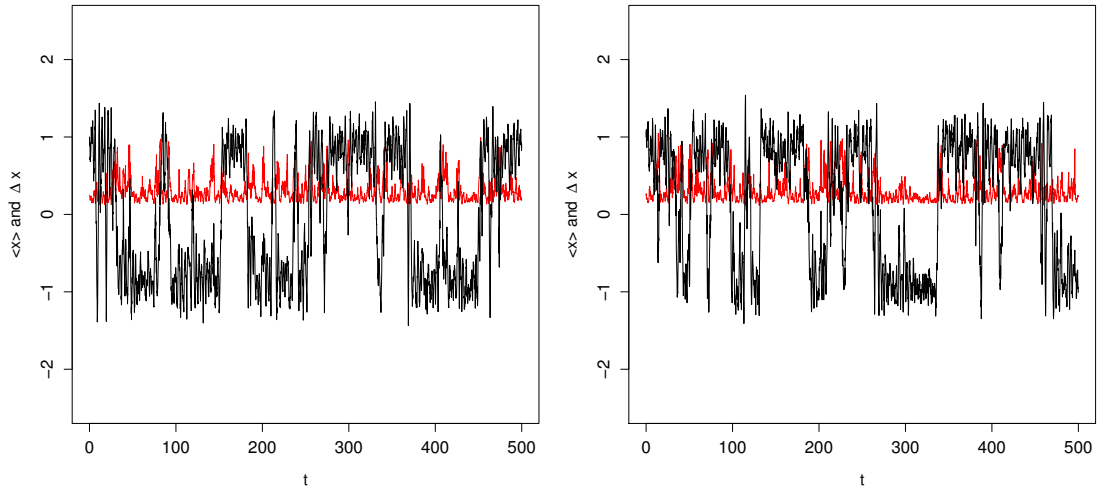
become more similar to the classical counterpart. This is reflected by the fact that at such temperatures the spread along the position coordinate stays localised around its initial value throughout time evolution in both semiclassics and quantum mechanics.

Finally in figure 3.5 we show an example where the semiclassical equations (3.79)-(3.82) fail to deliver meaningful results. This happens when the value of the coupling coefficient is very low, $\gamma = 0.01$. By looking at the red line representing Δq in figure 3.5a, we see that unphysical results for the trajectory are obtained after Δq has taken especially large values. In the quantum-mechanical counterpart of this trajectory, shown in figure 3.5b, we see that Δx stays localised around 0.2 throughout time evolution and the trajectory remains trapped at $q = 1$, similarly to the classical case. In particular Δq reaches values as high as 1.35, when the total distance between the intercepts of $V(q)$ along the positive and negative axes is $2\sqrt{2} = 2.83$. In equation (3.80) we see that $\dot{b} \propto \gamma T$ and from equation (3.37) we have that $\Delta q \propto (\sqrt{b})^{-1}$, hence Δq does indeed get large when γ is small and T is not very large, like the present case. So it makes sense to expect that our semiclassical scheme can yield unphysically large values for the position uncertainty within regions of (T, γ)-space characterised by small γ's. As a result the semiclassical trajectory features oscillations of increasingly large amplitude, up to the point where we find $q(t)$ beyond -4 and 4. On the other hand, we saw in the previous examples sthat the quantum-mechanical trajectories can occasionally feature large uncertainties but the motion remains localised near the potential minima. This can be related to what we saw in the examples with $T = 0.01$, that a purely quantum-mechanical system at low temperature can have a large uncertainty in the position but as it intereferes with itself the trajectory stays near the bottom of the wells; in the semiclassical case interference effects are not captured so large uncertainties can result in very large, and occasionally unphysically large oscillations over the energy barrier.

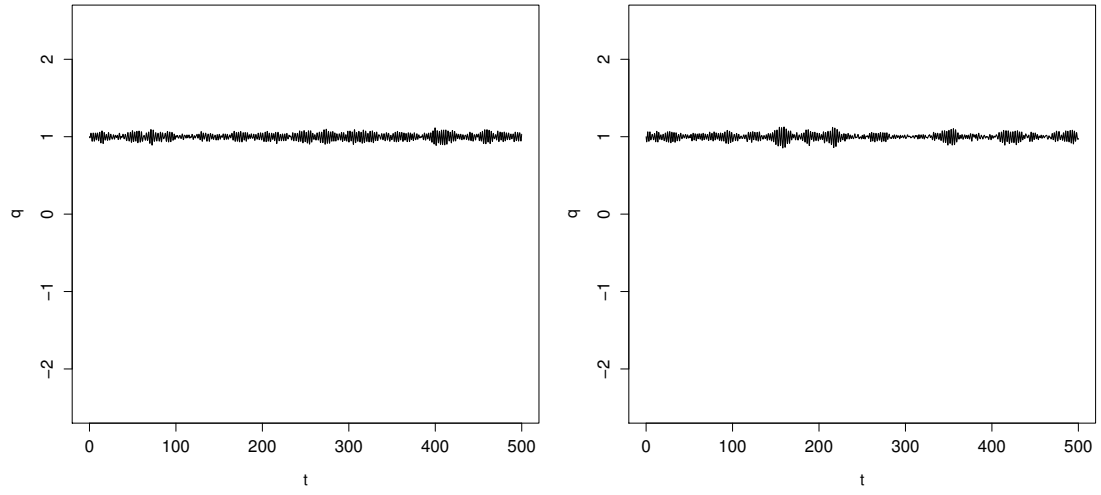
Having dived into the features of open quantum dynamics we can move on to the final stage of our discussion: in the next chapter we show how temperature-dependent quantum dynamics can be used to obtain the quantum-mechanical transmission coefficient in a novel way.



(A) (B)

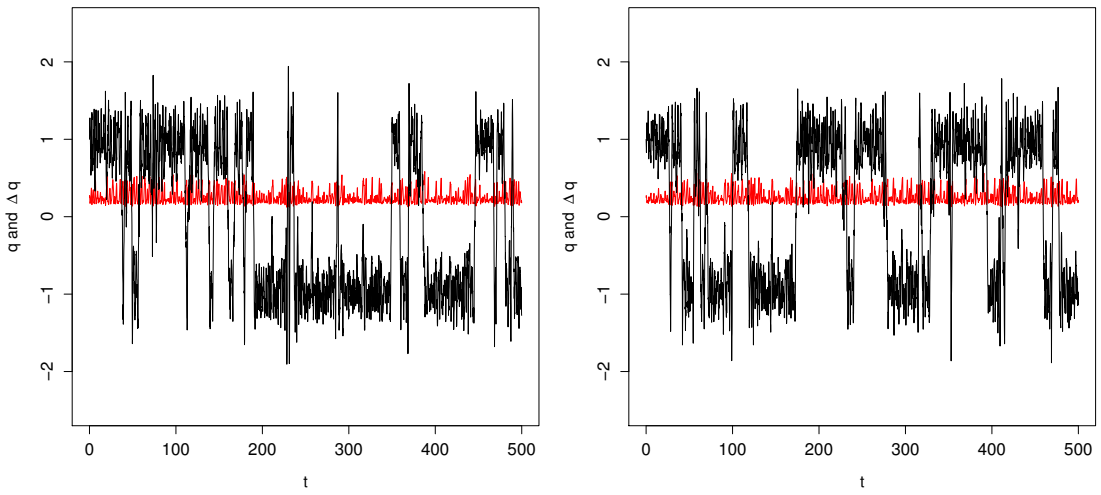


(C) (D)

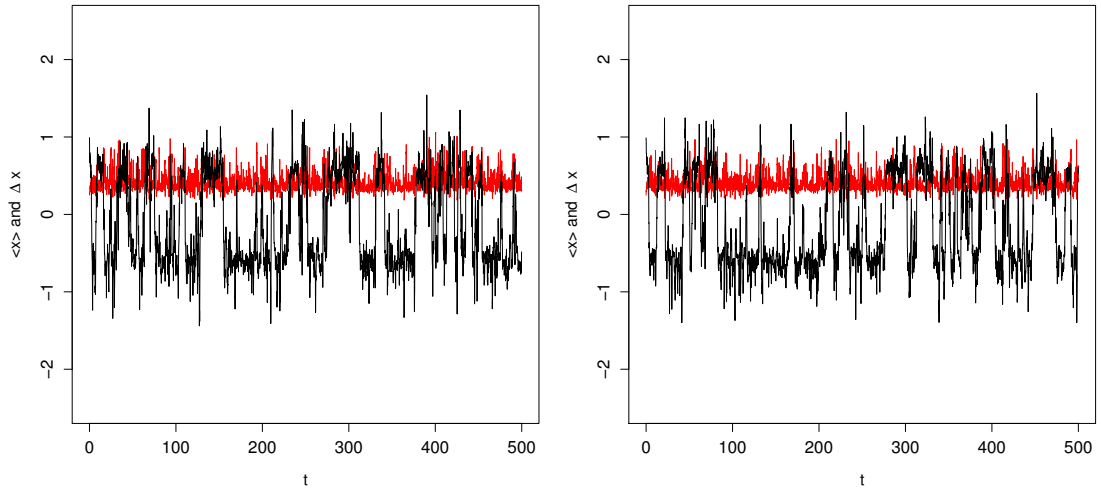


(E) (F)

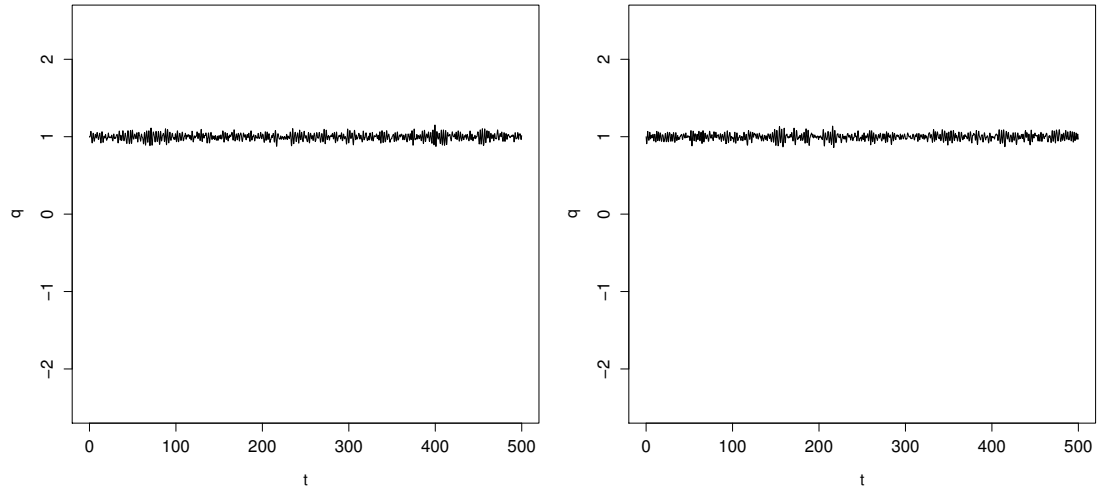
FIGURE 3.1: $T = 0.01$, γ=0.1. Top panel, in (A) and (B): stochastic semiclassical dynamics from equations (3.79)-(3.82). Middle panel, in (C) and (D): stochastic quantum dynamics from equation (3.23). Bottom panel, in (E) and (F): stochastic classical dynamics from equations (2.63) and (2.64).



(A) (B)

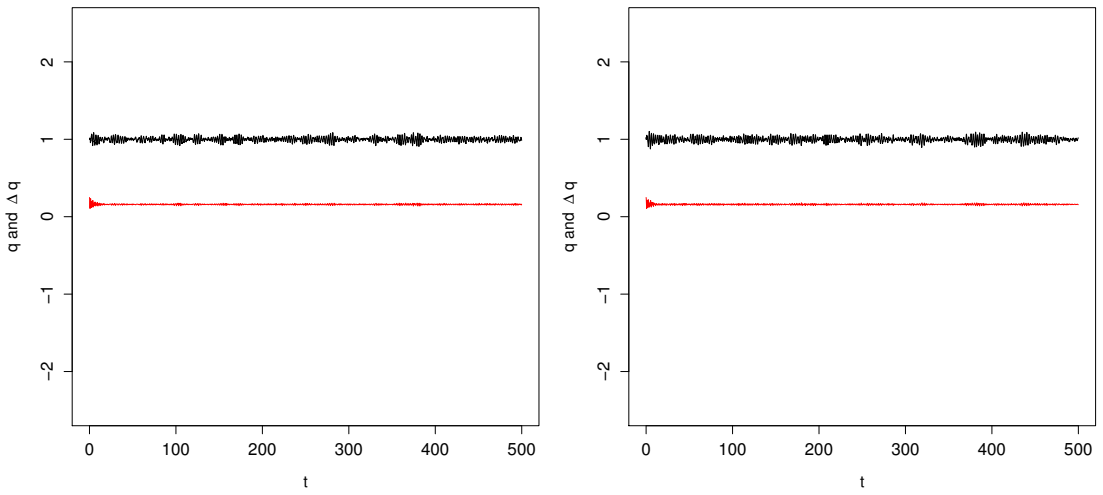


(C) (D)

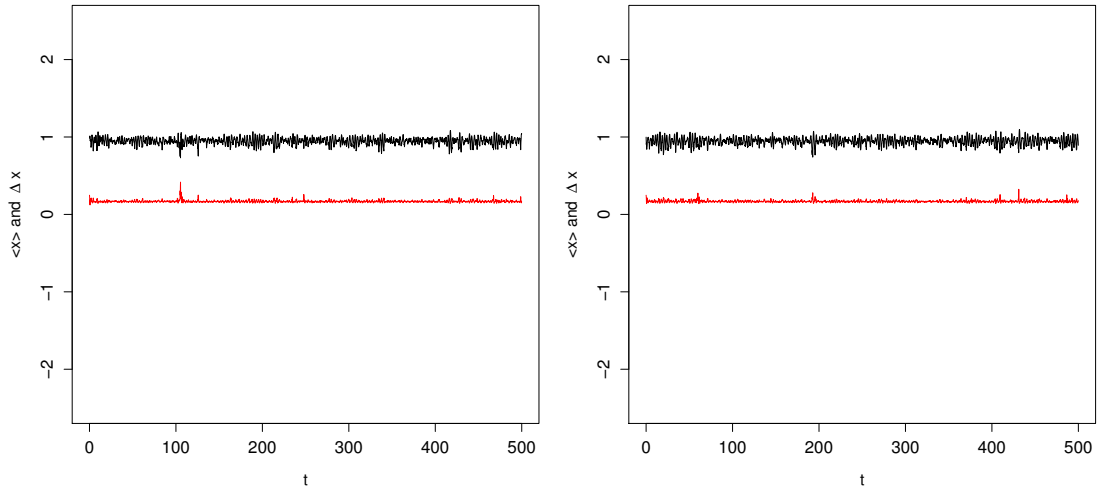


(E) (F)

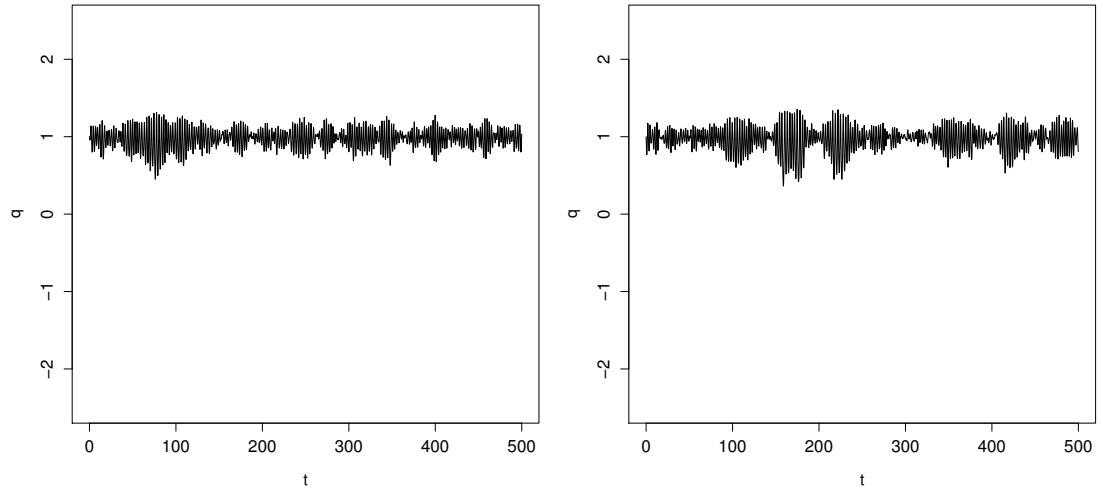
FIGURE 3.2: $T = 0.01$, γ=0.5. Top panel, in (A) and (B): stochastic semiclassical dynamics from equations (3.79)-(3.82). Middle panel, in (C) and (D): stochastic quantum dynamics from equation (3.23). Bottom panel, in (E) and (F): stochastic classical dynamics from equations (2.63) and (2.64).



(A) (B)

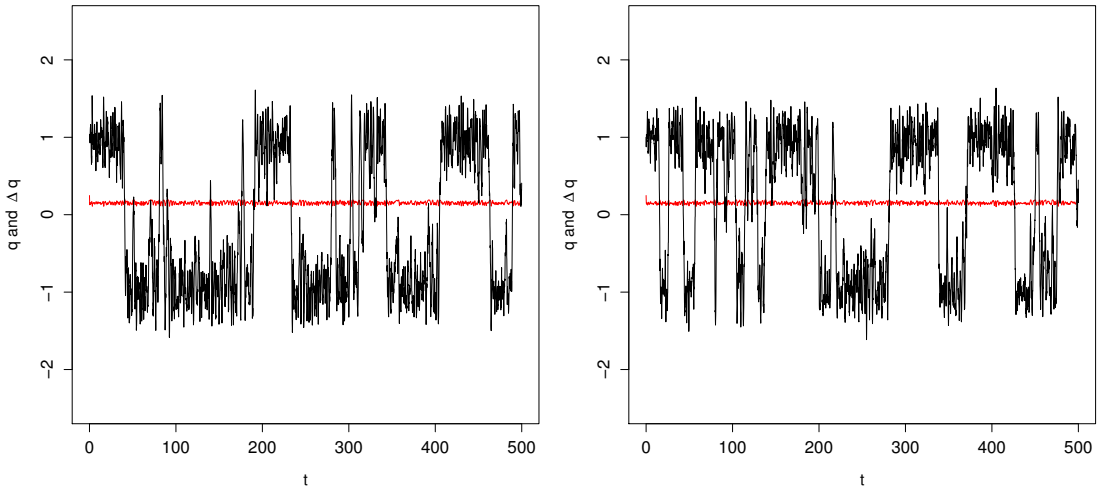


(C) (D)

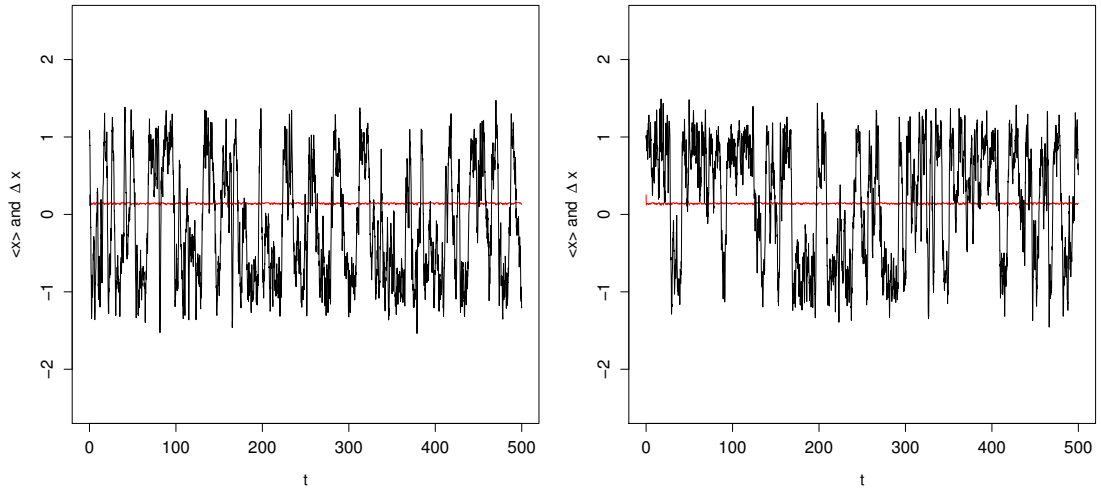


(E) (F)

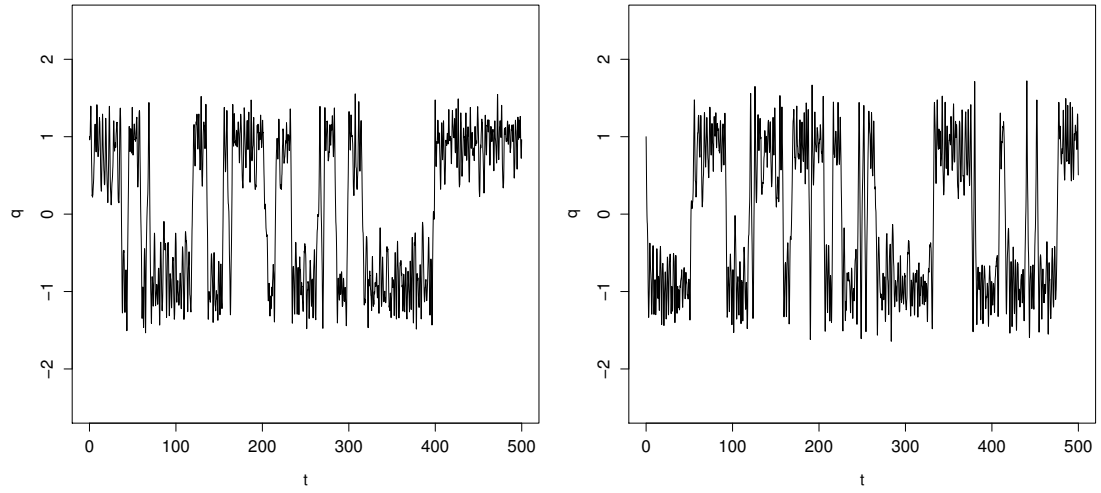
FIGURE 3.3: $T = \gamma = 0.1$. Top panel, in (A) and (B): stochastic semiclassical dynamics from equations (3.79)-(3.82). Middle panel, in (C) and (D): stochastic quantum dynamics from equation (3.23). Bottom panel, in (E) and (F): stochastic classical dynamics from equations (2.63) and (2.64).



(A) (B)

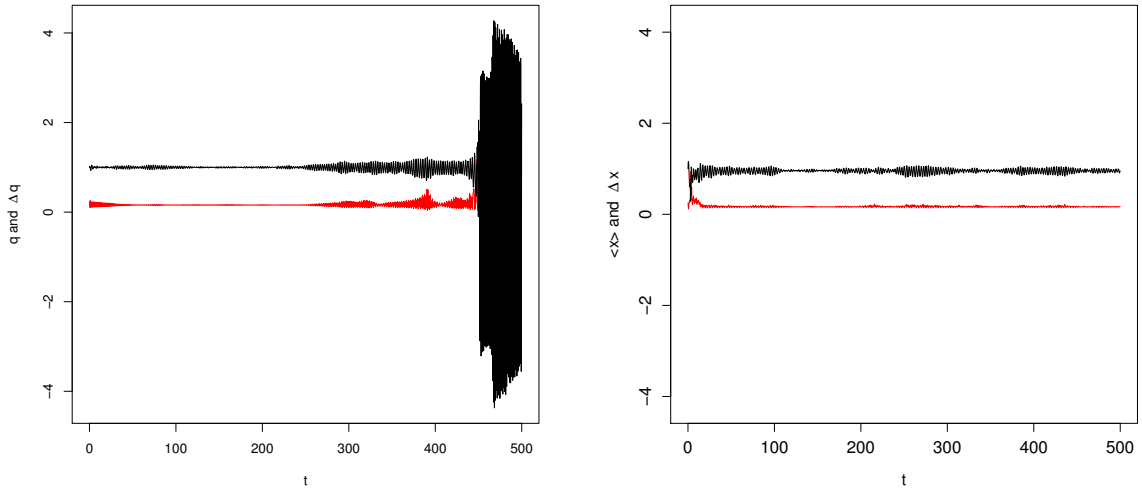


(C) (D)

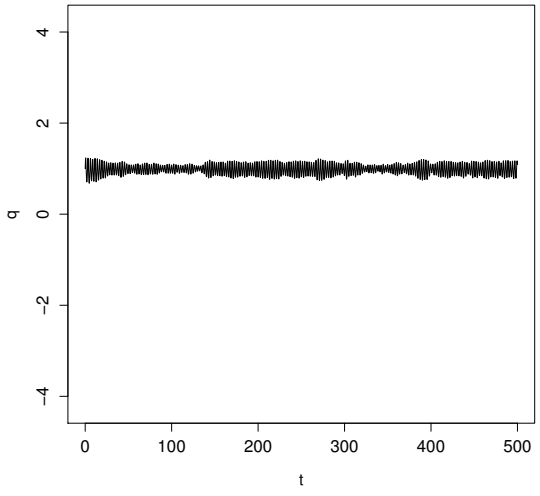


(E) (F)

FIGURE 3.4: $T = \gamma = 0.5$. Top panel, in (A) and (B): stochastic semiclassical dynamics from equations (3.79)-(3.82). Middle panel, in (C) and (D): stochastic quantum dynamics from equation (3.23). Bottom panel, in (E) and (F): stochastic classical dynamics from equations (2.63) and (2.64).



(A) (B)



(C)

FIGURE 3.5: $T = 0.1$, γ=0.01. In (A): stochastic semiclassical dynamics from equations (3.79)-(3.82). In (B): stochastic quantum dynamics from equation (3.23). In (C): stochastic classical dynamics from equations (2.63) and (2.64).

Chapter 4

Quantum transition rate theory of a 1-d double-well system

In this chapter we first present our formulation of the quantum-mechanical transmission coefficient $\kappa(t)$; the novelty we introduce is the fact that the time-dependent state function $\theta(t)$ is written in terms of the density operator, which evolves according to the Lindblad equation. Hence our expression enables us to study the dynamical effects arising in quantum TRT explicitly as a function of the temperature and the coupling coefficient γ, analogously to the Langevin-based approach we took in classical TRT. The quantum transmission coefficient we introduce features the expectation values of the position and momentum operator which substitute the classical position and momentum appearing in the classical transmission coefficient. We use Gaussian coherent states to perform the expectation values and to define the intial configuration of our system: in classical TRT one initiates the system by giving the particle a position and a momentum; in quantum-mechanics, where the uncertainty principle would not allow to do the same, using Gaussian coherent states we place the centre of the wave packet at the desired point in phase space.

We study in detail quantum transition rate theory using our formulation for $\kappa(t)$. In particular, we compute numerically the open quantum trajectories that will feed into the calculation of the transmission coefficient for different values of T and γ. This allows

us to see in which parameter regimes we expect TRT to apply, and where we expect it not to be applicable – similarly to what we did in chapter 2 in the classical case. We then compute the quantum transmission coefficient in these regimes and compare it to the classical counterpart. We find that in certain regions of (T, γ)-space the quantum and classical correlation functions share some strong qualitative similarities, while in other regimes, especially at low temperature, we observe significant divergences between the two. As predicted by a result well-known in the literature ([16]), we find that the quantum correlation function vanishes at $t = 0$, so that a TST value of the quantum rate cannot be defined via the limit as $t \to 0^+$ of the reactive flux correlation function as it is done in the classical case. We find that the quantum transmission coefficient displays the "plateau" predicted by classical TRT in parameter regimes where the separation of time scales between macroscopic transitions and microscopic fluctuations applies. In comparison to the classical value of the plateau, the quantum-mechanical value we obtain tends to be smaller. On the other hand, we observe that when such separation does not apply the quantum correlation function decays to zero exponentially fast, similar to what we find classically.

4.1 Novel formulation of quantum transition rate theory

We saw in the previous section that there is still no consensus as to how to translate the transition rate and its TST approximation to quantum-mechanics. Here we propose an entirely different approach by incorporating the quantum dynamics of activated processes explicitly into the formulation of the quantum transition rate. The importance of this aspect has also been noted in the context of quantum TST ([1]), however it is apparent that it is even more pivotal in transition rate theory, which is by nature a dynamical theory.

In particular we wish to study the dynamical effects arising in quantum transition rate

theory by directly evaluating the average over momenta in equation (2.48), suitably translated into its operator version. Let us now outline our procedure to obtain a quantum-mechanical expression for the transmission coefficient. For clarity we re-write equation (2.48) here:

$$\kappa^c(t) = \frac{1}{\langle p_0 \rangle_{p_0^+}} \langle p_0 \theta^c(t)|_{q_0=q^*} \rangle_{p_0}. \tag{4.1}$$

We focus on the average over momenta in the numerator as this is the contribution containing the dynamical information we are interested in, while $\langle p_0 \rangle_{p_0^+}$ is a constant.

Our approach differs from previous formulations in that we do not define a quantum-mechanical analogue of the classical transition rate and then attempt to derive the quantum transmission coefficient from it; instead we evaluate a quantum-mechanical version of the momentum average appearing in the classical transmission coefficient introduced by Chandler in reference [31]. In chapter 2 we stressed that the transmission coefficient contains the dynamical information which allows us to answer the key questions of transition rate theory: whether TRT can be applied to the system under study; whether the TST approximation is accurate for the system of interest; and to obtain the value of the true transition rate k^c. Further, generalising the path-sampling expression for $\kappa^c(t)$ to quantum-mechanics directly allows one to bypass the well-known problem that the quantum-mechanical version of the TST rate is zero, as we do not include the transition-state contribution to the rate and we consider only the dynamical contribution given by the transmission coefficient. Nevertheless, as we shall see, the transmission coefficient we derive shares with alternative formulations the property of vanishing in the limit as $t \to 0$.

The correlation function in equation (4.1) counts the number of trajectories which, starting at the dividing point q^* at $t = 0$, are found in the positive x-semiaxis at time t; this is weighted by the initial momentum p_0 corresponding to each trajectory and averaged over the distribution of initial momenta. In the classical case we saw that $\theta^c(t)$ is a heaviside step function $H[q(t)]$ of $q(t)$ meaning that if the trajectory at time t is in the positive x-semiaxis θ^c is equal to one, and it is zero otherwise. This definition relies on the position of the classical particle being identifiable with a δ-function of $q(t)$; in quantum mechanics this is no longer the case, and there is a finite probability that an individual particle is

in the positive semiaxis at any given time. We introduce the quantum analogue of the heaviside step function as the projection operator $\hat{P}$, which in position representation can be written:

$$\hat{P} = \int_0^\infty |x\rangle\langle x| \mathrm{d}x. \tag{4.2}$$

In one dimension, the quantum-mechanical analogue of $\theta^c(t)$, which we call $\theta(t)$, is obtained by computing the expectation value of the projection operator $\hat{P}$ in the quantum state at time t which gives the *probability* to find the particle in the positive q-semiaxis at time t. The probability to find a quantum particle described by the density operator $\hat{\rho}$ in state B – *i.e.*, the positive x-semiaxis, is given by the trace of the projection operator $\hat{P}$ in equation (4.2) acting on the density operator, that is:

$$\theta(t) = \mathrm{tr}\ \hat{P}\hat{\rho}. \tag{4.3}$$

In comparison to the definition of the characteristic function θ^c in classical mechanics, in the quantum-mechanical case θ varies continuously from 0 to 1, as one would expect.

We now need to identify a quantum-mechanical analogue of the momentum p_0 and the position q_0 appearing in the classical expression (4.1). We choose to use a Gaussian wave packets to describe the quantum initial states. This is for two reasons. Firstly, in the classical system the average is taken over trajectories that are initially located at the dividing point q^* and whose initial momentum is sampled from a Boltzmann distribution, however in quantum mechanics position and momentum cannot both be simultaneously well-defined. A coherent state is as close as we can get to having both values well-defined. Secondly, coherent states provide a picture of quantum states that closely resembles the classical idea of a particle, thus making such states conceptually convenient tools in TRT. Then in the quantum-mechanical case the quantities p_0 and q_0 are given by with the expectation values with respect to Gaussian states $|\psi\rangle$ of the quantum observables at time zero:

$$p_0 \quad \mapsto \langle\psi(0)|\hat{p}|\psi(0)\rangle = \langle\hat{p}_0\rangle \tag{4.4}$$

$$q_0 \quad \mapsto \langle\psi(0)|\hat{x}|\psi(0)\rangle = \langle\hat{x}_0\rangle. \tag{4.5}$$

The quantum-mechanical transmission coefficient $\kappa(t)$ can now be obtained by performing an average over a distribution of expected momenta $\langle\hat{p}_0\rangle$, which we indicate with the symbol $\mathcal{M}_{\langle\hat{p}_0\rangle}$ in order not to confuse averaging with computing the quantum expectation values. Overall, for $\kappa(t)$ we have:

$$\kappa(t) = \mathcal{M}_{\langle\hat{p}_0\rangle}[\langle\hat{p}_0\rangle\theta(t)|_{\langle\hat{x}_0\rangle=q^*}]. \tag{4.6}$$

Here $\langle\hat{p}_0\rangle$ is the expectation value of the momentum operator at $t = 0$ and the state function $\theta(t)$ is computed via equation (4.3) using initial states such that $\langle\hat{x}_0\rangle = q*$. By means of equation (4.6) one can study the time-dependent effects arising in quantum transition rate theory. The novelty we introduce is that the time evolution of the density operator encoded in the state function $\theta(t)$ takes into account the interaction of the quantum particle with a heat bath.

We choose to define the initial states as minimum-uncertainty Gaussian wave packets in p and q. This provides a physical interpretation of the different behaviour displayed by quantum and classical transmission coefficients for very small times. While classical states in coordinate space can be thought of as δ-functions centred at $q(t)$, a coherent state can be described as a Gaussian wave packet of a given width whose mean is centred at $q(t)$. For infinitely small times, that is in the limit as $t \to 0^+$, a δ-function that was centred at $q = 0$ at $t = 0$ is fully localised at $q' = q(0 + \delta t) \approx q(0)$; conversely the quantum wave packet will have only moved its mean to the new location $q' \approx q(0)$. In other words, assuming that at $t = 0$ a classical and a quantum particle are centred at $q = 0$ and are given a positive momentum, the probability to find the classical particle in the positive semiaxis at $t = 0 + \delta t$ is 1, whereas the probability to find the quantum particle in the positive semiaxis at $t = 0 + \delta t$ is $\frac{1}{2} + \epsilon$, where ϵ is a very small positive number. So for very small times δt the average appearing in equation (4.6) is still zero since it entails a product of an odd by an even function integrated over the entire p-axis, while the average in equation (4.1) is positive.

Our approach is conceptually rather simple compared to previous formulations in that it essentially rephrases the classical transmission coefficient in terms of the expectation values of the position and momentum operators and a quantum mechanical version of

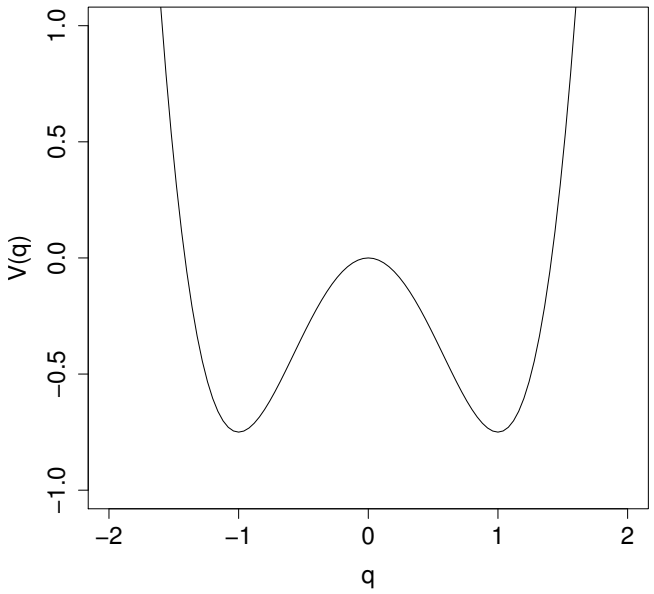


FIGURE 4.1: Schematic representation of the potential used in the quantum mechanical simulations to compute the dynamical trajectories and transmission coefficient κ. We use the dimensionless units discussed in appendix B.

the state function $\theta(t)$. Additionally, because the evolution of the density operator is given by a deterministic, linear first-order differential equation our approach is also computationally accessible for simple systems. What distinguishes the approach proposed here from other formulations of quantum TRT is that we explicitly bring the quantum activated dynamics into the formulation of the quantum rate. In the next sections we apply this approach to a 1-dimensional double-well system and compare the results with what we found in the classical case, presented in chapter 2.

4.2 Model and implementation

Here we investigate the dynamics and transition rate theory generated in the quantum-mechanical counterpart of the model used in chapter 2. To compute the quantum-mechanical rate $\kappa(t)$ we use the theory based on the evolution of the density operator outlined in section 3.1; to study the quantum dynamics we employ the QSD method outlined in section 3.2. In particular we study a hydrogen atom moving a 1-d double-well

potential such as the one we used in both the classical and semiclassical case, represented here in picture 4.1. For more details about how our toy model is related to a model of hydrogen in iron see appendix B.

Our implementation of both temperature-dependent quantum dynamics and quantum transition rate theory relies on the representation of state vectors in terms of coherent states. While for the semiclassical dynamics examined in chapter 3 we adopted a coordinate representation of coherent states, here we express coherent states in matrix form using the harmonic oscillator basis [61]. A quantum state $|\psi\rangle$ is thus expressed as

$$|\psi\rangle_z = e^{-\frac{1}{2}|z|^2} \sum_{n=0}^{\infty} \frac{z^n}{\sqrt{n!}} |n\rangle, \tag{4.7}$$

where $|n\rangle$ indicates the n-th eigenvector of the harmonic oscillator Hamiltonian and z is the eigenvalue of the annihilation operator $\hat{a}$ associated to the eigenvector ψ. The Glauber coherent state above can be seen as an eigenstate of the annihilation operator $\hat{a}$ and it is a localised state in phase space, with equal uncertainties in p and q given by $\sqrt{\frac{\hbar}{2}}$ [62]. The $|n\rangle$ eigenstates of the harmonic oscillator Hamiltonian in the harmonic oscillator basis are just vectors of zeroes with a 1 at the n-th entry; hence implementing equation (4.7) reduces to computing the following vector:

$$|\psi\rangle_z = e^{-\frac{1}{2}|z|^2} \begin{pmatrix} \frac{z^0}{\sqrt{0!}} \\ \frac{z^1}{\sqrt{1!}} \\ \dots \end{pmatrix}. \tag{4.8}$$

In this formalism, the initial momentum and position of the wave vector are assigned via the eigenvalue z in coordinate representation, that is:

$$z = \sqrt{\frac{m\omega}{2\hbar}} q + \mathrm{i} \frac{1}{\sqrt{2m\omega\hbar}} p, \tag{4.9}$$

where we have used the notation $p = \langle \hat{p} \rangle$ and $q = \langle \hat{x} \rangle$.

For the calculation of quantum-mechanical trajectories, equation (4.8) can be used to give the initial state a position and momentum of choice; in quantum transition rate

theory we always pick $q = 0$ and p from a Boltzmann distribution, analogously to what we did in the classical case to evaluate the trasmission coefficient κ^c - see equation (2.48).

For the quantum-mechanical transmission coefficient defined in equation (4.6), which we report here:

$$\kappa(t) = \mathcal{M}_{\langle\hat{p}_0\rangle}[\langle\hat{p}_0\rangle\theta(t)|_{\langle\hat{x}_0\rangle=q^*}], \tag{4.10}$$

we integrate the deterministic Lindblad equation using a standard order-four Runge-Kutta algorithm, as explained in more detail in appendix D. Once the density operator is known at all desired times, the quantum state function θ can be determined, which gives the time-dependent contribution to κ. The quantum state function $\theta(t)$, defined in equation (4.3) can be written as follows

$$\text{tr } \hat{P}\hat{\rho} = \sum_n \int_0^\infty \langle n|x\rangle\langle x|\hat{\rho}|n\rangle \mathrm{d}x \tag{4.11}$$

$$= \sum_{nm} \int_0^\infty \langle n|x\rangle\langle x|m\rangle\rho_{mn}\mathrm{d}x, \tag{4.12}$$

where $|n\rangle$, $|m\rangle$ are the harmonic oscillator eigenstates and ρ_{mn} are the matrix elements $\langle m|\hat{\rho}|n\rangle$. The eigenfunctions $\psi_n(x) = \langle x|n\rangle$ can be expressed as follows:

$$\psi_n(x) = \frac{1}{\sqrt{2^n n!}} \left(\frac{m\omega}{\pi\hbar}\right)^{\frac{1}{4}} e^{-\frac{m\omega}{2\hbar}x^2} H_n\left(\sqrt{\frac{m\omega}{\hbar}}x\right), \tag{4.13}$$

where m and ω are the harmonic oscillator's parameters and H_n indicates the Hermite polynomial:

$$H_n(z) = (-1)^n e^{z^2} \frac{\mathrm{d}^n}{\mathrm{d}z^n} e^{-z^2}. \tag{4.14}$$

Overall, for the quantum-mechanical state function $\theta(t)$ we find:

$$\theta(t) = \sum_{nm} \rho_{mn}(t) I_{nm}, \tag{4.15}$$

where:

$$I_{nm} = \frac{1}{\sqrt{\pi}} \int_0^\infty \frac{H_n(x)}{\sqrt{2^n n!}} \frac{H_m(x)}{\sqrt{2^m m!}} e^{-x^2} \mathrm{d}x. \tag{4.16}$$

We compare the quantum transmission coefficient in equation (4.10) to its classical counterpart, κ^c, which we introduced in chapter 2 and we re-write here:

$$\kappa^c(t) = \sqrt{\frac{2\pi\beta}{m}}\langle p_0\theta^c(t)|_{q_0=q^*}\rangle_{p_0}. \tag{4.17}$$

However, because our definition of the transmission coefficient in quantum mechanics only considers the average over momenta in the equation above, and does not include the multiplicative factor in front of the average which is related to the classical transition state theory contribution to the rate, we actually compare κ to the following quantity:

$$\tilde{\kappa}^c(t) = \langle p_0\rangle_{p_0^+}\kappa^c(t) = \langle p_0\theta^c(t)|_{q_0=q^*}\rangle_{p_0}, \tag{4.18}$$

where we use the classical momentum factor $\langle p_0\rangle_{p_0^+} = \sqrt{\frac{m}{2\pi\beta}}$ which was previously introduced in equation (2.38). Note however that because in our system of units $m = 1$, in reference to equation (2.42) we have that $\tilde{\kappa}^c(t) = \langle p_0\rangle_{p_0^+}\kappa^c(t) = \langle v\rangle\kappa^c(t)$.

Along with the quantum rates, we also compute the open QSD dynamics, given in equation (3.23), by means of a modified version of the fourth-order Runge-Kutta algorithm, as outlined in appendix D. We also evaluate the time-dependent position uncertainty Δx of the wave packet along x, as a measure of the degree of localisation of the quantum state in time; this is defined as the standard deviation of the operator $\hat{x}$, defined as in euqation 3.88. In the following two section we present the results for the dynamics first, and the results for the rates next.

4.3 Results – quantum and classical dynamics

We start by looking at the quantum and classical trajectories in a low-temperature regime, with $T = 0.01$; the relevant figures are 4.2 for the quantum-mechanical case and 4.3 for the classical case. Firstly we notice that in this low-temperature regime quantum and classical dynamics differ significantly, as we expect. In particular the quantum dynamics features many more transitions across the barrier then the classical counterpart.

By comparing quantum and classical dynamics at $T = 0.01$ and $\gamma = 0.001$, in figures 4.2a, 4.2b, and 4.3a, 4.3b respectively, we observe that the quantum trajectories are characterised by a much more erratic motion than the classical ones: in the latter case, we have regular oscillations across the energy barrier with frequent recrossings, and regular asymmetric oscillations within the potential wells, which trap the classical trajectories for long periods of time. In the quantum-mechanical case the trajectories behave quite erratically and get trapped in the metastable states only for short periods of time. Trapping can take place in this regime, as we see in figure 4.2b for $t > 150$ units of time; however it seems that crossings over the barrier remain likely after the trajectory has been trapped. We also see that the quantum trajectories feature a large position uncertainty Δx throughout the duration of the simulation. Recall that the initial value of Δx is $\frac{\hbar}{2} \approx 0.25$ and the width of the wells is $\sqrt{2} \approx 1.41$. With the quantum dynamics starting at the hyperbolic fixed point $q = 0$ we see that the position uncertainty jumps from 0.25 to just above 1 within 2 units of time, arguably as a consequence of the particle's probability distribution spreading itself over both sides of the energy barrier. So the oscillations across the barrier could be partly due to the delocalisation of the wave packet. We also expect quantum interference effects to play an important role at a very low value of the coupling to the heat bath, which would explain why we have such an erratic motion across and below the energy barrier. Interference could also have to do with the fact that the quantum dynamics stays confined approximately within the central region of the potential, and does not appear to ever go to regions beyond the two metastable states.

In the classical case, figures 4.3a and 4.3b, we see that transitions through $q^* = 0$ are less frequent than in the quantum-mechanical case, but still present: in both realisations trapping takes place only after 100 units of time or more. Here we have well-defined lower-frequency oscillations across the barrier as well as higher-frequency oscillations about the metastable states. In both cases the dynamics is very regular because γ is very low, with the asymmetry of the potential wells causing the trajectories to oscillate about a point at some distance from the energy minimum when they are trapped in one of the wells.

In figures 4.2c and 4.2d we have two realisations of the quantum dynamics obtained with $T = 0.01$ and $\gamma = 0.1$. With this higher value of γ, the transitions across the dividing point are more visibly regular and more frequent than before. The uncertainty in x is on average rather large throughout the simulations, but not as large as with $\gamma = 0.001$. As in the previous example it makes sense to think that we observe oscillations across the barrier as a result of the delocalisation of quantum states for $t > 0$. At the same time with a larger value of the coupling to the heat bath decoherence is likely to come into play, and this would be consistent with the fact that we find more regular oscillations across the barrier now that the dissipative contribution to the dynamics is larger, and the quantum dynamics is more susceptible to the motion along the classical periodic orbits. Additionally a larger γ provides more thermal "kicks" to the quantum trajectories, which contribute to more frequent transitions across $q = 0$. If we compare these trajectories with their classical counterparts, shown in figures 4.3c and 4.3d, we see that unlike in the quantum-mechanical case these get trapped in one of the wells and remain there for long periods of time, suggesting that the classical dynamics is more affected by the damping effect of the coupling coefficient than to its stochastic contribution to the motion.

Figures 4.2e and 4.2f, where $T = 0.01$ and $\gamma = 0.5$, provide a similar example: the quantum trajectories undergo frequent and regular oscillations across the barrier driven by the delocalisation of the wave function in combination with strong stochasticity in the dynamics. The classical counterparts in figures 4.3e and 4.3f, on the other hand, display a completely different behaviour as they get immediately trapped by one of the metastable states and remain there for the entire duration fo the simulation.

In regard to the type of transmission coefficients we expect to find in the quantum and classical case with $T = 0.01$, it is reasonable to expect that the quantum correlation function with $T = 0.01$ and $\gamma = \{0.1, 0.5\}$ decays to zero exponentially fast due to the fact that there is no time scale sepratation between oscillations at the minima and across the barrier, as the latter take place very frequently. In the classical case, on the other hand, the time correlation functions will likely display a nice plateau due to the fact that transitions across the barrier are very rare in these regimes. With $T = 0.01$ and $\gamma = 0.001$ it is hard to make a predictions; surely we do not expect to see a plateau in

the quanutm-mechanical transmission coefficient, and we may or may not see one in the classical one.

In figures 4.4 and 4.5 we show the quantum and classical dynamics in a medium-temperature regime, with $T = 0.1$. In comparison to the previous set of examples at $T = 0.01$, here we immediately notice that the quantum wave packets feature much smaller widths along the x-axis and quantum and classical dynamics look a lot more similar to one another than they did before.

When $T = 0.1$ and $\gamma = 0.01$ we find some similarities between quantum and classical dynamics. The quantum dynamics is shown in figures 4.4a and 4.4b, while the classical one is given in figures 4.5a and 4.5b. Both quantum and classical trajectories feature a series of initial oscillations across the barrier which eventually result in trapping within one of the potential wells. The fact that the value of the coupling coefficient is low is more visible in the classical dynamics than the quantum one: while the quantum trajectories are quickly trapped in one metastable state and, once there, remain in close proximity of the energy minimum, the two classical examples show wide oscillations about the minima. Also, in the case of figure 4.5a, we see that the classical trajectories can take a long time to get trapped in this regime. On the other hand the quantum-mechanical trajectories behave as if we were in a highly dissipative regime; but this is just a result of the fact that in this temperature regime the wave function is quite localised and the stochastic "kicks" coming from γ are not strong enough to move it make it transition across the barrier. We expect that the quantum and classical transmission coefficients obtained in this regime will feature some kind of plateau, however this might be less well-defined in the classical case.

Similarly in figures 4.4c and 4.4d, where $T = \gamma = 0.1$ dimensionless units, we observe that the uncertainty Δx stays consistently small throughout time evolution and the quantum trajectories remain trapped in one of the wells for the entire time. We observe a very similar behaviour in the classical case, shown in figures 4.5c and 4.5d, where the classical trajectories also stay trapped for most of the duration of the simulation. The trajectories here show that we are in a regime where the separation of time scales required by TRT is valid in both quantum and classical case, suggesting the corresponding transmission

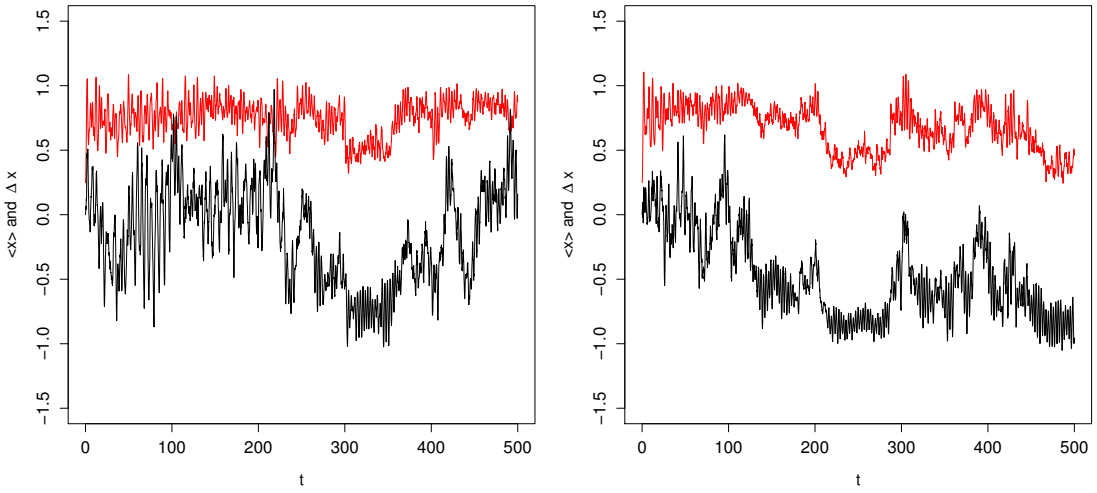
coefficients will display a visible plateau, and the dynamics displayed in the two cases are remarkably similar, so the shape of the two correlation functions should look rather similar. This makes $T = \gamma = 0.1$ an interesting regime in that one appreciates how the time scale separation necessary for classical TRT to be applicable tends to hold at low temperatures, when crossings are rare; but in quantum-mechanics this is when delocalisation effects become significant and can bring about transitions that again defy the basic TRT assumption.

Yet at relatively high temperatures we can also appreciate significant differences between quantum and classical dynamics: when $T = 0.1$ and $\gamma = 0.5$, the quantum trajectories shown in figures 4.4e and 4.4f display an intermediate behaviour where transitions over the energy barrier appear to take place rarely, but not *very* rarely. This is a very interesting example. Note how $\langle \hat{x} \rangle$ tends to remain between the saddle point and the energy minimum instead of oscillating about the metastable state as one would intuitively expect. This is likely to be due to the wave packet being asymmetric with on average more probability on one side of the minimum. There could also be some delocalisation effect whereby part of the probability gets trapped one one side of the barrier and the remaining part is on the other side; this would also explain why we have occasional transitions across the energy barrier. By looking at these trajectories one would struggle to predict the shape of the correponding time correlation function, $\kappa(t)$. The classical case is quite different in that the trajectories simply get trapped by the metastable states and remain there: this is the case in both figures 4.5e and 4.5f.

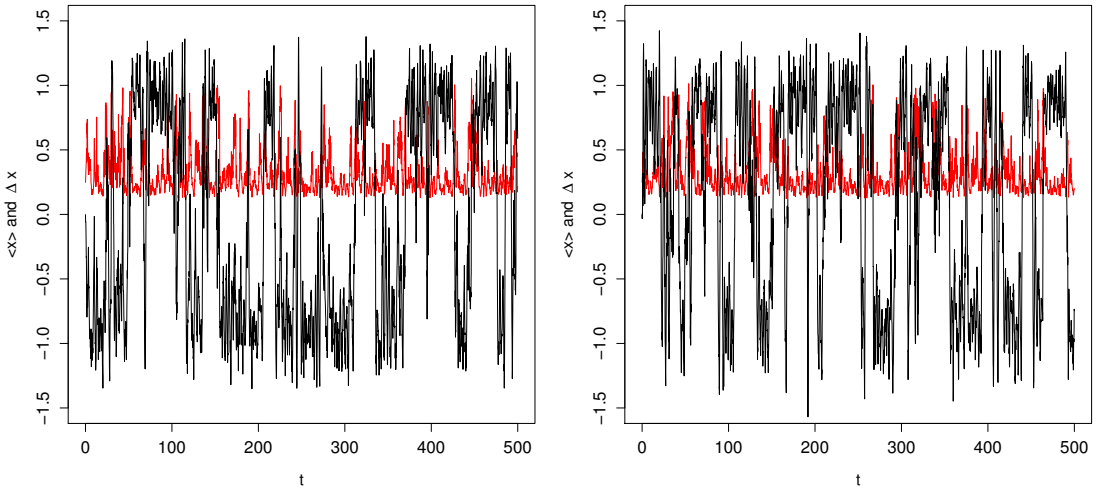
Lastly in figures 4.6 and 4.7 we show quantum and classical trajectories at high temperatures, namely $T = 0.25$ and $T = 0.5$. In figures 4.6a and 4.6b we show the quantum dynamics obtained with $T = 0.25$ and $\gamma = 0.001$. With a high temperature and a very low coupling to the heat bath we find a behaviour that in some way resembles what we found with $T = 0.01$ and $\gamma = 0.001$: transitions across the dividing point q^* are overall very frequent and the same time the value of Δx tends to stay high throughout time evolution; also the motion of the quantum particle is very irregular. Being the value of the coupling to the heat bath we can expect that interference effects are important in this regime as they were in the previous case with $T = 0.01$; this combined with

the fact that the wave packet is highly delocalised in x partly accounts for the oscillations taking place across the barrier, and for the fact that oscillations are in general quite erratic. However we also see that with a temperature $T = 0.25$ transitions across $q = 0$ are much more frequent than they were with $T = 0.01$. The classical trajectories in this regime also display some qualitative similarity to the case where $T = 0.01$ and $\gamma = 0.001$, among which the fact that because the value of γ is very low we also see semi-harmonic oscillations about the minima whenever the particle gets trapped in one of the wells. This is shown in figures 4.7a and 4.7b. Note that as before the classical dynamics appears significantly more regular than the quantum-mechanical one. This is a case where making conjectures as to what the corresponding transmission coefficients will look like is rather difficult; we could say though that with $T = 0.25$, despite the coupling coefficient being very low, we are likley to be in a region where the requirement $k_B T \ll E_b$, where in our case $E_b = 0.75$ is not satisfied, making it unlikely that either correlation function displays a plateau.

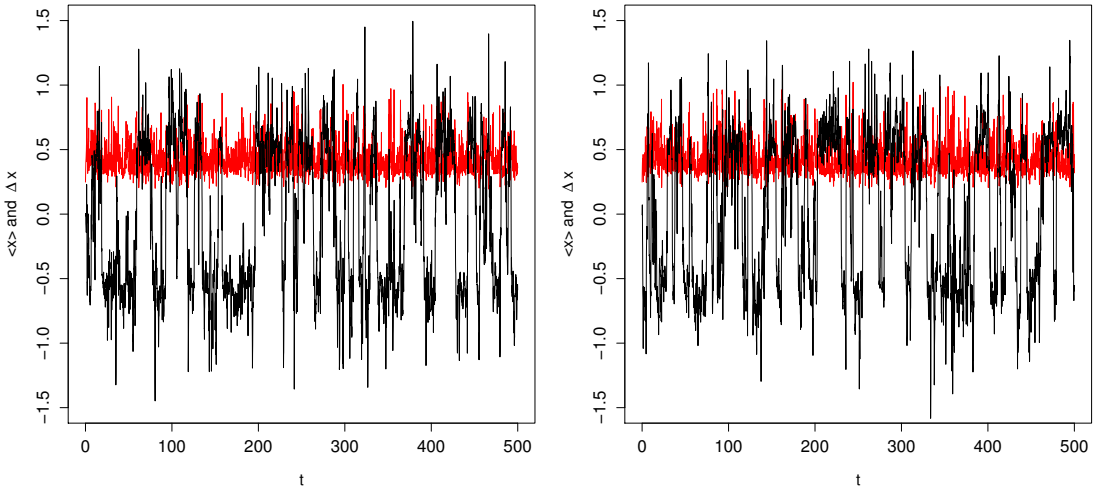
By raising both the temperature and the coupling coefficient to 0.5 we find a regime where quantum and classical dynamics are, as one would expect, very similar. This is apparent in figures 4.6c and 4.6d, showing the quantum dynamics at $T = \gamma = 0.5$ dimensionless units, and in figures 4.7c and 4.7d, showing the classical dynamics in the same regime. As the temperature is very high, quantum and classical dynamics are nearly the same; the fact that no prolonged trapping can take place in this regime implies that we expect both quantum and classical correlation functions to decay to zero following an exponential law. In the next section we will use the open trajectories discussed above to obtain the quantum transmission coefficient at a range of values of the temperature and the coupling coefficient, and compare it to the classical counterpart.



(A) (B)

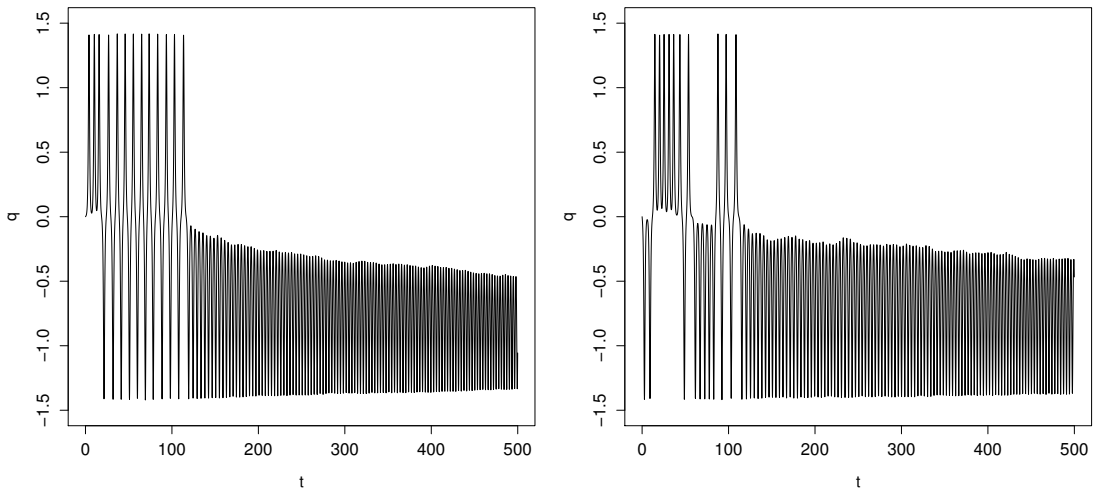


(C) (D)

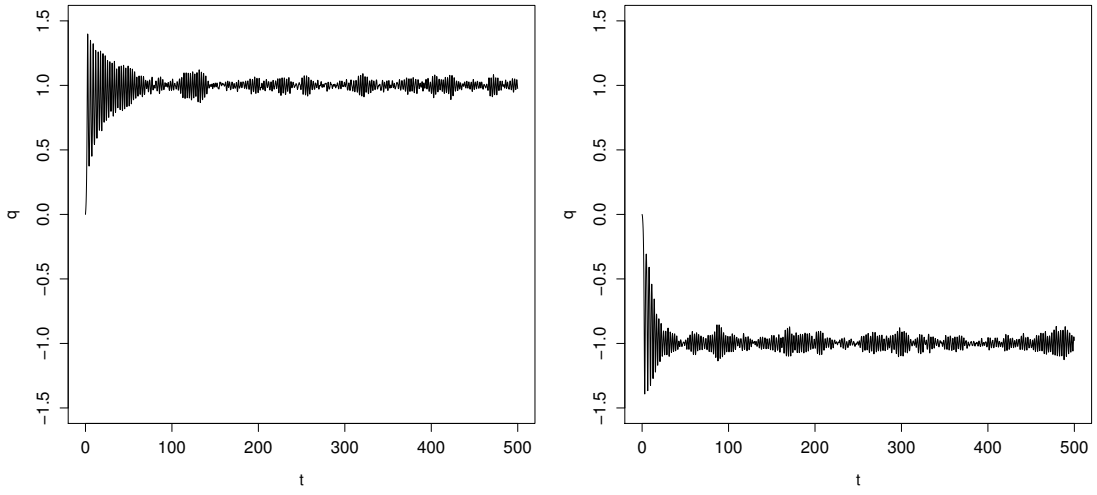


(E) (F)

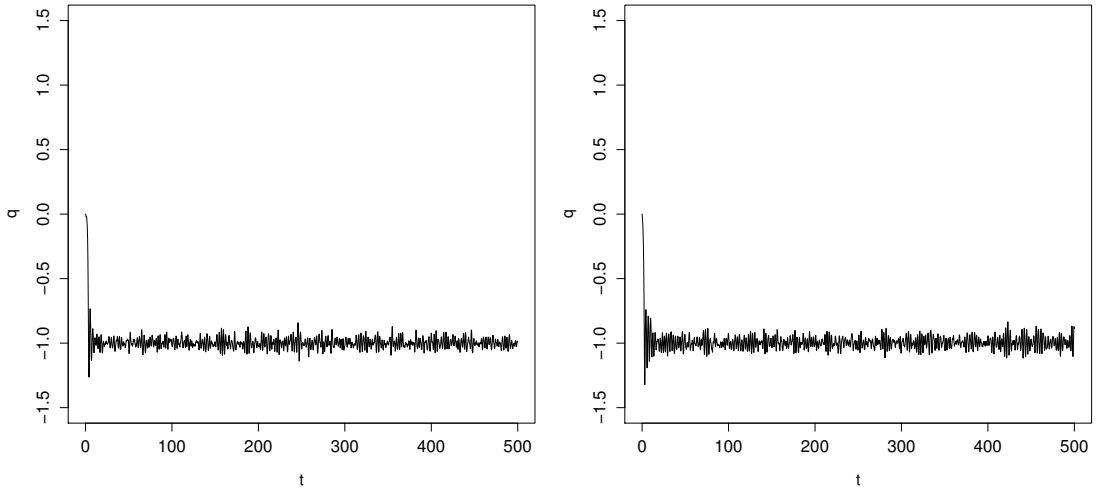
FIGURE 4.2: $T = 0.01$. Stochastic quantum dynamics in equation (3.88), obtained by integrating equation (C.8) via the numerical scheme outlined in equations (C.9)-(C.18). The quantum trajectory is pictured in black and the uncertainty in the position Δx is pictured in red. In the upper panel we show γ=0.001; in the middle panel, $\gamma = 0.1$; in the bottom panel, γ=0.5.



(A) (B)

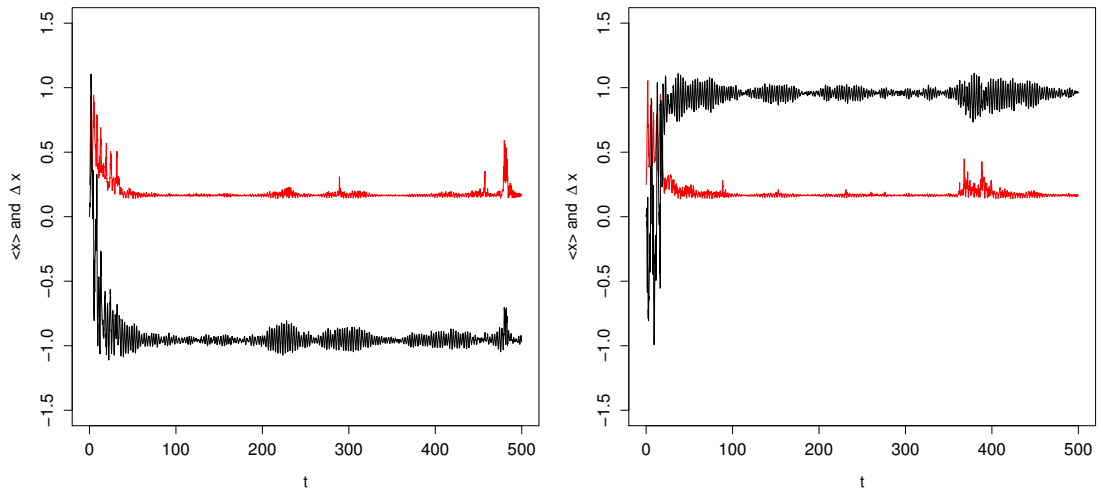


(C) (D)

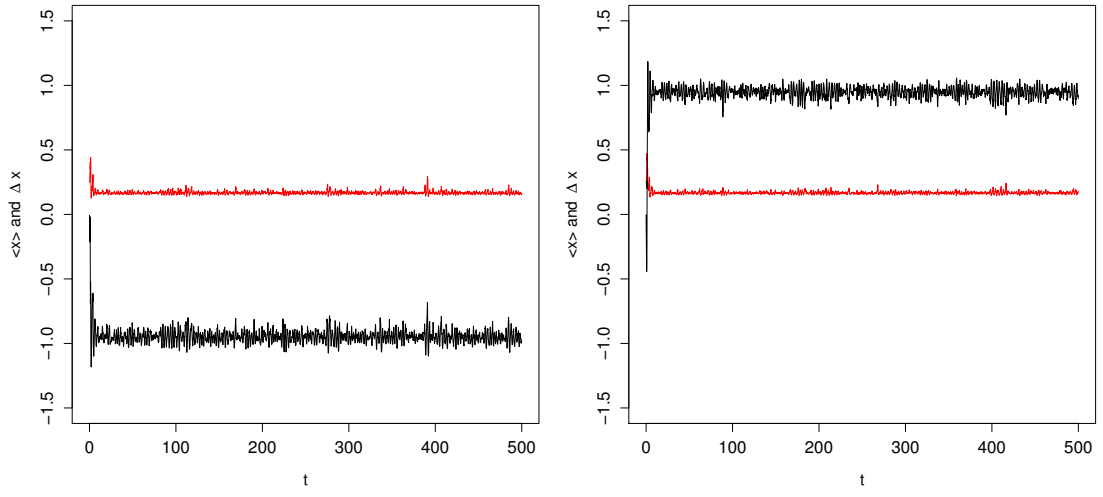


(E) (F)

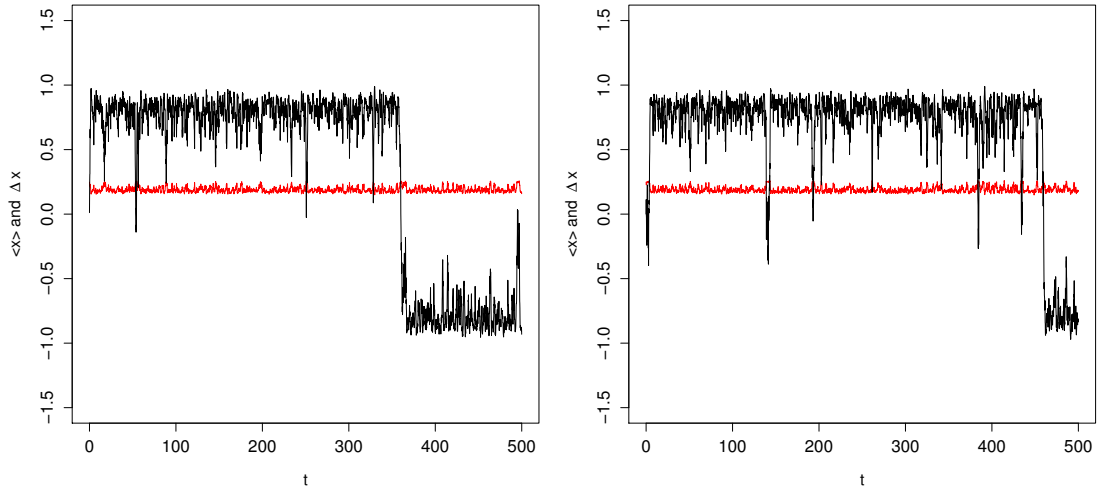
FIGURE 4.3: $T = 0.01$. One realisation of the stochastic classical trajectories, obtained by integrating the classical equations of motion (2.63) and (2.64) using the numerical scheme in equations (C.1) and (C.2). In the top panel we show γ=0.001; in the middle panel, $\gamma = 0.1$; in the bottom panel, γ=0.5.



(A) (B)

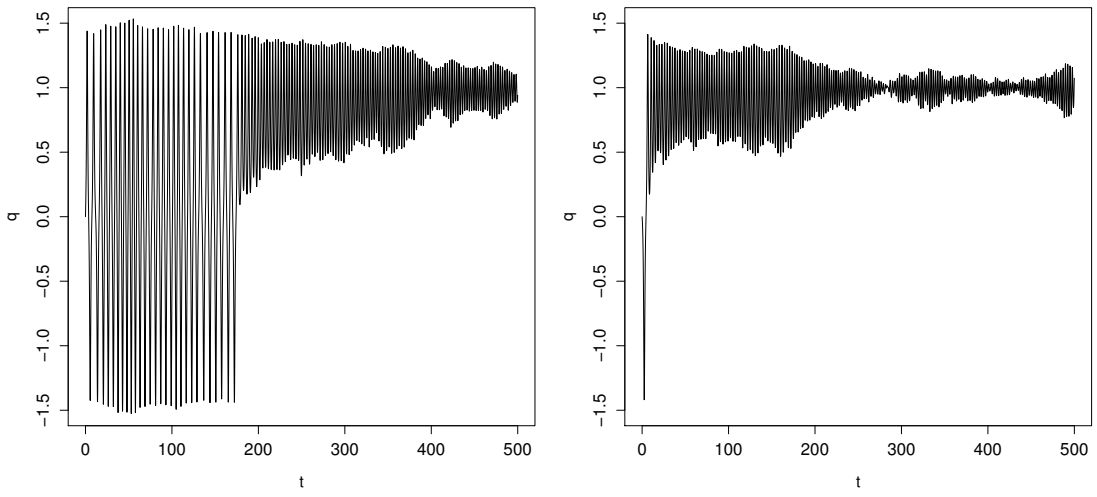


(C) (D)

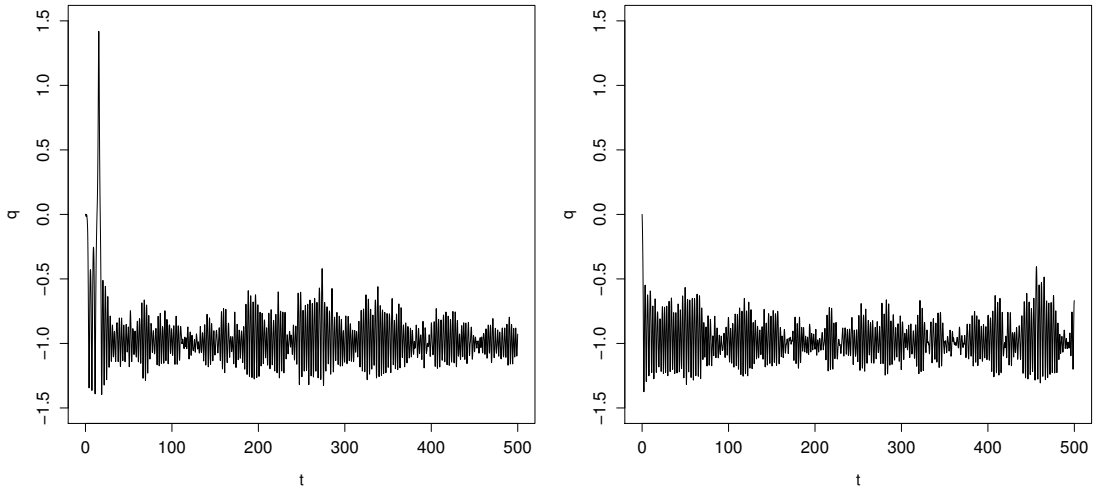


(E) (F)

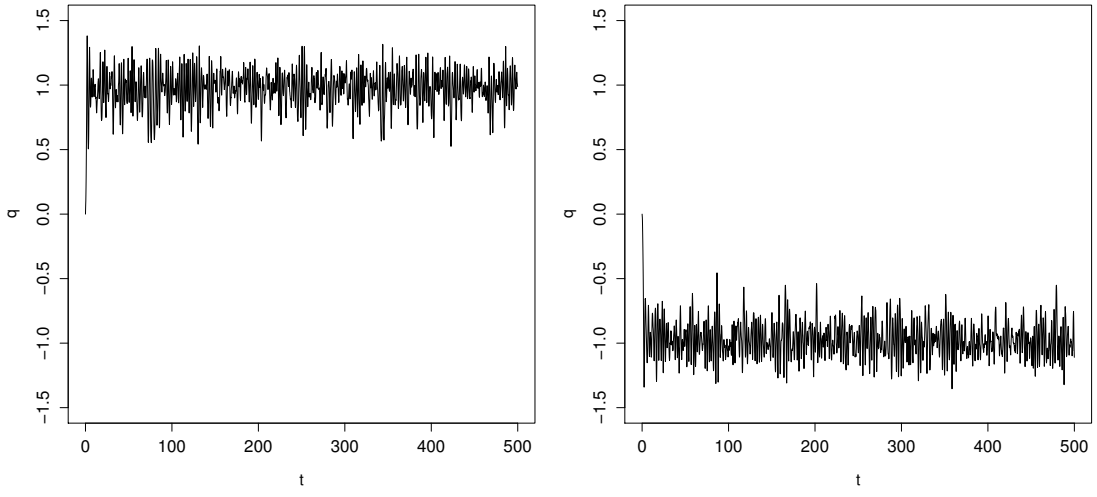
FIGURE 4.4: $T = 0.1$. Stochastic quantum dynamics in equation (3.88), obtained by integrating equation (C.8) via the numerical scheme outlined in equations (C.9)-(C.18). The quantum trajectory is pictured in black and the uncertainty in the position Δx is pictured in red. In the top panel we show γ=0.01; in the middle panel, $\gamma = 0.1$; in the bottom panel, γ=0.5.



(A) (B)

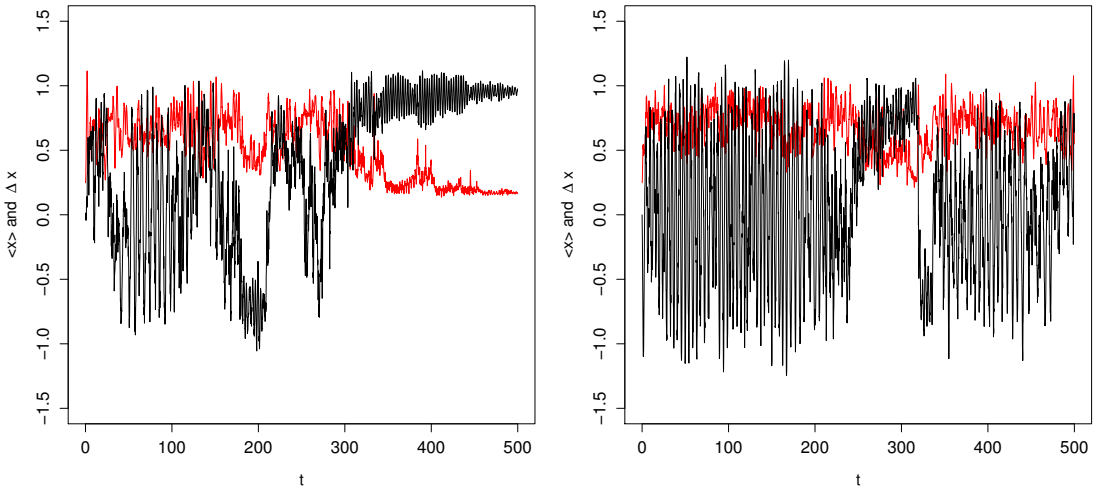


(C) (D)



(E) (F)

FIGURE 4.5: $T = 0.1$. One realisation of the stochastic classical trajectories, obtained by integrating the classical equations of motion (2.63) and (2.64) using the numerical scheme in equations (C.1) and (C.2). In (A) we show γ=0.01; in (B), $\gamma = 0.1$; in (C), γ=0.5.



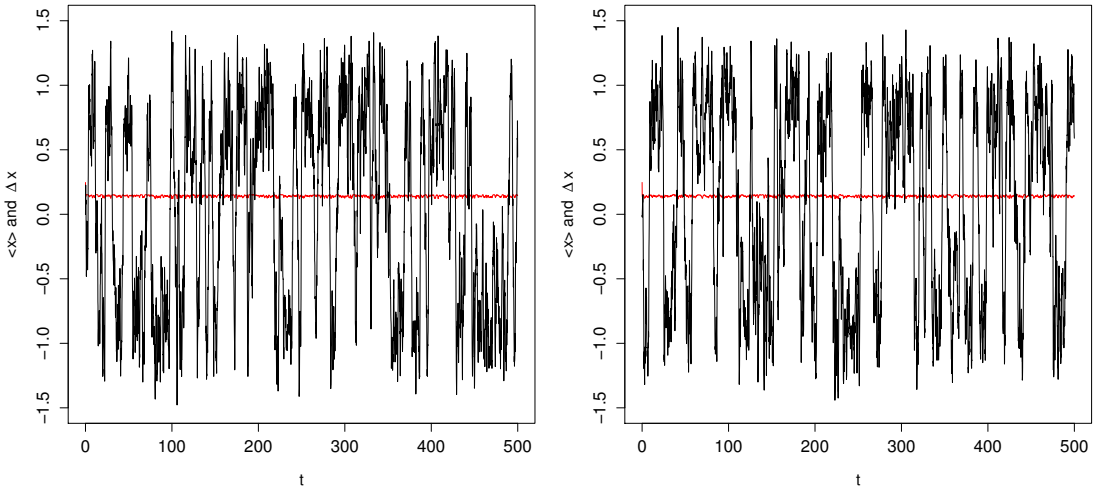
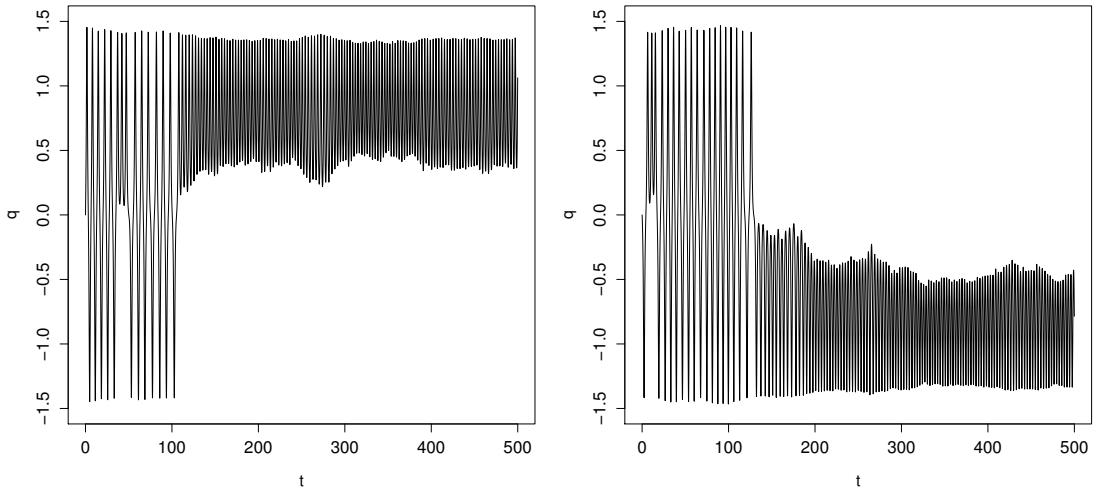
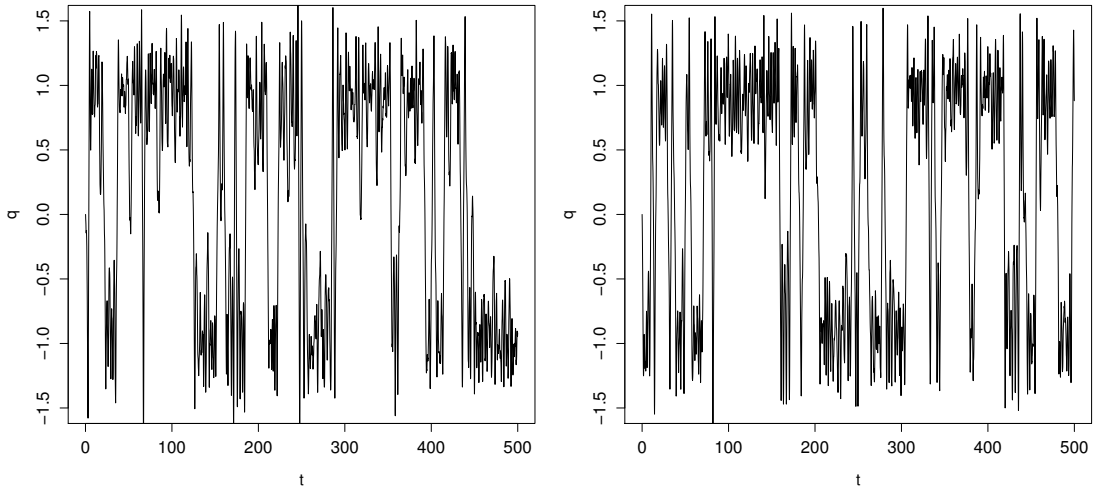


FIGURE 4.6: Stochastic realisation of the quantum dynamics in equation (3.88), obtained by integrating equation (C.8) via the numerical scheme outlined in equations (C.9)-(C.18). The quantum trajectory is pictured in black and the uncertainty in the position Δx is pictured in red. In the upper panel we show two realisations obtained for $T = 0.25$ and $\gamma = 0.001$; In the lower panel we show two realisations obtained for $T = \gamma = 0.5$.



(A) (B)



(C) (D)

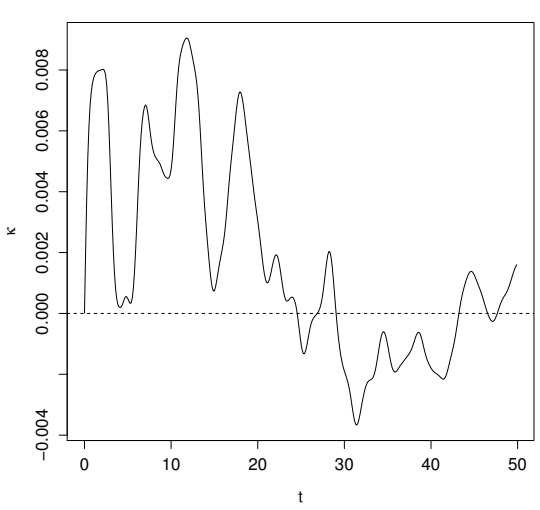
FIGURE 4.7: Stochastic realisation of the classical dynamics obtained by integrating the classical equations of motion (2.63) and (2.64) using the numerical scheme in equations (C.1) and (C.2). In the upper panel we show two realisations obtained for $T = 0.25$ and $\gamma = 0.001$; In the lower panel we show two realisations obtained for $T = \gamma = 0.5$.

4.4 Results – quantum transition rate theory

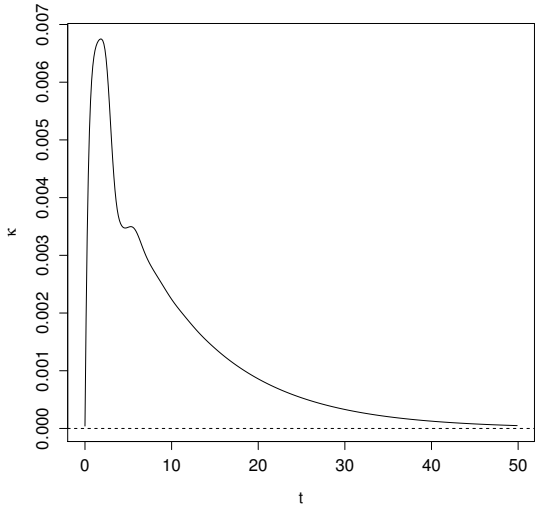
In this section we show the quantum transmission coefficients and their classical counterpart at a range of temperatures. The first feature we notice in all examples of quantum rates is that the time correlation function $\kappa(t)$ always starts at zero as opposed to starting at a positive value, as we have in the classical case: all plots in figures 4.8, 4.11 and in the left-hand-side panel of figure 4.13 show a curve starting at zero and immediately reaching a small positive number which we call $\kappa(\delta t)$. This confirms the literature results presented in chapter 2, which predict that in the limit as $t \to 0^+$ the quantum transition rate is always zero. Conversely, the classical transmission coefficient $\kappa^c(t)$ starts at a positive value equal to $\langle v \rangle$, as per equation (4.18) and discussion therein.

In figure 4.8 are shown the quantum transmission coefficients corresponding to a low-temperature region in (T, γ)-space, that is $T = 0.01$. The corresponding classical transmission coefficients computed for the same values of T and γ are reported here in figure 4.9. Firstly we notice how in this low-temperature regime quantum and classical transmission coefficients differ significantly; this is reflected by differences between quantum and classical dynamics we observed in the previous section. By comparing figures 4.8 and 4.9, we observe that the first non-zero value reached by $\kappa(t)$, which we call $\kappa(\delta t)$, is roughly one order of magnitude smaller than $\tilde{\kappa}^c(0)$. In particular we notice that the value of $\kappa(\delta t)$ in figure 4.8a is approximately 0.008 and the value of $\tilde{\kappa}^c(0)$ for the same values of T and γ, in figure 4.9a, is approximately 0.04, that is $\tilde{\kappa}^c(0) \approx 5\kappa(\delta t)$. In the case where $T = 0.01$ and $\gamma = 0.1$ we find a similar result, and with $T = 0.01$ and $\gamma = 0.5$ we have $\tilde{\kappa}^c(0) \approx 10\kappa(\delta t)$.

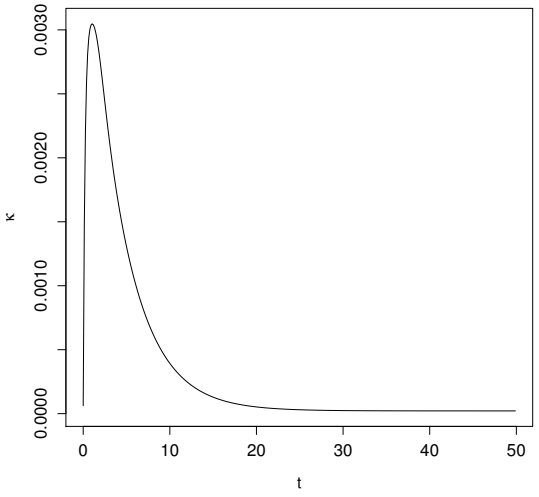
By looking at figures 4.8a and 4.9a it is apparent that when $T = 0.01$ and $\gamma = 0.001$ quantum and classical transmission coefficient display some analogies as well as some differences. Both correlation functions feature wide initial fluctuations; however in the classical case these look like damped harmonic oscillations converging to a positive constant, while in the quantum-mechanical one the oscillatory pattern is less clear. In figure 4.10 we consider the correlation functions in figures 4.8a and 4.9a for a period of 200 units of time. In both cases we have initial oscillations resulting in a "plateau", more clearly identifiable in the classical case than in the quantum-mechanical one; we also see



(A) $T = 0.01$, γ=0.001



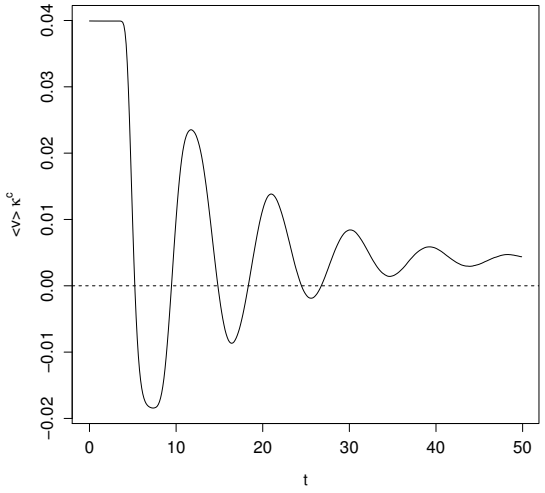
(B) $T = 0.01$, γ=0.1



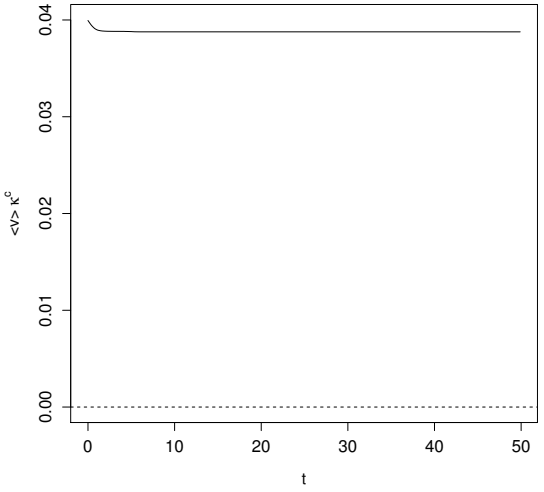
(C) $T = 0.01$, γ=0.5

FIGURE 4.8: Quantum-mechanical transmission coefficient computed using equation (4.10) and the numerical procedure summarised in section 4.2 and appendix C. In (A) we show $T = 0.01$ and γ=0.001; in (B), $T = 0.01$ and $\gamma = 0.1$; in (C), $T = 0.01$ and γ=0.5.

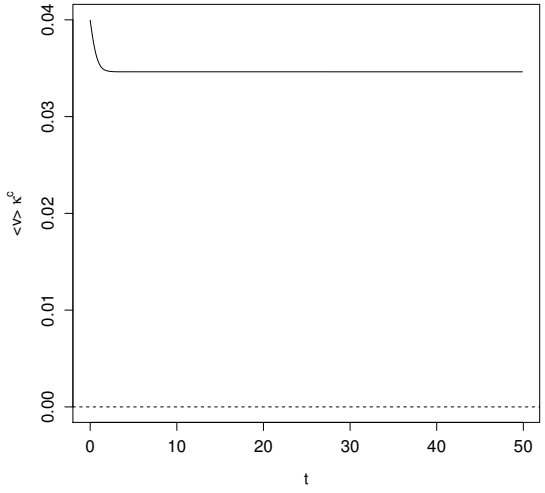
that figure 4.10a features a lower-frequency oscillatory pattern on top of the short-time oscillations we have in both quantum and classical case. In the dynamics corresponding to this regime we found that indeed quantum and classical trajectories differ significantly, as shown in figures 4.2a, 4.2b and 4.3a, 4.3b. However it is interesting to notice that by looking at the quantum trajectories one would find it difficult to tell whether the corresponding transmission coefficient will reach a plateau or not. Additionally, although it



(A) $T = 0.01$, γ=0.001



(B) $T = 0.01$, γ=0.1

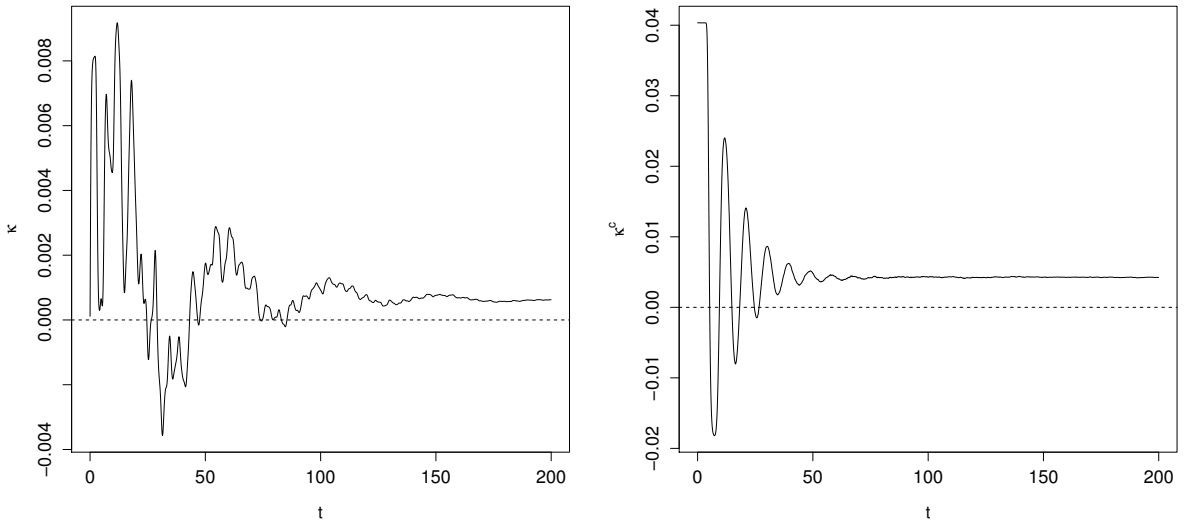


(C) $T = 0.01$, γ=0.5

FIGURE 4.9: Classical transmission coefficient $\tilde{\kappa}^c(t)$ in equation (4.18) computed via equation (2.48) and the numerical scheme in equations (C.1) and (C.2). In (A) we have $T = 0.01$ and γ=0.001; in (B), $T = 0.01$ and $\gamma = 0.1$; in (C), $T = 0.01$ and γ=0.5.

is clear that the quantum trajectories have a more complex behaviour than the classical ones in this regime, it is also difficult to link the characteristics of the quantum dynamics to the existence of a double frequency in $\kappa(t)$, which can be verified by taking the relevant Fourier transform.

In figure 4.8b, when $T = 0.01$ and $\gamma = 0.1$, $\kappa(t)$ displays a behaviour that is markedly different from the classical correlation function $\tilde{\kappa}^c(t)$. The latter, shown in figure 4.9b,



(A) (B)

FIGURE 4.10: Quantum and classical transmission coefficients at T=0.01 and γ=0.001 (previously shown in figures 4.8a and 4.9a respectively), simulated for a longer period of 200 units of time. In (A) we have $\kappa(t)$, in (B) we have $\tilde{\kappa}^c(t)$.

features a well-defined plateau $\tilde{\kappa}^c(t_{pl}) \approx 0.039$, while the quantum correlation function peaks at $\kappa(\delta t) \approx 0.007$ and then decays exponentially fast. As stressed above, this is due to the fact that in this regime the quantum dynamics diverges significantly from the classical one. In fact in figures 4.2c, 4.2d and 4.3c, 4.3c we found that the quantum trajectories frequently cross the energy barrier so that oscillations taking place at the metastable states are characterised by a frequency that is not much greater than that relative to the transitions across the barrier; on the other hand the classical trajectories quickly get trapped by the energy minima and remain trapped for long times. In other words, no separation of time scales can be made in this regime for the quantum-mechanical case, despite the low temperature. This further demonstrates how the quantum dynamics adds a layer of complexity to the discussion of TRT: not only does the theory requires the energy separation $E_b \gg k_B T$, we also see that the temperature needs be high enough for the quantum dynamics not to be affected by delocalisation effects too much, as these bring about frequent low-temperature transitions across the energy barrier.

When $T = 0.01$ and $\gamma = 0.5$, in figure 4.8c, we have a scenario similar to the one just discussed: $\kappa(t)$ rapidly decays to zero. Conversely $\tilde{\kappa}^c(t)$ features a plateau just below

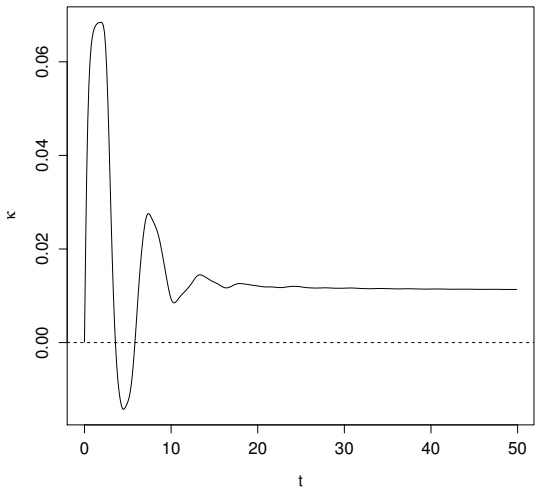
0.035. Such a stark difference between quantum and classical transmission coefficients is reflected by the trajectories in figures 4.2e, 4.2f and 4.3e, 4.3f, where we see how the quantum dynamics is driven by a large uncertainty in the position coordinate and frequently crosses the barrier, while the classical counterpart features no transitions over prolonged periods of time.

In figures 4.11 and 4.12 we show the quantum and classical trasmission coefficients obtained for an intermediate value of the temperature, $T = 0.1$. Here we find that quantum and classical correlation functions display more similarities than before. In particular we note that the short-time behaviour of $\kappa(t)$ and $\tilde{\kappa}^c(t)$ are now quantitatively more similar than they were with $T = 0.01$: when $T = 0.1$ and $\gamma = 0.01$ we have $\kappa(\delta t) \approx 0.07$ and $\tilde{\kappa}^c(0) \approx 0.13$, that is $\tilde{\kappa}^c(0) \approx 2\kappa(\delta t)$; the same holds when $T = \gamma = 0.1$; with $T = 0.1$ and $\gamma = 0.5$ we have $\tilde{\kappa}^c(0) \approx 3\kappa(\delta t)$. Overall in this medium-temperature regime $\kappa(\delta t)$ and $\tilde{\kappa}^c(0)$ are found to be of the same order of magnitude in the cases considered.

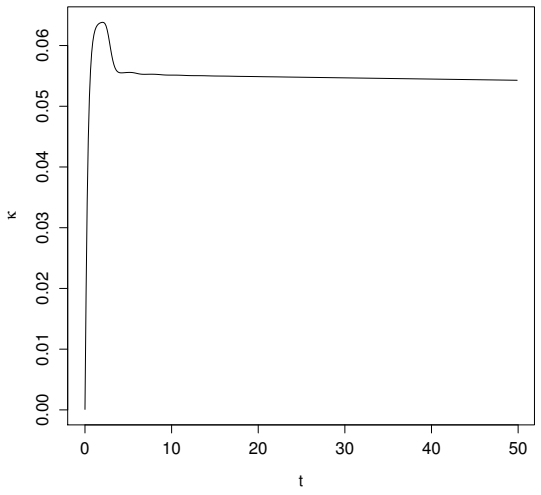
The time correlation functions shown in figures 4.11a and 4.12a, obtained with $T = 0.1$ and $\gamma = 0.01$ share some strong similarities. In the quantum-mechanical case the time correlation function displays a short-time relaxation resulting in a plateau, $\kappa(t_{pl}) \approx 0.01$, which is reached at $t_{pl} \approx 20$ units of time. The classical counterpart reaches a fairly oscillatory "plateau", $\tilde{\kappa}^c(t_{pl}) \approx 0.01$, after a short-time relaxation displayed up until $t_{pl} \approx 30$ units of time. In fact in the previous section we found that the dynamics generated in the quantum and classical case display strong qualitative similarities in this regime. At the same time the trajectories shown in figures 4.4a, 4.4b and 4.5a, 4.5b also account for the differnce between $\kappa(t)$ and $\tilde{\kappa}^c(t)$ in this regime, which is that the quantum-mechanical correlation function reaches its plateau at about $t_{pl} = 20$ units while the classical counterpart flattens only at $t_{pl} \approx 30$: in fact we saw that in this medium-temperature regime the classical trajectories are more likey to recross the barrier than the quantum counterpart.

In figures 4.11b and 4.12b we observe that both $\kappa(t)$ and $\tilde{\kappa}^c(t)$ display a plateau, starting at approximately $t_{pl} = 5$ units of time in the former case and at approximately $t_{pl} = 10$ units of time in the latter case. As before, the orders of magnitude of these rates are the same, with $\kappa(t_{pl}) \approx 0.055$ and $\tilde{\kappa}^c(t_{pl}) \approx 0.065$. The marked analogy between transmission

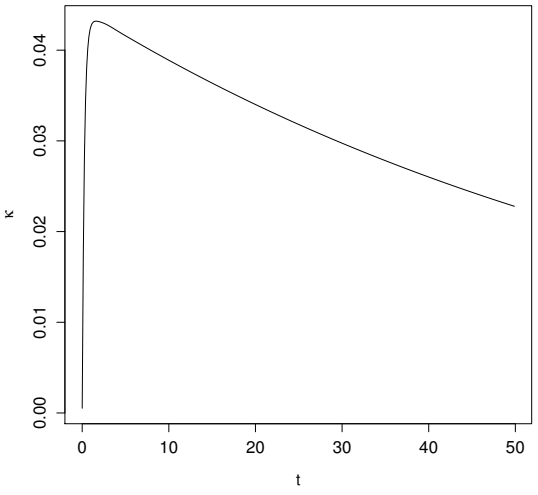
coefficients is reflected by the similar types of dynamics found in this regime, as discussed in the previous section with reference to figures 4.4c, 4.4d and 4.5c, 4.5d.



(A) $T = 0.1$, γ=0.01



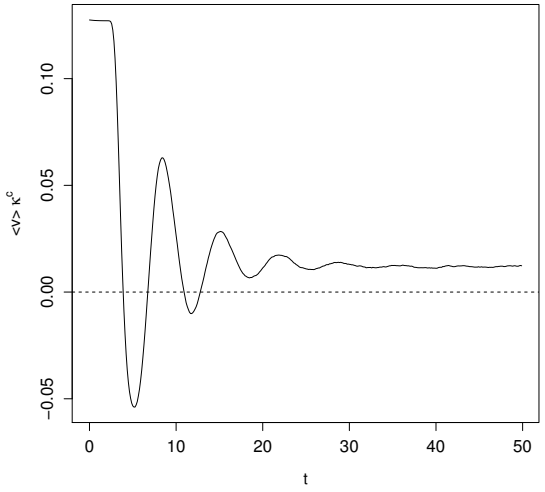
(B) $T = \gamma = 0.1$



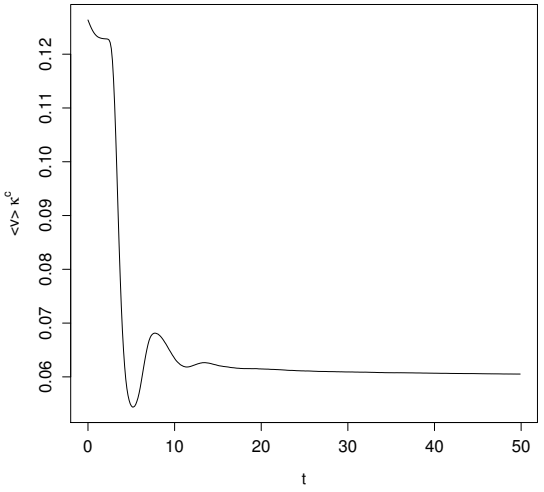
(C) $T = 0.1$, γ=0.5

FIGURE 4.11: Quantum-mechanical transmission coefficient computed using equation (4.10). In (A) we show $T = 0.1$ and γ=0.01; in (B), $T = \gamma = 0.1$; in (C), $T = 0.1$ and γ=0.5.

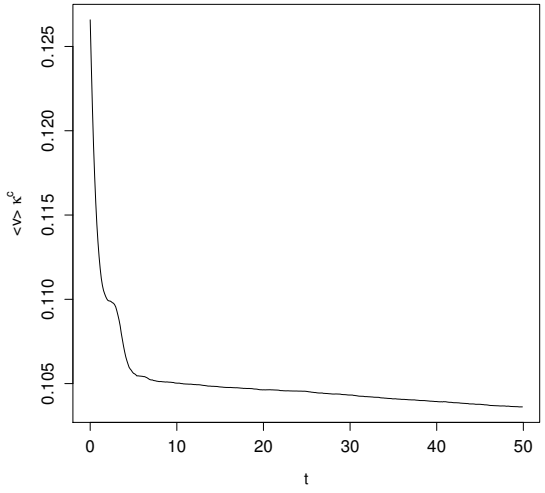
With $T = 0.1$ and $\gamma = 0.5$, shown in figure 4.11c for the quantum-mechanical case, we do not observe an exponential decay in the transmission coefficient as we did with the same value of the coupling coefficient and $T = 0.01$, see figure 4.8c. Despite the temperature here being ten times larger, we find that $\kappa(t)$ decays to zero more slowly than it did with $T = 0.01$. This is an interesting region in (T, γ)-space where we do not observe a



(A) $T = 0.1$, γ=0.01



(B) $T = \gamma = 0.1$



(C) $T = 0.1$, γ=0.5

FIGURE 4.12: Classical transmission coefficient $\tilde{\kappa}^c(t)$ in equation (4.18). In (A) we have $T = 0.1$ and γ=0.01; in (B), $T = \gamma = 0.1$; in (C), $T = 0.1$ and γ=0.5.

simple exponential decay in the quantum transmission coefficient, and yet a flat plateau cannot be identified either, and $\kappa(t)$ decays linearly to zero. The corresponding classical transmission coefficient also displays a linearly decaying "plateau", analogously to the quantum-mechanical counterpart. The qualitative similarity between these transmission coefficients is reflected by the dynamics we found in this regime for the quantum and classical case, as shown in figures 4.4e, 4.4f and 4.5e, 4.5f, in that in both cases we have trajectories that stay trapped within the potential wells for long periods of time.

However it is also clear from the dynamics that crossings and recrossings over the barrier are more frequant in the quantum case than they are in the classical one in the present regime. This is peculiar considering the fact that both the temperature and the coupling coefficient are quite high.

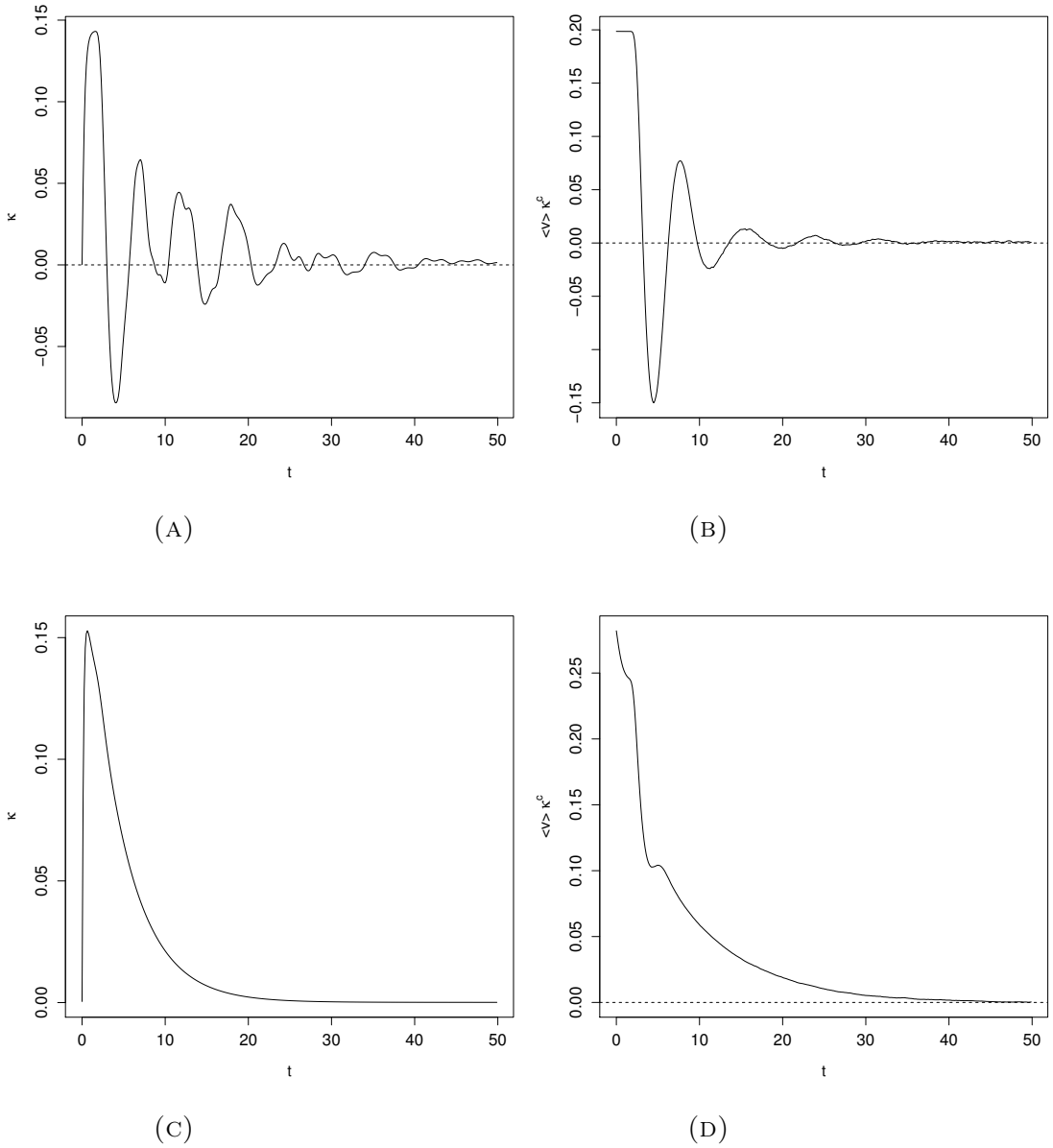


FIGURE 4.13: Upper panel: in (A), quantum-mechanical transmission coefficient with $T = 0.25$ and $\gamma = 0.001$; in (B), classical transmission coefficient with $T = 0.25$ and $\gamma = 0.001$. Lower panel: in (C), quantum-mechanical transmission coefficient with $T = \gamma = 0.5$; in (D), classical transmission coefficient with $T = \gamma = 0.5$.

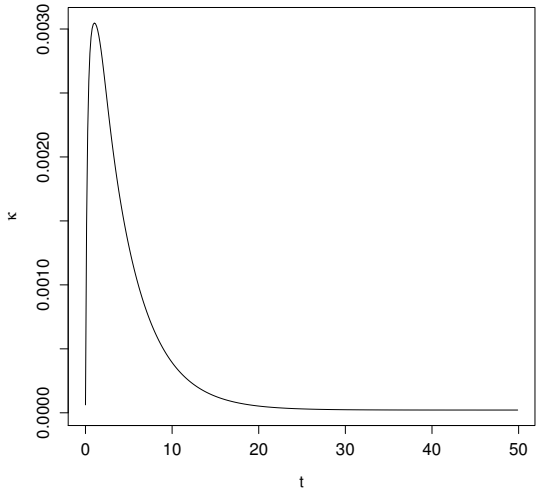
In figure 4.13 we show the quantum and classical transmission coefficients in two high-temperature regimes, with $T = 0.25$ and $T = 0.5$. We immediately see that both with

$T = 0.25$ (upper panel of figure 4.13) and $T = 0.5$ (lower panel of figure 4.13) $\kappa(t)$ and $\tilde{\kappa}^c(t)$ are qualitatively and quantitatively similar; also note that in both regimes $\kappa(\delta t)$ is of the same order of magnitude as $\tilde{\kappa}^c(0)$.

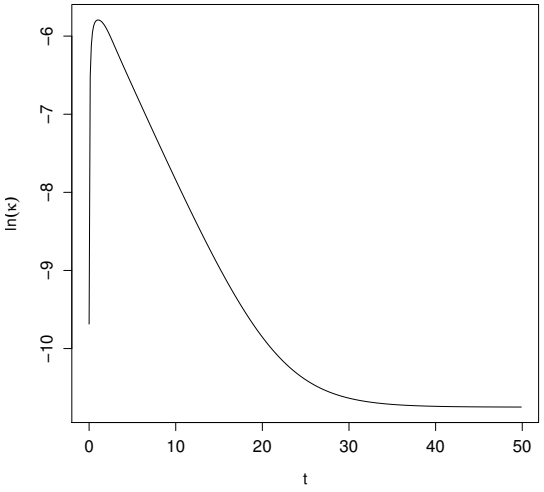
We also note some minor differences. If we look at figures 4.13a and 4.13b, showing our results for $T = 0.25$ and $\gamma = 0.001$, we observe something analogous to the case of figures 4.8a and 4.9a: the quantum-mechanical transmission coefficient features a richer structure than the classical counterpart. In particular, while $\tilde{\kappa}^c(t)$ oscillates smoothly to zero after the initial relaxation, the quantum-mechanical correlation function displays in addition several small disruptions to the overall oscillatory trend. This makes sense if we consider that while the temperature here is relatively high the value of the coupling coefficient is very low. The trajectories found in this regime for the quantum-mechanical case, shown in figures 4.6a and 4.6b confirm that with such a low value of the coupling to the heat bath the quantum dynamics is enriched by a large uncertainty in the position coordinate which we do not have in classics.

When both T and γ are equal to 0.5 units we find that $\kappa(t)$ behaves much like its classical counterpart, as shown in figures 4.13c and 4.13d. We observe analogous exponential decays in both quantum and classical cases, as we expect from the general theory of transition rates at high temperatures. The strong similarity between $\kappa(t)$ and $\tilde{\kappa}^c(t)$ in this regime is mirrored by very similar trajectories in the quanutm and classical case, as discussed in the previous section in regard to figures 4.6c, 4.6d and 4.7c, 4.7d.

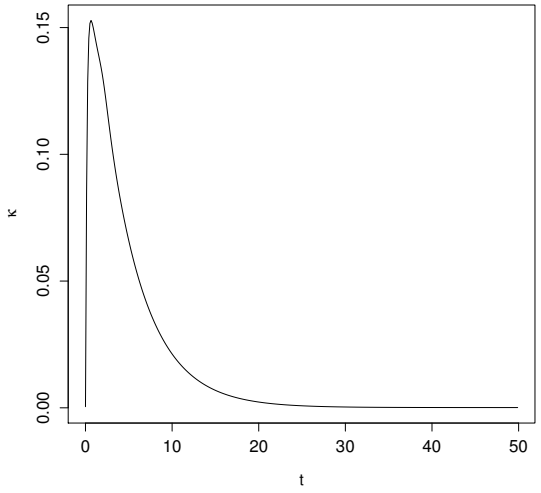
One may ask whether there is a difference between the exponential decays exhibited by the quantum rate with $T = 0.01$ and $\gamma = 0.5$, shown in figure 4.8c, and that obtained with $T = \gamma = 0.5$. To this end we compare them to the plots of the corresponding logarithms, as shown in figure 4.14. Here we can see that in fact the two exponential decays do differ, as the rate of decay shown in figure 4.14b is roughly double the one displayed in figure 4.14d. This can be explained by analysing the trajectories in figures 4.2e, 4.2f and 4.6c, 4.6d, where we find that when $T = 0.01$ and $\gamma = 0.5$ one has approximately 30 crossings every 100 units of time, while when $T = \gamma = 0.5$ one has approximately half that number.



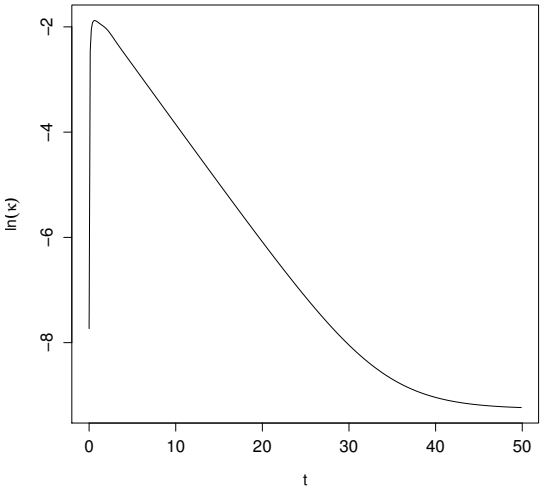
(A) $T = 0.01$, γ=0.5



(B) $T = 0.01$, γ=0.5



(C) $T = 0.5$, γ=0.5



(D) $T = 0.5$, γ=0.5

FIGURE 4.14: Quantum transmission coefficients from figures 4.8 and 4.13, with corresponding logarithm on the right-hand side. In (A) we show $T = 0.01$ and $\gamma = 0.5$, and in (B) the corresponding logarithm. In (C) we show $T = \gamma = 0.5$, and in (D) the corresponding logarithm.

We have studied quantum TRT using our formulation of the quantum transmission coefficient based on explicit knowledge of the open quantum dynamics. We have analysed and compared to the classical case both the activated quantum trajectories at a range of values of T and γ, and the quantum transmission coefficient, $\kappa(t)$ itself. The coupling of quantum trajectories to a heat bath affects the dynamics in a variety of non-trivial ways: in time scales where tunnelling does not play a role, we observe a rich interplay of

delocalisation and intereference effects, which especially at low temperatures make the quantum correlation function behave quite differently from the classical counterpart. It is apparent that the inclusion of temperature-dependent effects in the study of quantum TRT is crucial if one wants to compute the rate exactly at a range of temperature regimes.

Chapter 5

Conclusions and outlook

In this work I have presented a method to compute quantum-mechanical transition rates derived from the transition path-sampling expression introduced by Chandler for the dynamical contribution to the classical transition rate, the so-called transmission coefficient [31]. This approach consists in writing the quantum rate as an average over a distribution of momenta where the quantum-mechanical state function is expressed in terms of the time-dependent density operator $\hat{\rho}(t)$; the classical position and momentum appearing in Chandler's expression are substituted with the expectation values of the corresponding quantum operators.

The importance of this formulation relies on the fact that it incorporates open quantum dynamics into the expression for the quantum rate, in a manner that, to my knowledge, provides a new perspective in quantum transition rate theory. In fact the seminal paper by Miller ([15]) where he derives a formula for the quantum rate based on scattering theory, as well many subsequent works, focus more on developing a quantum theory for the transition-state theory (TST) approximation to the transition rate, which by definition neglects all dynamical effects entering the rate. The approach to open quantum dynamics I use here is based on the Lindblad equation for the density operator, which was first derived by Lindblad in 1976 [49].

In the classical transition path-sampling formulation of the transition rate one needs to be able to access the open classical dynamics in order to determine the fraction of trajectories

that are found in the "final", or "reactive" state at time t; without temperature-dependent effects the trajectories would follow a deterministic motion according to the shape of the potential and no transition rate could be defined. One way to introduce thermal effects in the dynamics is by adding a dissipative and a stochastic term to the equation of motion of the momentum coordinate – thus obtaining the classical Langevin equation, originally obtained by Langevin to describe the evolution of classical Brownian particles [41].

The question of how to derive a quantum-mechanical counterpart of the Langevin equation has been ongoing for a long time [48]. By using a coherent states representation of quantum states I show analytically that in the classical limit a stochastic Schrödinger equation based on a modified version of the Caldeira-Leggett model for quantum Brownian motion converges to the Langevin equation. This is done by deriving semiclassical equations of motion corresponding to the open quantum evolution under the assumption that the wave function can be described as a Gaussian wave packet in phase space, as proposed by Heller for the case of unitary dynamics [33]. The quantum evolution in Hilbert space I use is the so-called quantum-state diffusion (QSD) equation for state vectors ([53]), which can be shown to correspond to the Lindblad equation upon taking the average over stochastic realisations of the quantum dynamics [54].

This enables me to carry out two interlinked numerical investigations: on one hand I compare open classical and quantum dynamics at a range of temperatures and values of the coupling to the heat bath, based on Langevin and QSD equations respectively; on the other hand I present a comparison of the classical and quantum-mechanical transmission coefficients in the same temperature and coupling regimes, based on the classical path-sampling formulation and my expression for the quantum-mechanical transmission coefficient. Parallel to this, I apply the semiclassical scheme obtained using coherent states to compare the effects arising in the open dynamics in the semiclassical, quantum-mechanical and classical case. In all numerical simulations I study a hydrogen atom moving in a symmetric double-well potential mimicking a 1-dimensional model of iron.

The semiclassical equations of motion prove able to describe the transitions across the energy barrier that characterise the quantum trajectories at low temperatures; however,

the semiclassical scheme tends to overestimate the amplitude of these oscillations, arguably as a result of the fact that in semiclassics quantum interference is not taken into account (see, for example, reference [63]). I also find that for very low values of the coupling coefficient the semiclassical dynamics can yield unphysical results which arise when the uncertainty in the position coordinate takes particularly large values. This suggests that with appropriate values of the temperature and the coupling coefficient and provided the tunnelling time of the system is significantly larger than the other dynamical time scales in the system, the semiclassical dynamics could be used as a cheaper approximation to study quantum transmission coefficients.

My study of the quantum dynamics in terms of the QSD equation versus the classical Langevin equation shows that the quantum dynamics at low temperatures is dominated by delocalisation and interference effects. In particular for low values of the temperature and the coupling coefficient the quantum trajectories display irregular, erratic oscillations about the metastable states which can be related to interference effects, accompanied by transitions across the barrier that can be explained in terms of highly delocalised wave packets – see section 4.3, figure 4.2, top panel. At low temperatures and medium to high values of the coupling coefficient, decoherence comes into play and the dynamics is mainly characterised by transitions across the barrier – see section 4.3, figure 4.2, middle and lower panels. By looking at the quantum and classical trajectories at a range of values of the temperature and the coupling coefficient I am also able to determine in which regimes the assumptions of transition rate theory are likely to apply – in section 4.3, pages 81-85.

The results I obtain in quantum transition rate theory are consistent with my findings in open quantum dynamics. I am able to verify a result often cited in the literature, that the quantum-mechanical correlation function giving the rate vanishes in the limit as $t \to 0$. I find that the first non-zero value taken by the quantum transmission coefficient at very small times gets closer to the value of the classical correlation function at $t = 0$, which defines the classical TST value of the transition rate, as temperature increases. Additionally I determine in what regions of parameter space the quantum rate constant can be obtained from the plateau value of the transmission coefficient, which turns out to be dependent on having a large enough temperature and coupling coefficient such

that delocalisation and interference effects are negligible, but also on not having them so large that thermally activated transitions across the energy barrier take place frequently. The values I obtain for the rate constant in quantum-mechanics also appear to converge to the classical counterpart in the limit as temperature gets large, however generally we find that the quantum rate is smaller than the classical one.

This work can be the basis for several potential future investigations. Firstly, the semiclassical dynamics I obtained by representing quantum states as Gaussian wave packets could be investigated numerically for different systems by varying the value of $\hbar$, and for different hydrogen isotopes by varying the mass of the particle. Further, while I directly translate the classical path-sampling expression for the transmission coefficient into quantum-mechanical terms, one could attempt to re-derive the path-sampling formula in the quantum-mechanical language directly. This may or may not lead to a different expression for the quantum transmission coefficient than the one I use. A detailed analytical work on this aspect would be extremely valuable to a scientific community that has been struggling for decades to find computationally easy ways to include dynamical effects in quantum transition rate theory – and quantum dynamics based on the Lindblad equation offers just that, although it might not be viable for high-dimensional real-life problems. Another very exciting line of work would be to use the framework proposed here to compare the results obtained for quantum TRT to other numerical *ad hoc* methodologies that have been devised over the past couple of decades to evaluate the "dynamical corrections" arising in quantum-mechanical TST [30]. Other useful comparisons could be carried out between the results obtained via the method I propose and via a class of recently developed DPI-based formulations of quantum TST [22], [23]. Moreover the open quantum dynamics I obtain using the QSD equation could be compared to that generated by evolving DPI "polymers" in time, which has been poposed a way to compute quantum-dynamical effects more cheaply [29]. Lastly, the semiclassical dynamics I derive here could be employed to compute the transition rate, so that an analysis of the semiclassical rates thus obtained in comparison to the quantum results I find would prove a very useful contribution.

Appendix A

Derivation of the classical Langevin equation

It is useful to see how the Langevin equation emerges from a model where a classical particle is subject to the force $V(q)$ and interacts with a bath of classical harmonic oscillators to which it is coupled via the inverse time γ. Here we follow the derivation presented in reference [40]. For clarity we call P and Q the conjugate coordinates of the particle and $\{p_j\}$ and $\{q_j\}$ those of the oscillators. The particle's Hamiltonian is :

$$H = \frac{1}{2m}P^2 + V(Q), \tag{A.1}$$

while that of the bath is:

$$H_b = \sum_j \frac{1}{2}p_j^2 + \frac{1}{2}\omega_j^2\left(q_j - \frac{\gamma_j}{\omega_j}Q\right)^2, \tag{A.2}$$

where we assume that the oscillators' masses are all equal to unity and ω_j, γ_j indicate the frequency of the j-th oscillator and its coupling to the particle respectively. The resulting equations of motion are:

$$\dot{Q} = \frac{1}{m}P \qquad \dot{P} = -V_q(Q) + \sum_j \gamma_j\left(q_j - \frac{\gamma_j}{\omega_j^2}Q\right) \tag{A.3}$$

$$\dot{q_j} = p_j \qquad \dot{p_j} = -\omega_j^2 q_j + \gamma_j Q. \tag{A.4}$$

If $Q(t)$ is known the solution for $q_j(t)$ reads:

$$q_j(t) = q_j(0)\cos\omega_j t + p_j(0)\frac{\sin\omega_j t}{\omega_j} + \gamma_j \int_0^t \mathrm{d}s\; Q(s)\frac{\sin\omega_j(t-s)}{\omega_j}. \tag{A.5}$$

Using integration by parts this can be written as

$$q_j(t) - \frac{\gamma_j}{\omega_j^2}Q(t) = \left[q_j(0) - \frac{\gamma_j}{\omega_j^2}Q(0)\right]\cos\omega_j t + p_j(0)\frac{\sin\omega_j t}{\omega_j} - \gamma_j \int_o^t \mathrm{d}s\frac{p(s)}{m}\frac{\cos\omega_j(t-s)}{\omega_j^2}. \tag{A.6}$$

Inserting this into the dynamical equation for P yields:

$$\dot{P} = -V_q(Q) - \int_0^t \mathrm{d}sK(s)\frac{p(t-s)}{m} + \xi(t), \tag{A.7}$$

where we have introduced the *memory kernel* $K(t)$:

$$K(t) = \sum_j \frac{\gamma_j^2}{\omega_j^2}\cos\omega_j t, \tag{A.8}$$

and $\xi(t)$ is given by:

$$\xi(t) = \sum_j \gamma_j p_j(0)\frac{\sin\omega_j t}{\omega_j} + \sum_j \gamma_j\left[q_j(0) - \frac{\gamma_j}{\omega_j^2}Q(0)\right]\cos\omega_j t. \tag{A.9}$$

By defining the spectrum of $\{\omega_j\}$ and $\{\gamma_j\}$ a specific form is assigned to the memory kernel; when this is done in such a way that $K(t)$ is a δ-function, the force $\xi(t)$ is white or Markovian. Equation (A.9) provides a definition of the "random" force as a deterministic quantity that depends on the microscopic dynamics of the bath's degrees of freedom. However in the Langevin approach we choose to neglect the microscopic characterisation of $\xi(t)$ and focus on how the bath affects the system of interest on average. Because such average effects on the system appear to be random, $\xi(t)$ is substituted by a random process with specific average properties reflecting the physics of the interaction between the system and the bath.

Appendix B

A system of dimensionless units of measure

In this appendix we provide further details about the system of dimensionless units used throughout the thesis. In both quantum and classical mechanics we have an atom of mass m moving in a double-well potential characterised by an energy barrier E_b and a distance between minima, or metastable states, which we call d. In figure B.1 we provide a sketch of the potential used in dimensionless units. This potential, which we use for all the numerical work in this thesis, is given by $V(q) = -V_1 q^2 + V_2 q^4$, where V_1 and V_2 are chosen so that the distance between minima is equal to 2 and the height of the barrier is $\frac{3}{4}$.

We introduce the scaling parameters m_0, E_0 and d_0 such that:

$$\left[\frac{m}{m_0}\right] = \left[\frac{E_b}{E_0}\right] = \left[\frac{d}{d_0}\right] = 1, \tag{B.1}$$

where the symbol [ ] means "dimensions of". Throughout this work with deal primarily with quantities that depend on the time t, the coupling coefficient γ and the temperature T. Using m_0, E_0 and d_0 we can determine the derived scaling parameters for t, γ and T. In our system the Boltzmann constant k_B equals 1, hence $T_0 = E_0$. From dimensional

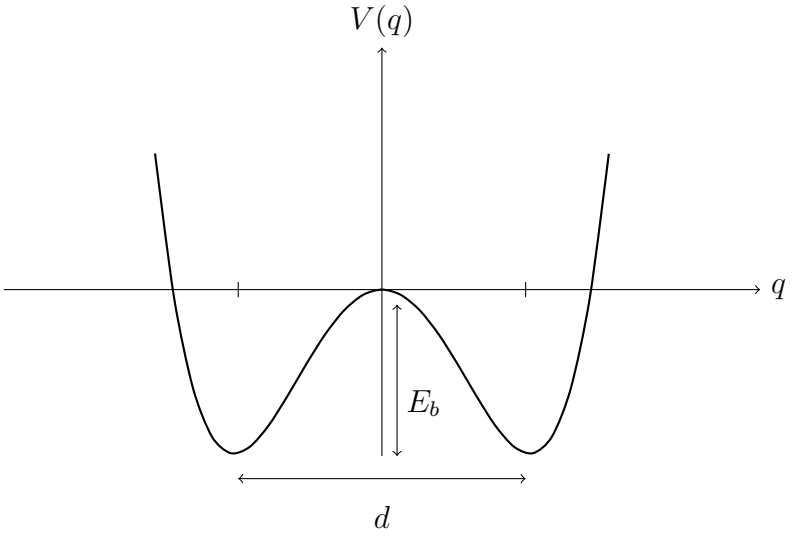


FIGURE B.1: Schematic representation of the potential used in the quantum mechanical simulations. In dimensionless units the values of d and E_b are 2 and $\frac{3}{4}$ respectively.

analysis we further find:

$$t_0 = d_0\sqrt{\frac{m_0}{E_0}}, \quad \gamma_0 = \frac{1}{t_0} = \frac{1}{d_0}\sqrt{\frac{E_0}{m_0}}, \tag{B.2}$$

and we have:

$$\left[\frac{t}{t_0}\right] = \left[\frac{\gamma}{\gamma_0}\right] = 1. \tag{B.3}$$

That is, when we refer to quantities expressed "in dimensionless units", we mean that they are scaled by the relevant parameters given as combinations of m_0, E_0 and d_0. To refer our results to a physical system we assign appropriate numerical values to the scaling parameters m_0, d_0 and E_0. In particular, if we set m_0 equal to the mass of the hydrogen atom, d_0 equal to the distance between tethrahedral sites in α-Fe and E_0 equal to the energy barrier separating tetrahedral sites in α-Fe, which has been calculated to be 0.089 eV ([30], [64]), we have the following values for the conversion factors:

$$d_0 = 1.014 \text{ Å}, \quad m_0 = 1.674 \times 10^{-27} \text{ kg} \quad \text{and} \quad E_0 = 0.089 \text{ eV}. \tag{B.4}$$

This yields the conversion factor for time as $t_0 = 8.016 \times 10^{-2}$ ps. In quantum mechanics fixing m_0, d_0 and E_0 also automatically rescales Planck's constant. In the case of hydrogen in an iron lattice considered here this yields a factor of $\hbar_0 = 8.575 \times 10^{-34}$ Js, and in dimensionless units the value of $\hbar$ is 0.123.

Appendix C

Methods of numerical integration for open dynamics

C.1 Classical Langevin equation

In classical dynamics, the Verlet algorithm can be used to evaluate numerically the solution of the classical equations of motion to second-order accuracy in the time step [65]. Here we want to evaluate the Langevin equation (2.63)-(2.64) numerically, hence we introduce a modified version of the Verlet algorithm that was devised specifically to take into account the dissipative and noise terms; this reads [43]:

$$q(t_k+\Delta t) = q(t_k) + \Delta t\, \dot{q}(t_k) + \frac{\Delta t^2}{2m}\left[f(t_k) + \gamma \dot{q}(t_k)\right] + \frac{\lambda}{m}\Delta t^{3/2}\left[\frac{\phi(t_k)}{2} + \frac{\theta(t_k)}{2\sqrt{3}}\right] \tag{C.1}$$

$$\begin{aligned}\dot{q}(t_k+\Delta t) = \dot{q}(t_k)\left[1 - \frac{\gamma}{m}\Delta t\right] + \frac{\Delta t}{2m}\left[f(t_k) + f(t_k+\Delta t)\right] - \frac{\gamma}{2m^2}\Delta t^2\left[f(t_k) + \gamma \dot{q}(t_k)\right] \\ + \frac{\lambda}{m}\sqrt{\Delta t}\phi(t_k) - \frac{\gamma\lambda}{m^2}\Delta t^{3/2}\left[\frac{\phi(t_k)}{2} + \frac{\theta(t_k)}{2\sqrt{3}}\right],\end{aligned} \tag{C.2}$$

where $k = 1, 2, ...$ labels the time steps in the simulation, Δt is the time steps of integration, $f(t) = -V'(q(t))/m$, and $\phi(t)$ and $\theta(t)$ indicate two independent variables sampled from a normal distribution generated at time t. One notes immediately that when $\gamma = 0$, so that also $\lambda = 0$, the algorithm reduces to the standard velocity Verlet.

C.2 Semiclassical dynamics

In semiclassics, we wish to evaluate numerically the coupled equations (3.79)-(3.82), which we report here:

$$\mathrm{d}a = \left[-\frac{1}{2}V_{xx} - \frac{2}{m}(a^2 - b^2) - 2\gamma a - \frac{2\hbar\gamma}{r^2}ab\right]\mathrm{d}t \tag{C.3}$$

$$\mathrm{d}b = \left[-\frac{4}{m}ab - 2\gamma b + \frac{\gamma r^2}{\hbar} + \frac{\hbar\gamma}{r^2}(a^2 - b^2)\right]\mathrm{d}t \tag{C.4}$$

$$\mathrm{d}q = \frac{p}{m}\mathrm{d}t + \frac{\sqrt{\gamma}}{2}\frac{r}{b}\mathrm{d}\xi^R - \frac{\hbar\sqrt{\gamma}}{2r}\mathrm{d}\xi^R - \frac{\hbar\sqrt{\gamma}}{2r}\frac{a}{b}\mathrm{d}\xi^I \tag{C.5}$$

$$\mathrm{d}p = -(V_x + 2\gamma p)\mathrm{d}t + r\sqrt{\gamma}\frac{a}{b}\mathrm{d}\xi^R + r\sqrt{\gamma}\mathrm{d}\xi^I - \frac{\hbar\sqrt{\gamma}}{r}\left(\frac{a^2 + b^2}{b}\right)\mathrm{d}\xi^I. \tag{C.6}$$

We do this by means of a simple first-order algorithm, where at each time step Δt the variables $\{y\} = \{a, b, q, p\}$ are approximated as

$$y_{t+\Delta t} = y_t + \mathrm{d}y, \tag{C.7}$$

and $\mathrm{d}y$ is given by the stochastic processes above.

C.3 Lindblad and QSD equations

The Lindblad equation is a deterministic first-order differential equation, which can be evaluated numerically by means of a Runge-Kutta algorithm with order-four accuracy in the time step. The Runge-Kutta scheme is one of the most well-known methods for computing differential equations numerically so we will not report it here, however one can easily find it for example in reference [66].

For a numerical investigation of the QSD equation for pure state vectors (3.23), which we report here:

$$|\mathrm{d}\psi\rangle_t = -\frac{\mathrm{i}}{\hbar}H|\psi\rangle\mathrm{d}t + \gamma(2\langle L^\dagger\rangle L - L^\dagger L - \langle L^\dagger\rangle\langle L\rangle)|\psi\rangle\mathrm{d}t + \sqrt{\gamma}(L - \langle L\rangle)|\psi\rangle\mathrm{d}\xi, \tag{C.8}$$

where $\mathrm{d}\xi = \mathrm{d}\xi^R + \mathrm{i}\mathrm{d}\xi^I$, we adopt a generalisation of the order-four Runge-Kutta method proposed by Wilkie and Çetinbaş [67]. We summarise the key steps of the algorithm here. Let $a(|\psi\rangle, t)$ and $b(|\psi\rangle, t)$ such that the equation above reads:

$$|\mathrm{d}\psi\rangle_t = a(|\psi\rangle, t)\mathrm{d}t + \sum_{j=1,2} b_j(|\psi\rangle, t)\mathrm{d}\xi_j; \tag{C.9}$$

now let:

$$f(|\psi\rangle, t) = \left[a(|\psi\rangle, t) - \frac{1}{2}\sum_{j=1,2} b_j(|\psi\rangle, t)\frac{\partial b_j}{\partial |\psi\rangle}\right]\mathrm{d}t + \sum_{j=1,2} b_j(|\psi\rangle, t)\mathrm{d}\xi_j. \tag{C.10}$$

If we define the functions k_1, k_2, k_3 and k_4 in the standard Runge-Kutta fashion, that is:

$$k_1 = f(|\psi\rangle, t) \tag{C.11}$$
$$k_2 = f(|\psi\rangle + \frac{1}{2}k_1, t + \frac{1}{2}\mathrm{d}t) \tag{C.12}$$
$$k_3 = f(|\psi\rangle + \frac{1}{2}k_2, t + \frac{1}{2}\mathrm{d}t) \tag{C.13}$$
$$k_4 = f(|\psi\rangle + k_3, t + \mathrm{d}t), \tag{C.14}$$

we can obtain the value of the wave vector at time $t + \mathrm{d}t$:

$$|\mathrm{d}\psi\rangle_{t+\mathrm{d}t} = |\mathrm{d}\psi\rangle_t + \frac{1}{6}(k_1 + 2k_2 + 2k_3 + k_4). \tag{C.15}$$

With reference to equation (C.8) above, we have the following:

$$a(|\psi\rangle, t) = \left[-\frac{\mathrm{i}}{\hbar}H + \gamma(2\langle L^\dagger\rangle L - L^\dagger L - \langle L^\dagger\rangle\langle L\rangle)\right]|\psi\rangle, \tag{C.16}$$

$$b_1(|\psi\rangle, t) = \sqrt{\gamma}(L - \langle L\rangle)|\psi\rangle \quad \text{and} \quad b_2(|\psi\rangle, t) = \mathrm{i}\sqrt{\gamma}(L - \langle L\rangle)|\psi\rangle. \tag{C.17}$$

Hence overall:

$$f(|\psi\rangle, t) = \left[-\frac{\mathrm{i}}{\hbar}H + \gamma(2\langle L^\dagger\rangle L - L^\dagger L - \langle L^\dagger\rangle\langle L\rangle)\right]|\psi\rangle\mathrm{d}t + \sqrt{\gamma}(L - \langle L\rangle)|\psi\rangle(\mathrm{d}\xi^R + \mathrm{i}\mathrm{d}\xi^I), \tag{C.18}$$

which allows to evaluate equations (C.11)-(C.14) and (C.15) for each time step over the required duration of the simulation.

Appendix D

Brownian motion and Itô calculus

Here we review some basic notions that are of relevance in the study of quantum Brownian motion, following reference [50]. Let us start with the classical case. Here we firstly have the two basic properties applying to a Brownian motion that takes place along the coordinate x:

$$\mathcal{M}_{\mathrm{d}x}\mathrm{d}x_t = 0 \quad \text{and} \quad \mathcal{M}_{\mathrm{d}x}(\mathrm{d}x_t)^2 = a^2\mathrm{d}t, \tag{D.1}$$

where $\mathcal{M}_{\mathrm{d}x}$ indicates the average over small displacements $\mathrm{d}x$ and a is a positive constant. If we now introduce the normalised stochastic differential $\mathrm{d}w$ such that:

$$\mathcal{M}_{\mathrm{d}w}\mathrm{d}w_t = 0 \quad \text{and} \quad \mathcal{M}_{\mathrm{d}w}(\mathrm{d}w_t)^2 = \mathrm{d}t, \tag{D.2}$$

then we have the Langevin-Itô equation:

$$\mathrm{d}x_t = a\mathrm{d}w_t. \tag{D.3}$$

In Itô calculus differentials of order $(\mathrm{d}t)^2$ and above are neglected, and since the variance of $\mathrm{d}w$ is of order $\mathrm{d}t^2$ one can simplify the notation above and write:

$$(\mathrm{d}w)^2 = \mathrm{d}t. \tag{D.4}$$

Further we should note the rule by which we obtain the differential of a functions f of the stochastic process $\mathrm{d}x$; this follows from the well-known Itô's lemma:

$$\mathrm{d}f = (\mathrm{d}x)f_x + \frac{1}{2}(\mathrm{d}x)^2 f_{xx}, \tag{D.5}$$

where, as usual, f_x and f_{xx} indicate the first and second order derivatives of f with respect to x. For the product of two functions of $\mathrm{d}x$, f and g, we have:

$$\mathrm{d}(fg) = f\mathrm{d}g + (\mathrm{d}f)g + (\mathrm{d}f)(\mathrm{d}g). \tag{D.6}$$

In classics we had a Langevin equation of the form:

$$\mathrm{d}x_t = v\mathrm{d}t + a\mathrm{d}w_t, \tag{D.7}$$

with real v and a giving the magnitude of drift and diffusion respetively and $\mathrm{d}w$ is the Wiener process. In quantum-mechanics we deal with stochastic differential equations of the form:

$$\mathrm{d}z_t = u\mathrm{d}t + b\mathrm{d}\xi_t, \tag{D.8}$$

where u and b can be complex and $\mathrm{d}\xi$ is now a complex Wiener process, that is:

$$\mathrm{d}\xi_t = \mathrm{d}\xi_t^R + \mathrm{i}\mathrm{d}\xi_t^I, \tag{D.9}$$

where $\mathrm{d}\xi^R$ and $\mathrm{d}\xi^I$ are real Wiener process which satisfy the following properties:

$$\mathcal{M}_{\mathrm{d}\xi^\diamond}\mathrm{d}\xi^R = \mathcal{M}_{\mathrm{d}\xi^\diamond}\mathrm{d}\xi^I = 0, \quad \mathcal{M}_{\mathrm{d}\xi^\diamond}\mathrm{d}\xi^R\mathrm{d}\xi^I = 0, \quad \text{and} \quad \mathcal{M}_{\mathrm{d}\xi^\diamond}(\mathrm{d}\xi^R)^2 = \mathcal{M}_{\mathrm{d}\xi^\diamond}(\mathrm{d}\xi^I)^2 = \mathrm{d}t, \tag{D.10}$$

where $\mathcal{M}_{\mathrm{d}\xi^\diamond}$ indicates the average over stochastic differentials $\mathrm{d}\xi^R$ or $\mathrm{d}\xi^I$.

Bibliography

[1] H. Waalkens, R. Schubert, and S. Wiggins. Wigner's dynamical transition state theory in phase space: classical and quantum. *Nonlinearity*, 21:R1, 2008. URL http://stacks.iop.org/0951-7715/21/i=1/a=R01.

[2] A. Einstein. Über die von der molekularkinetischen Theorie der Wärme geforderte Bewegung von in ruhenden Flüssigkeiten suspendierten Teilchen. *Annalen der Physik*, 322:549–560, 1905. URL http://dx.doi.org/10.1002/andp.19053220806.

[3] M. A. Islam. Einstein-Smoluchowski diffusion equation: a discussion. *Physica Scripta*, 70(2-3):120, 2004. URL http://iopscience.iop.org/1402-4896/70/2-3/008.

[4] C.D. Beachem. A new model for hydrogen-assisted cracking (hydrogen embrittlement). *Metallurgical Transactions*, 3:441–455, 1972. URL http://dx.doi.org/10.1007/BF02642048.

[5] H. K. Birnbaum and P. Sofronis. Hydrogen-enhanced localised plasticity: a mechanism for hydrogen-related fracture. *Materials Science and Engineering: A*, 176: 191–202, 1994. ISSN 0921-5093. URL http://www.sciencedirect.com/science/article/pii/092150939490975X.

[6] R. A. Oriani and P. H. Josephic. Equilibrium aspects of hydrogen-induced cracking of steels. *Acta Metallurgica*, 22:1065–1074, 1974. ISSN 0001-6160. URL http://www.sciencedirect.com/science/article/pii/0001616074900613.

[7] S. Arrhenius. Über die Reaktionsgeschwindigkeit bei der Inversion von Rohrzucker durch Säuren. *Zeitschrift für physikalische Chemie*, 4:226–248, 1889.

[8] R. Kubo. Statistical-mechanical theory of irreversible processes. i. general theory and simple applications to magnetic and conduction problems. *Journal of the Physical Society of Japan*, 12:570–586, 1957. URL http://dx.doi.org/10.1143/JPSJ.12.570.

[9] R. Kubo, M. Yokota, and S. Nakajima. Statistical-mechanical theory of irreversible processes. ii. response to thermal disturbance. *Journal of the Physical Society of Japan*, 12:1203–1211, 1957. URL http://journals.jps.jp/doi/abs/10.1143/JPSJ.12.1203.

[10] D. Chandler. Statistical mechanics of isomerization dynamics in liquids and the transition state approximation. *The Journal of Chemical Physics*, 68:2959–2970, 1978. URL http://scitation.aip.org/content/aip/journal/jcp/68/6/10.1063/1.436049.

[11] D. G. Bourgin. Unimolecular reactions. *Proceedings of the National Academy of Sciences*, 15:357–362, 1929.

[12] E. Wigner. On the quantum correction for thermodynamic equilibrium. *Physical Review*, 40:749–759, 1932. URL https://link.aps.org/doi/10.1103/PhysRev.40.749.

[13] T. Yamamoto. Quantum statistical mechanical theory of the rate of exchange chemical reactions in the gas phase. *The Journal of Chemical Physics*, 33:281–289, 1960. URL http://scitation.aip.org/content/aip/journal/jcp/33/1/10.1063/1.1731099.

[14] C. P. Flynn and A. M. Stoneham. Quantum theory of diffusion with application to light interstitials in metals. *Physical Review B*, 1:3966–3978, 1970. URL http://link.aps.org/doi/10.1103/PhysRevB.1.3966.

[15] W. H. Miller. Quantum mechanical transition state theory and a new semiclassical model for reaction rate constants. *The Journal of Chemical Physics*, 61:1823–1834, 1974. URL http://dx.doi.org/10.1063/1.1682181.

[16] J. Costley and P. Pechuka. Short-time behavior of quantum correlation functions in rate theory. *Chemical Physics Letters*, 83:139–144, 1981. ISSN 0009-2614. URL http://www.sciencedirect.com/science/article/pii/0009261481803065.

[17] R. P. Feynman. Space-time approach to non-relativistic quantum mechanics. *Reviews of Modern Physics*, 20:367–387, 1948. URL http://link.aps.org/doi/10.1103/RevModPhys.20.367.

[18] R. P. Feynman and A. R. Hibbs. *Quantum mechanics and path integrals*. McGraw-Hill, 1965.

[19] M. J. Gillan. Quantum simulation of hydrogen in metals. *Physical Review Letters*, 58:563–566, 1987. URL http://link.aps.org/doi/10.1103/PhysRevLett.58.563.

[20] M. J. Gillan. Quantum-classical crossover of the transition rate in the damped double well. *Journal of Physics C: Solid State Physics*, 20:3621, 1987. URL http://stacks.iop.org/0022-3719/20/i=24/a=005.

[21] G. A. Voth, D. Chandler, and W. H. Miller. Rigorous formulation of quantum transition state theory and its dynamical corrections. *The Journal of Chemical Physics*, 91:7749–7760, 1989. URL http://scitation.aip.org/content/aip/journal/jcp/91/12/10.1063/1.457242.

[22] T. J. H. Hele and S. C. Althorpe. Derivation of a true ($t \to 0^+$) quantum transition-state theory. i. uniqueness and equivalence to ring-polymer molecular dynamics transition-state-theory. *The Journal of Chemical Physics*, 138, 2013. URL http://scitation.aip.org/content/aip/journal/jcp/138/8/10.1063/1.4792697.

[23] S. C. Althorpe and T. J. H. Hele. Derivation of a true ($t \to 0^+$) quantum transition-state theory. ii. recovery of the exact quantum rate in the absence of recrossing. *The Journal of Chemical Physics*, 139:084115, 2013. URL http://dx.doi.org/10.1063/1.4819076.

[24] I. R. Craig and D. E. Manolopoulos. Quantum statistics and classical mechanics: Real time correlation functions from ring polymer molecular dynamics. *The Journal of Chemical Physics*, 121:3368–3373, 2004. URL http://link.aip.org/link/?JCP/121/3368/1.

[25] I. R. Craig and D. E. Manolopoulos. Chemical reaction rates from ring polymer molecular dynamics. *The Journal of Chemical Physics*, 122:084106, 2005. doi: 10.1063/1.1850093. URL http://dx.doi.org/10.1063/1.1850093.

[26] B. J. Braams and D. E. Manolopoulos. On the short-time limit of ring polymer molecular dynamics. *The Journal of Chemical Physics*, 125, 2006. URL http://scitation.aip.org/content/aip/journal/jcp/125/12/10.1063/1.2357599.

[27] J. O. Richardson and S. C. Althorpe. Ring-polymer molecular dynamics rate-theory in the deep-tunneling regime: Connection with semiclassical instanton theory. *The Journal of Chemical Physics*, 131:214106, 2009. URL http://dx.doi.org/10.1063/1.3267318.

[28] T. J. H. Hele, M. J. Willatt, A. Muolo, and S. C. Althorpe. Boltzmann-conserving classical dynamics in quantum time-correlation functions: "Matsubara dynamic". *The Journal of Chemical Physics*, 142:134103, 2015. URL http://dx.doi.org/10.1063/1.4916311.

[29] H. Kimizuka, H. Mori, and S. Ogata. Effect of temperature on fast hydrogen diffusion in iron: a path-integral quantum dynamics approach. *Physical Review B*, 83:094110, 2011. URL http://link.aps.org/doi/10.1103/PhysRevB.83.094110.

[30] A. T. Paxton and I. H. Katzarov. Quantum and isotope effects on hydrogen diffusion, trapping and escape in iron. *Acta Materialia*, 103:71–76, 2016. ISSN 1359-6454. URL http://www.sciencedirect.com/science/article/pii/S1359645415007430.

[31] D. Chandler. Roles of classical dynamics and quantum dynamics on activated processes occurring in liquids. *Journal of Statistical Physics*, 42:49–67, 1986.

[32] K. Hepp. The classical limit for quantum mechanical correlation functions. *Communications in Mathematical Physics*, 35(4):265–277, 1974. URL https://doi.org/10.1007/BF01646348.

[33] E. J. Heller. Time-dependent approach to semiclassical dynamics. *The Journal of Chemical Physics*, 62:1544–1555, 1975. URL http://dx.doi.org/10.1063/1.430620.

[34] D. Chandler. *Introduction to modern statistical mechanics*. Oxford University Press, 1987.

[35] J. A. Montgomery, D. Chandler, and B. J. Berne. Trajectory analysis of a kinetic theory for isomerization dynamics in condensed phases. *The Journal of Chemical Physics*, 70:4056–4066, 1979. URL http://scitation.aip.org/content/aip/journal/jcp/70/9/10.1063/1.438028.

[36] P. Hänggi, P. Talkner, and M. Borkovec. Reaction-rate theory: fifty years after Kramers. *Reviews of Modern Physics*, 62:251–341, 1990. URL http://link.aps.org/doi/10.1103/RevModPhys.62.251.

[37] L. Onsager. Reciprocal relations in irreversible processes. i. *Physical Review*, 37: 405–426, 1931. URL https://link.aps.org/doi/10.1103/PhysRev.37.405.

[38] L. Onsager. Reciprocal relations in irreversible processes. ii. *Physical Review*, 38: 2265–2279, 1931. URL https://link.aps.org/doi/10.1103/PhysRev.38.2265.

[39] D. Manolopoulos. Lecture notes on chemical reaction dynamics. URL http://manolopoulos.chem.ox.ac.uk/Lectures/SummerSchoolLectures.

[40] R. Zwanzig. *Nonequilibrium statistical mechanics*. Oxford University Press, 2001.

[41] P. Langevin. Sur la théorie du mouvement brownien. *CR Acad. Sci. Paris*, 146 (530-533):530, 1908.

[42] M. Tuckerman. *Statistical mechanics: theory and molecular simulations*. Oxford Graduate Texts, 2010.

[43] E. Vanden-Eijnden and G. Ciccotti. Second-order integrators for Langevin equations with holonomic constraints. *Chemical Physics Letters*, 429:310–316, 2006. ISSN 0009-2614. URL http://www.sciencedirect.com/science/article/pii/S0009261406011092.

[44] W. H. Miller, S. D. Schwartz, and J. W. Tromp. Quantum mechanical rate constants for bimolecular reactions. *The Journal of Chemical Physics*, 79:4889–4898, 1983. URL http://scitation.aip.org/content/aip/journal/jcp/79/10/10.1063/1.445581.

[45] G. A. Voth. Feynman path integral formulation of quantum mechanical transition-state theory. *The Journal of Physical Chemistry*, 97:8365–8377, 1993.

[46] H.-P. Breuer and F. Petruccione. *The theory of open quantum systems*. Oxford University Press on Demand, 2002.

[47] R. P. Feynman. Statistical mechanics: a set of lectures. 1998.

[48] U. Weiss. *Quantum dissipative systems*. World scientific, 2012.

[49] G. Lindblad. On the generators of quantum dynamical semigroups. *Communications in Mathematical Physics*, 48:119–130, 1976. URL http://dx.doi.org/10.1007/BF01608499.

[50] I. Percival. *Quantum state diffusion*. Cambridge University Press, 1998.

[51] A. O. Caldeira and A. J. Leggett. Quantum tunnelling in a dissipative system. *Annals of physics*, 149:374–456, 1983. URL http://www.sciencedirect.com/science/article/pii/0003491683902026.

[52] L. Diósi. Calderia-Leggett master equation and medium temperatures. *Physica A: Statistical Mechanics and its Applications*, 199:517–526, 1993. URL http://www.sciencedirect.com/science/article/pii/037843719390065C.

[53] N. Gisin. Quantum measurements and stochastic processes. *Physical Review Letter*, 52:1657–1660, 1984. URL https://link.aps.org/doi/10.1103/PhysRevLett.52.1657.

[54] N. Gisin and I. C. Percival. The quantum-state diffusion model applied to open systems. *Journal of Physics A: Mathematical and General*, 25:5677, 1992. URL http://stacks.iop.org/0305-4470/25/i=21/a=023.

[55] P. Dirac. *Quantum Mechanics*. Clarendon Press, 1958.

[56] E.-M. Graefe and R. Schubert. Complexified coherent states and quantum evolution with non-Hermitian Hamiltonians. *Journal of Physics A: Mathematical and Theoretical*, 45:244033, 2012. URL http://stacks.iop.org/1751-8121/45/i=24/a=244033.

[57] E.-M. Graefe, H. J. Korsch, A. Rush, and R. Schubert. Classical and quantum dynamics in the (non-Hermitian) Swanson oscillator. *Journal of Physics A: Mathematical and Theoretical*, 48:055301, 2015. URL http://stacks.iop.org/1751-8121/48/i=5/a=055301.

[58] S. Gao. Dissipative quantum dynamics with a Lindblad functional. *Physical Review Letters*, 79:3101–3104, 1997. URL https://link.aps.org/doi/10.1103/PhysRevLett.79.3101.

[59] B. Pokharel, P. Duggins, M. Misplon, W. Lynn, K. Hallman, D. Anderson, A. Kapulkin, and A. K. Pattanayak. Dynamical complexity in the quantum to classical transition. 2016. URL https://arxiv.org/abs/1604.02743.

[60] W. T. Strunz and I. C. Percival. Classical mechanics from quantum state diffusion - a phase-space approach. *Journal of Physics A: Mathematical and General*, 31(7): 1801, 1998. URL http://stacks.iop.org/0305-4470/31/i=7/a=014.

[61] H. J. Korsch and M. Glück. Computing quantum eigenvalues made easy. *European Journal of Physics*, 23:413, 2002. URL http://stacks.iop.org/0143-0807/23/i=4/a=305.

[62] W.-M. Zhang, D. H. Feng, and R. Gilmore. Coherent states: Theory and some applications. *Reviews of Modern Physics*, 62:867–927, 1990. URL https://link.aps.org/doi/10.1103/RevModPhys.62.867.

[63] W. H. Miller. The semiclassical initial value representation: a potentially practical way for adding quantum effects to classical molecular dynamics simulations. *The Journal of Physical Chemistry A*, 105:2942–2955, 2001. URL http://pubs.acs.org/doi/abs/10.1021/jp003712k.

[64] I. Katzarov. Private communication.

[65] L. Verlet. Computer "experiments" on classical fluids. i. thermodynamical properties of Lennard-Jones molecules. *Physical Review*, 159:98–103, 1967. URL https://link.aps.org/doi/10.1103/PhysRev.159.98.

[66] W. Press, S. Teukolsky, W. Vetterling, and B. Flannery. *Numerical recipes in C - the art of scientific computing*. Cambridge University Press, 1992.

[67] J. Wilkie and M. Cetinbas. Variable-stepsize Runge-Kutta methods for stochastic Schrödinger equations. *Physics Letters A*, 337:166–182, 2005. URL http://www.sciencedirect.com/science/article/pii/S0375960105001581.